2017

Friction and Environmental Sensitivity of Molybdenum Disulfide: Effects of Microstructure

John Francis Curry
Lehigh University

Friction and Environmental Sensitivity of Molybdenum Disulfide: Effects of Microstructure

by

John F. Curry

Presented to the Graduate and Research Committee
of Lehigh University
in Candidacy for the Degree of
Doctor of Philosophy

in

Mechanical Engineering

Lehigh University

August 2017

Approved and recommended for acceptance as a dissertation draft

_____

Date

_____

Accepted Date

Committee Members:

_____

Advisor: Dr. Brandon Krick, Mechanical Engineering and Mechanics

_____

Dr. Herman F. Nied, Mechanical Engineering and Mechanics

_____

Dr. Frank Zhang, Mechanical Engineering and Mechanics

_____

Dr. Nicholas Strandwitz, Materials Science & Engineering

Acknowledgements

It certainly takes a village. While I've learned a bit over the past four years, my life has been full of people helping me learn and grow as a person. This section of acknowledgements is meant for them and only serves as a small token of my appreciation.

Like most, my parents are a cornerstone of my personality, who I am and who I want to be. Claire and James have been and will always be superstars in my mind. They are the most caring, understanding and supportive people I'll be lucky enough to have known. They always valued education among my siblings and I, but as the third child I was never pressured to do be overly involved in school or extra-curricular and the freedom was admittedly relaxing, and made me interested in pursuing academics nonetheless. They are truly wonderful people and it really is tough to adequately describe the impact they've had on my life in just a few sentences.

The same goes for my brother Matt and sister Catherine. I attribute most of my understandings of social norms and some of my observational skills to their interactions with my parents - this, of course, at a young age when nobody seemed to get along. I am proud to say that all grown up we've become very close and our relationships are something I treasure.

The one person that has been with me constantly throughout this process is my lovely co-pilot and partner in life, Brionna O'Connor. Brionna was with me from the very start of my graduate career and amid the uncontrolled beard growth, dips in hygiene, stay at home and work weekends and a sounding board for all advisor related woes, she's always been there and perfectly supportive. Not to mention the support her family has

also extended to me. They are an ironclad clan of stellar, welcoming human beings that I view as an extension of my own family.

Also, part of the extended family is my longtime best friend Ben Lehar, a person I've been lucky enough to live with and live in proximity to for the past decade or more. Ben is someone that inherently understands life, people and all the nuances (at least in my opinion!). He is a fiercely loyal, reliable and a genuinely kind-hearted person that I am very lucky to know.

An equal share of thanks goes to everyone in the Tribology Laboratory at Lehigh University: Mark Sidebottom, Guosong Zeng, our advisor Brandon Krick and many others who have spent time in the lab I have come to consider a close friend. Mark Sidebottom is one of the most out-going people I have ever met and superstar baker while Guosong Zeng happens to be an undercover superstar with a huge heart. They are both intensely smart people that have contributed so much to my academic career over the years. Special mention also goes to supremely intelligent, mental bear trap Chris Junk and all of his wonderful coffee, chocolate and stories he has shared with the lab in the past year or two. I also can't forget my favorite undergrad Zakaria Hsain for all the help in lab and time spent talking about world views and opinions.

Mark, Guosong and I may be Brandon's first graduate students, but the level of work ethic, detail and effort he has put into his career as a University Professor with a highly active focus in research is mind boggling. The lab operates at full speed, because everybody is having so much fun and learning every day. We were extremely lucky to have such a socially and academically involved lab, an environment which Brandon fully supports and encourages. Brandon gave us car loads of lab snacks before the STLE

presentation crunches, march madness bracket challenges, frequent lab lunches, Christmas parties, hiking excursions, road trips and many more but in general enabled many life-long friendships. One of the most exciting aspects of graduating from this lab is knowing that I can work with these wonderful people for the rest of my career.

The fine folks at Lehigh University also deserve special mention here as their help and friendship over the years made Lehigh such a joy to be a part of. Jen Smith was almost like a second mother to me, helping me constantly when I needed it, just being there to talk to in general and someone who I will miss a lot. The same goes for Barbara McGuire who somehow made everyone in the Mechanical Engineering Department call me the Pope - very classy.

It wouldn't be right if I didn't acknowledge the fine folks at Sandia National Laboratories. Nic Argibay and Mike Chandross were like a second set of advisors to me and also great friends. Nic is just pure joy and likely the most loving person I have encountered (truthfully), supremely smart and highly creative. The same can be said of Mike Chandross, who may have lots of foul jokes, but is super reliable, smart and outgoing (tell nobody). I very much look forward to working with them and the same goes for Mike Dugger, Brendan Nation, Andrew Kustas, Mark Wilson and Rand Garfield.

There are also those who deserve thanks for providing a lot of initial motivation and interest when first starting out in the lab. The Tribology Lab at the University of Florida under my grand advisor Greg Sawyer is just larger than life. Angela, Juan, Kyle, multiple Sam’s, multiple Alex's, Sean and many more are awesome people that I look forward to seeing every year at STLE and hopefully more in between. There are also the

gentlemen of University of Delaware under the mythic D.L. Burris. Axel, Ben and Nick are great people that I also look forward to seeing more of. Also, special mention to Jeff Ewin out of the University of Florida as well for being an all-around great guy and providing samples that I wish I had time to test! Last but not least is Mike Counts from WD-40. Without Mike's friendship and the support from WD-40 I would not have a PhD today for which I am forever grateful.

Again, these few pages are far too short to adequately thank everyone for the friendship and knowledge they've imparted over the years. If you've stuck it out and made it to the end of this, thank you for dealing with the plethora of positive adjectives, descriptors and overall bad grammar. To those not specifically mentioned, feel free to hassle me.

Table of Contents

List of Tables

List of Figures

Abstract

For nearly a century, molybdenum disulfide has been employed as a solid lubricant to reduce the friction and wear between surfaces. MoS2 is in a class of unique materials, transition metal dichalcogens (TMDC), that have a single crystal structure forming lamellae that interact via weak van der Waals forces. This dissertation focuses on the link between the microstructure of MoS2 and the energetics of running film formation to reduce friction, and effects of environmental sensitivities on performance. Nitrogen impinged MoS2 films are utilized as a comparator to amorphous PVD deposited MoS2 in many of the studies due to the highly ordered surface parallel basal texture of sprayed films. Comparisons showed that films with a highly ordered structure can reduce high friction behavior during run-in. It is thought that shear induced reorientation of amorphous films contributes to typically high initial friction during run-in.

In addition to a reduction in initial friction, highly ordered MoS2 films are shown to be more resistant to penetration from oxidative aging processes. High sensitivity, low-energy ion scattering (HS-LEIS) enabled depth profiles that showed oxidation limited to the first monolayer for ordered films and throughout the depth (4-5 nm) for amorphous films. X-ray photoelectron spectroscopy supported these findings, showing far more oxidation in amorphous films than ordered films.

Many of these results show the benefits of a well run-in coating, yet transient increases in initial friction can still be noticed after only 5 – 10 minutes. It was found that the transient return to high initial friction after dwell times past 5 – 10 minutes was not due to adsorbed species such as water, but possibly an effect of basal plane relaxation to a

commensurate state. Additional techniques and methods were developed to study the effect of adsorbed water and load on running film formation via spiral orbit XRD studies. Spiral orbit experiments enabled large enough worn areas for study in the XRD. Diffraction patterns for sputtered coatings at high loads (1N) showed more intense signals for surface parallel basal plane representation than lower loads (100mN). Tests run in dry and humid nitrogen (20% RH), however, showed no differences in reorientation of basal planes. Microstructure was found to be an important factor in determining the tribological performance of MoS2 films in a variety of testing conditions and environments. These findings will be useful in developing a mechanistic framework that better understands the energetics of running film formation and how different environments play a role.

1. Introduction

1.1 Historical Perspective of Tribology

Tribology is the study of surfaces in relative motion, the phenomenon that occur during sliding and attempts to understand the fundamental mechanisms that explain what happens. As Rabinowicz wrote, “we live in a solid world… the earth itself is solid, the stones and sand on its surface are solid, human beings, and their tools and machines are solid.” [1] The interaction between solids in relative motion, and specifically the study of the friction, wear and lubrication associated with their interactions, is the cornerstone of tribological research and development.

It is not hard to imagine the challenges faced throughout the history of engineering where the interaction between surfaces has played a critical role in the success or longevity of a mechanism or system. As far back as the stone ages (11,000 – 5,500 years ago), there is evidence of early tribologists creating the first man-made bearings for wheeled vehicles. Ancient Egyptians used water and various oils available to them as a lubricant to move large statues and stone slabs long distances. Perhaps the most important development in the science behind tribology came with Leonardo da Vinci (1452 – 1519) who demonstrated before anyone else that the force of friction was directly proportional to the applied load and independent of the apparent contact area. These laws put forward by da Vinci were again demonstrated and published nearly 200 years later by French inventor and physicist Guillaume Amonton (1663 - 1705) in his 1699 paper *De la Resistance Causée dans les Machines* (“On the Resistance Caused in Machines”) [2]–[4]. Almost like clockwork, another 200 years after Amonton’s published findings, Heinrich Hertz (1857 - 1894) began developing much of what we know about contact mechanics, which in

addition to Amonton's observations have become a large part of how we characterize the mechanisms behind sliding friction between surfaces in relative motion.

1.2 Materials Tribology in Mechanical Design

Moving mechanical assemblies of all shapes, sizes and materials across industries more than likely have a critical interface in which tribological materials are employed. The automobile, for example, is a mobile tribology laboratory. Additives are widely used in engine oils to help reduce friction and wear in the piston assembly and bearings along with other components such as the valve train, transmission (clutch plates), tires, brake pads, etc. [5]. The energy sector also stands to benefit greatly from reductions in friction and wear for gearboxes in wind turbine applications [6]. Bearings used in the gearbox undergo fatigue and begin to spall and wear over time and large, electrical contacts for the transmission of power also wear over time, reducing the efficiency of transmitting power. These are only a few examples of widespread applications of tribology and areas with potential gains in efficiency and prolonged service life. A recent study by Carpick et al revisited the groundbreaking reports by Jost [7]–[9], revealing the widespread economic gains by adapting tribological advances in research. Similar to Jost's previous findings, the authors concluded that between transportation, utility and industrial sectors, *11% of energy used can potentially be saved* with investments in recent developments in tribological research [6].

Development of spacecraft also pose many materials tribology engineering challenges. Launch vehicles and transport systems, spin stabilized satellites and large structures such as the US Skylab (1973 – 1979) and International Space Station (ISS; 1998 - present) all house many intricate moving mechanical assemblies that must provide proper lubrication

in the harsh environment of space. On unmanned missions, the ability to repair any one of the latched or locking mechanisms, actuators, gyroscopes, telescoping joints or pumps that are all specifically lubricated for a set of operating conditions could result in catastrophic failure. The cost of such failures is, of course, extremely prohibitive [10], [11].

Incorporating materials into mechanical designs for tribological applications is heavily reliant upon a variety of factors. As such, it is important to note that friction and wear are not strictly material parameters that you can look up in a table. The tribological response of a system is very much dependent on a variety of intrinsic and external factors such as loading conditions (applied load, contact geometry, sliding mode), environmental conditions (vacuum, different vapor phase of gaseous environments, varying temperatures), deposition techniques and resulting differences in microstructure. In addition to this, the basic laws that govern relationships between normal force, friction force and contact area set by da Vinci and Amonton also fall apart for certain classes of material pairs. Altogether, the endeavor of a tribologist to classify a system to the extent where guidelines or even predictive models can be applied becomes very challenging.

1.3 Solid Lubrication

For many applications, typical lubrication via liquids such as base or synthetic oils is commonplace. The automotive and metal working industries dominate use and consumption of lubricants [12] and it is more than likely most are familiar with using WD-40 to hush squeaky, bare metal contacts. There is, however, another class of commonly used lubricants that are solid or dry in nature. Teflon ^{TM} (PTFE) in “non-stick” coatings and graphite powder in automotive and metalworking are commonly used examples of what are referred to as solid lubricants. Solid lubrication is typically employed in systems

that, for one reason or another, are unable to use liquids for lubrication. High temperature and vacuum applications such as those found in space are conditions in which liquids typically cannot exist. In these situations, oil or grease based lubricants would outgas and unfavorably contaminate or react with other components in the assembly. In similar applications, the ability to reduce weight and save space by removing lubricant reservoirs is also beneficial.

Just as with liquid lubrication, the goal of solid lubrication is to separate an interface and prevent wear from occurring; reducing friction between interfaces if necessary. For solid lubricants, that interface is typically between two metal surfaces (bearings, gears, etc..). Much of our understanding of interactions between solid metal contacts stems from the work of Bowden and Tabor [13]. They had put forth that the friction force (F) could be calculated as the product of real contact area (A_r) and shear strength (τ) of the lubricant. This allows us to define the friction coefficient as follows

Equation 1-1

$$\mu = \frac{F}{L} = \frac{A_r \cdot \tau}{A_r \cdot P} = \frac{\tau}{P} = \frac{\tau_0}{P} + \alpha$$

with τ_0 representing the interfacial shear strength of the junction and α representing the lowest possible friction coefficient attainable for the material pair. This is possible by also substituting the applied normal load (L) with the product of A_r and the mean Hertzian contact pressure (P). Such a discovery made it easy to imagine what could be done to optimize the lubrication in a friction couple. Ideally, if you had a hard material (high P, low A_r) with a thin, low shear strength junction (low τ_0) you could drive the friction coefficient towards its lowest attainable value α. This was proven experimentally by Bowden and Tabor when they coated a steel substrate with a thin film of indium and

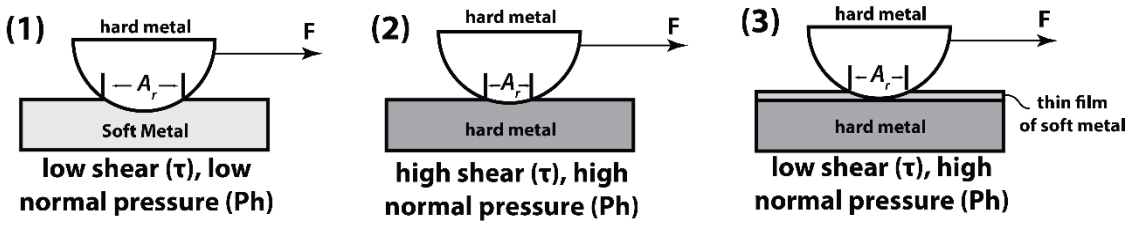

Fig. 1-1. Schematic detailing the relationship between contact pressure, shear strength and contact area to minimize friction. Ideally, a thin soft film will only slightly increase contact area while greatly reducing shear resulting in lower friction coefficients. [17]

showed that as the load was increased, the friction coefficient decreased. These results directly contradicted Amonton's first law of friction, stating friction coefficient is dependent upon the applied load. This can be explained by the fact that as the load increased, the deformation of the underlying substrate only produced a slight increase in contact area (Figure 1-1). This minimal increase in contact area only produces a slight change in friction force but nothing compared to the normal load and as such provides a decrease in friction coefficient. Hertz contact models have also been employed to calculate friction coefficient when we consider a sphere in elastic contact with a flat plane

Equation 1-2

$$\mu = \tau_0 \left(\frac{3R}{4E^*} \right)^{2/3} L^{-1/3} + \alpha$$

with R as the radius of the sphere and E^* as the reduced young's modulus. This relationship further proves the inapplicability of Amonton's laws and reveals an interesting relationship between friction coefficient and applied load:

Equation 1-3

$$\mu \propto L^{-1/3}$$

In addition to the inverse relationship in load providing a means to lower friction (low τ_0; low A_r), many material pairs further reduce τ_0 by the development of transfer films, running films and the entrapment of wear debris capable of extending the life of the film. Transfer of material to either sliding pair can be an important mechanism for preventing

direct contact of the coating material (preventing wear) and impart a further reduction in shear strength of the junction (lower τ_0) [14]–[16].

It is also important to realize that there are many different solid lubricants at a tribologist's disposal with their own benefits and drawbacks. One of the most important considerations when selecting the proper solid lubricant for the application are contact conditions (geometry, contact pressure, velocity), modes of sliding (rolling / sliding / reciprocating / unidirectional, etc…) and most importantly the environment and temperature of sliding. It is common practice, then, to pick a specific material based upon these criteria.

To accommodate a wide variety of applications in different environments, research and development has progressed on many different solid lubricant material systems. Typical examples of these solid lubricants soft metal materials (gold, silver, tin, indium), carbon-based (graphite/graphene, diamond-like-carbon (DLC), ultrananocrystalline diamond (UNCD), polymers (PTFE), and transition metal dichalcogenides (TMD) such as MoS_2 and WS2. An excellent review in tabular form of various solid lubricant films can be found in a review of solid lubricants by Scharf et al [17].

No one material can effectively operate in more than one type of environment or temperature range [17]. This can pose problems when applications span multiple operating environments. As such, composites of many materials in addition to a base lubricant such as MoS_2 have been employed to produce coatings better suited for use in multiple environments.

1.4 Motivation - Development of Robust, Environmentally Agnostic, Low Friction Coatings

Coatings are developed to match the operating conditions of their intended applications. With many different applications and possible solid lubricant material systems, it becomes difficult to know what the best choice is in every situation. There are, however, characteristics of a solid lubricant that are paramount, especially in the context of this dissertation. Specifically, the ability of a coating to provide consistent lubrication (low friction, low wear) in multiple environments are among the most important qualities in a successful solid lubricant. Consistent lubrication can be tied to various properties of the substrate-coating pair. Adhesion at the interface between coating and substrate, density and packing of the film, thickness and hardness can all play a role. How the coating reacts to sliding or aging in different environments varies greatly, is specific to each material system and can also greatly affect performance.

To aid in the development of robust, environmentally agnostic, low friction coatings we assess the role of microstructure on initial sliding behavior (run-in) and environmental sensitivity (oxidation). This is in part achieved by utilizing multiple deposition techniques capable of producing very different film microstructures. The tribological properties of these films are assessed in addition to multiple characterization techniques and atomistic simulations. The results and insights provided here aim to further our understanding of the fundamental mechanisms of friction in pure MoS_2 lubricated contacts.

2. Theoretical Background and Motivation for studying MoS_2

2.1 MoS_2 As a Tribological Material

Lubrication in extreme environments poses a unique and challenging problem where traditional lubricants such as oils and greases are not able to perform. Inert gas or vacuum environments as well as large temperature ranges such as those found in space is a great example of where dry films or solid lubricants on hard surfaces serve to reduce friction and wear of various mechanical components. Molybdenum Disulfide (MoS_2) is a well-known industrial solid lubricant with stellar tribological performance in such environments and the focus of this dissertation. MoS_2 is a transitional metal dichalcogenide (TMDC) in which a Mo atom is covalently bonded to two S atoms in a continuous S-Mo-S sheet (Figure 2-

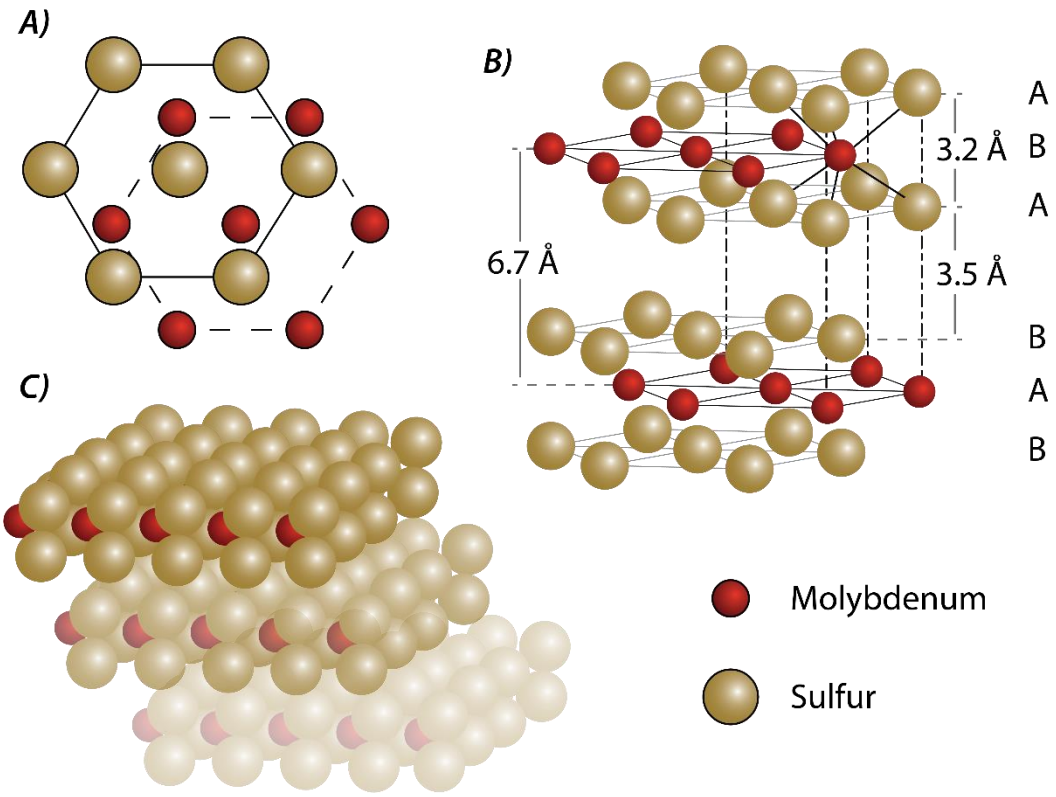

Fig. 2-1. A) Top and B) isometric view of hexagonal crystal structure of *MoS_2* and C) lamellar structure

1). These sheets or lamellae are separated by weak Van der Waals forces and upon applying a shear force, slide easily along their basal planes past one another.

2.2 Run-In & Environmental Dependencies

MoS2 nearly always experiences a transition in friction performance, known as "run in". In inert environments, run-in consists of a drop from initial friction to a lower steady state friction (Figure 2-2). Frictional transitions are accompanied with structural changes in the film[18]–[20], as well as formation of tribofilms[21]–[23]– a transfer film on the material in contact and a running film on the MoS2 surface. During the first few cycles of sliding, a transition occurs in which MoS_2 on the surface of the wear track undergoes shear-induced crystallization and reorientation[18]–[20], [24], [25] (and possibly joining and increasing in crystallite size), which orders the basal planes of these MoS_2 crystallites parallel to the substrate which allows for easy shear between lamellae[26] (Figure 2-3). Formation of a transfer film in the first few sliding cycles is thought to be a requirement in achieving low friction behavior of MoS_2 films. The ability of MoS_2 to

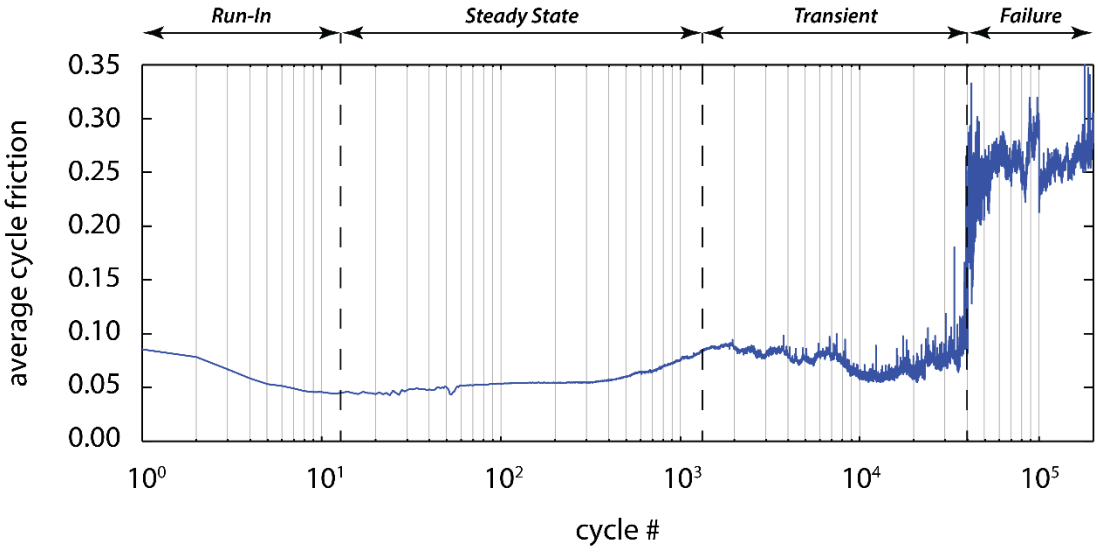

Fig. 2-2. Typical trace of friction coefficient during a long cycle experiment. Highlights the different phases during a test such as run-in, steady state, transient and failure

transfer to a counterface is well documented [21]–[23], but isolating the ability of transferred MoS_2 to provide lubrication has not yet been studied.

Presence of contaminants on the surface such as water, oxides and hydrocarbons are also thought to contribute to increased friction upon first sliding[27]–[30]. While many different theories exist in the literature, it is commonly accepted that water physically adsorbs to the surface of MoS_2 and/or diffuses into the near surface to disrupt the easy shear between lamella (Figure 2-4). Molecular oxygen on the other hand disrupts shear via the formation of oxides (Molybdenum Trioxide - MoO_3) at the reactive edge sites of MoS_2 crystals at higher temperatures (250°C). Lastly, the most prominent concern in low earth

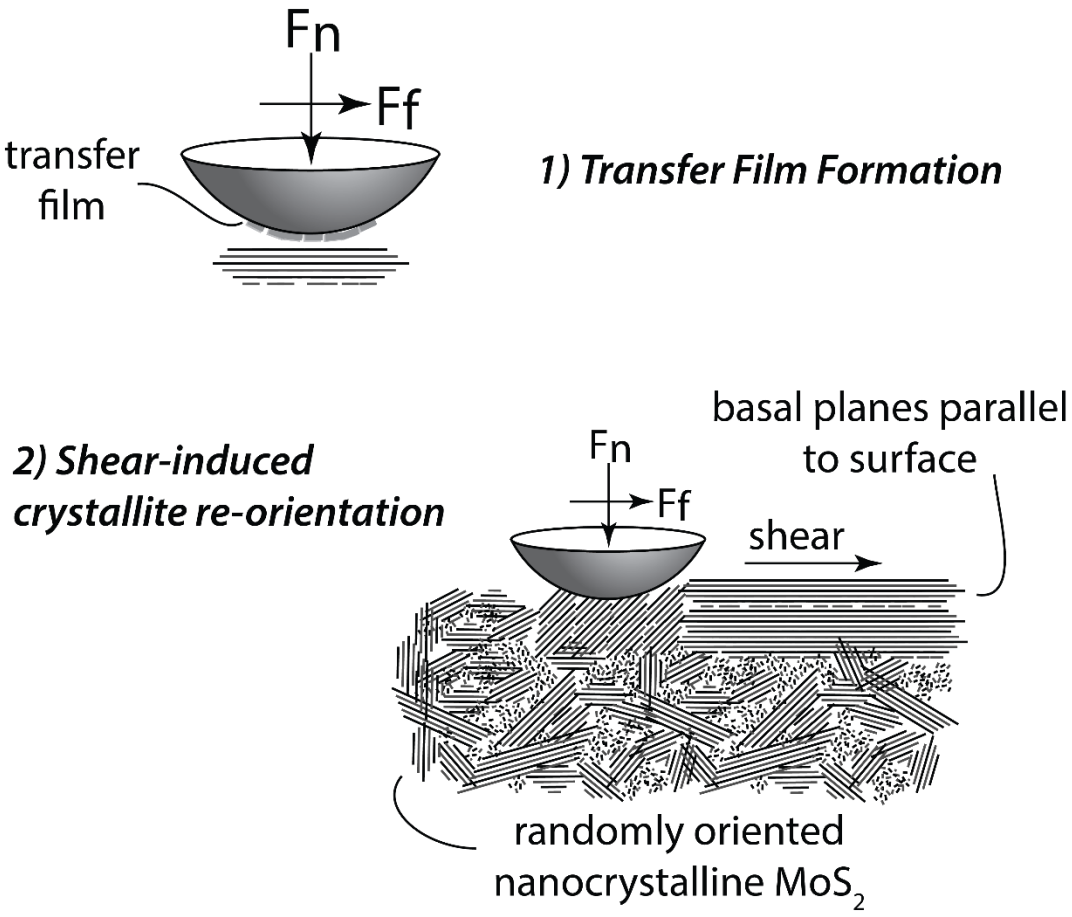

Fig. 2-3. Run-in processes of *MoS_2*, consisting of (1) initial material transfer and transfer film formation as well as (2) reorientation and crystallization of *MoS_2* parallel to sliding.

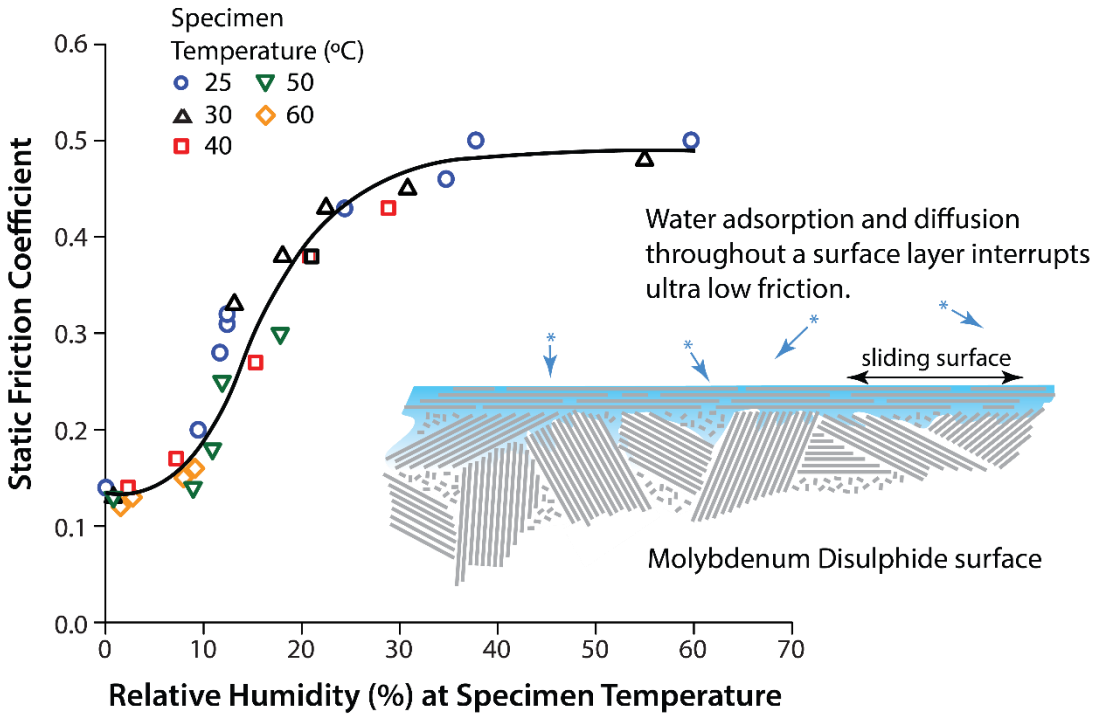

Fig. 2-4. Plot of static friction vs relative humidity. It is thought that water adsorbs and/or diffuses into the surface of *MoS_2* coatings, disrupting lamellar shear.

orbit (LEO) is the presence of atomic oxygen which is extremely reactive and quickly oxidizes the surface of MoS_2 coatings [31]–[36] (Figure 2-5).

Many different theories have been proposed as to the mechanisms behind the lubrication behavior of MoS_2 in environments containing water and oxygen. Studies done by Fusaro on burnished MoS_2 showed that friction in dry argon and dry air were low at $\mu = 0.02$ while higher in humid environments at $\mu = 0.08$; wear life was also the lowest in humid environments [37]. These results were similar to an earlier study by Salomon et al who showed that friction coefficient in dry argon and dry air were comparable at $\mu = 0.06 - 0.07$ while for humid environments was ~ 0.12 (7% RH) [38], [39]. Endurance testing however showed that samples run in humid environments lasted twice as long as those in

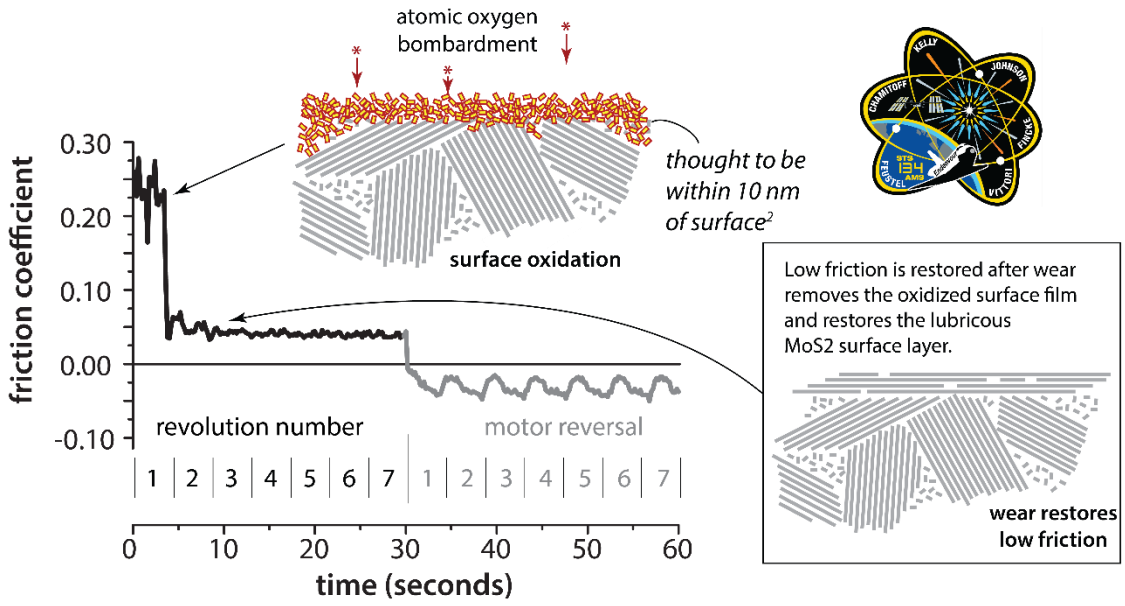

Fig. 2-5 A representative single cycle of sliding on *MoS_2* after exposure to atomic oxygen on the international space station (NASA MISSE 7) [167]. Initial sliding shows high friction attributed to wear of oxides on the surface.

oxygen. An accompanying x-ray analysis claimed the presence of oxides in the wear track of humid tested samples.

Many theories and conflicting results are present throughout the literature for the environmental effect on these coatings but a consensus is found in that water, more than oxygen, increases friction coefficient. Common hypotheses for the increase in friction in humid environments include: the physisorption of water in the sliding surface [40]–[42], bonding of water to active edge sites of MoS_2, water initiated oxidation [40], [43], film softening [44], surface tension of cavities on the surface [45] and hydrogen bonding between basal planes of MoS_2 [46]. Two of the most accepted and subsequently debated theories for the lubrication behavior of MoS_2 at room temperature argue that: 1) water itself causes an increase in the shear strength of the MoS_2 sliding interface or 2) a combination of thermal and mechanical processes cause water to oxidize MoS_2 and prevent easy shear of lamellae.

Early experiments done by Ross & Sussman showed that powder MoS_2 was easily oxidized in humid environments (at 85-100 °C) and the amount of oxidation rose with increasing humidity [43]. Over the next decade, a handful of tribological studies corroborated these findings [28], [40], [42], [47]. Generally, it was found that friction increased with humidity [41] and did so reversibly except at high humidity where friction was permanently degraded [42]. Many studies have also shown that storage or operation in humid environments degrade the low friction typically observed with any accompanying increase in oxidation [24], [39], [48].

A large aspect that had been missing from the literature up until recently was decoupling the effects of water and oxygen for humid testing. This was accomplished by testing in humid nitrogen. Khare et al showed via testing in dry nitrogen, humid nitrogen, dry air and humid air across a range of temperatures, that water did not contribute to the oxidation of MoS_2 [49], [50]. Pin on flat microtribometer experiments in humid nitrogen from room temperature up to 250°C revealed little to no oxygen Kα counts via EDS mapping. Friction also decreased with increased temperature in humid nitrogen which would make sense as adsorbed species such as water should be driven out and allow for easy shear between lamellae[41], [51], [52]. Testing in air after annealing in humid nitrogen did not produce high initial friction as opposed to samples annealed in environments containing oxygen. This showed oxidation and delamination of surface oxides did not occur after aging in humid environments, again pointing to the fact that water does not oxidize MoS_2. What they showed overall is that from room temperature until a transition temperature (~100°C), friction decreases as adsorbed water is driven out of the coating. Past the transition temperature friction begins to increase as oxides form.

Similar results but different oxidation temperatures were found by Windom et al using Raman to show that only dry air or oxygen environments produces oxides at elevated temperatures (~ 375 K) and not humid ones [53].

With the distinction shown by Windom and Khare, the mechanisms at play become much clearer. Any molecular oxygen present in the coating or at the surface can react with active edge sites of MoS_2 grains to form MoO_3 and does so more readily at elevated temperatures. Water serves to increase shear strength between MoS_2 lamellae and/or the transfer film adhered to the uncoated sliding member [54], possibly due to hydrogen bonding between lamellae [46].

A clear picture of the surface and subsurface effects of environmental constituents remains elusive though. While it is most likely that water physically adsorbs to the surface, it is unknown to what extent it diffuses into a coating [42], [47], [51] and how this diffusion effects the run-in processes critical to lubrication such as reorientation and crystallization of the nanocrystalline grains (byproduct of amorphous deposition). Similar questions can be asked of molecular and atomic oxygen. It is known that oxygen diffusion occurs in MoS_2 coatings and is affected largely by the crystal orientation and size of grains which in turn are affected by the deposition technique [22], [24], [35], [55]–[59]. The depths to which oxygen penetrates coatings during storage have been studied [24], [35], [36], [56] via various techniques (XPS, AES, RBS) but generally lack the proper resolution to distinguish absolute surface effects and gradients over thicknesses below 5-10 nm. More importantly, developing and optimizing deposition techniques to combat diffusion of water and oxygen via microstructural design is paramount to curbing the deleterious effects of storage in terrestrial environments.

2.3 MoS_2 Composites

2.3.1 Metal & Organic Doped

Studies by Niederhauser were some of the first to show the benefits of creating composite MoS_2 coatings either by adding interlayers of materials for strength and corrosion resistance or just combining other materials with MoS_2 such as PTFE and graphite [60] to obtain similar environmental safeguarding of lubrication. This has been supported throughout the literature with numerous examples such as: sulfiding steel substrates helps to improve adhesion [22], [60], incorporating additives such as other metals (Au, Ni, Ti, Pb) [61]–[64], carbon-based materials (Graphite, PTFE, DLC) [54], [55], [60], [65], and hard oxides or ceramics (YSZ, Sb_2O_3) [25], [66]–[71] all of which are capable of enhancing lubrication and endurance in dry and humid environments [63], [69].

2.3.2 MoS_2 Composites: Chameleon coatings

Coatings capable of maintaining beneficial lubricating behavior in whichever environment they are sliding in are referred to as adaptive or chameleon coatings. Put forward by Voevodin and Zabinski, the concept of chameleon coatings was to embed small reservoirs of solid lubricants (such as MoS_2 and graphite) within thermally stable and hard nanocrystalline or amorphous matrices (such as YSZ, Sb_2O_3) (Figure 2-6) [70]. For example, with a $MoS_2/Sb_2O_3/C$ composite, the Sb_2O_3 acts as a hard sliding surface to reduce contact area, a crack arrester to prevent large scale delamination/fatigue failure due to crack propagation, and a pump of sorts by pushing the solid lubricating components to the surface [67]. The $MoS_2/Sb_2O_3/C$ coating used in Zabinski's 2006 study was burnished, not sputtered onto the surface and survived millions of sliding cycles - an unprecedented feat of endurance for any form of MoS_2 coating. The deposition for most other chameleon

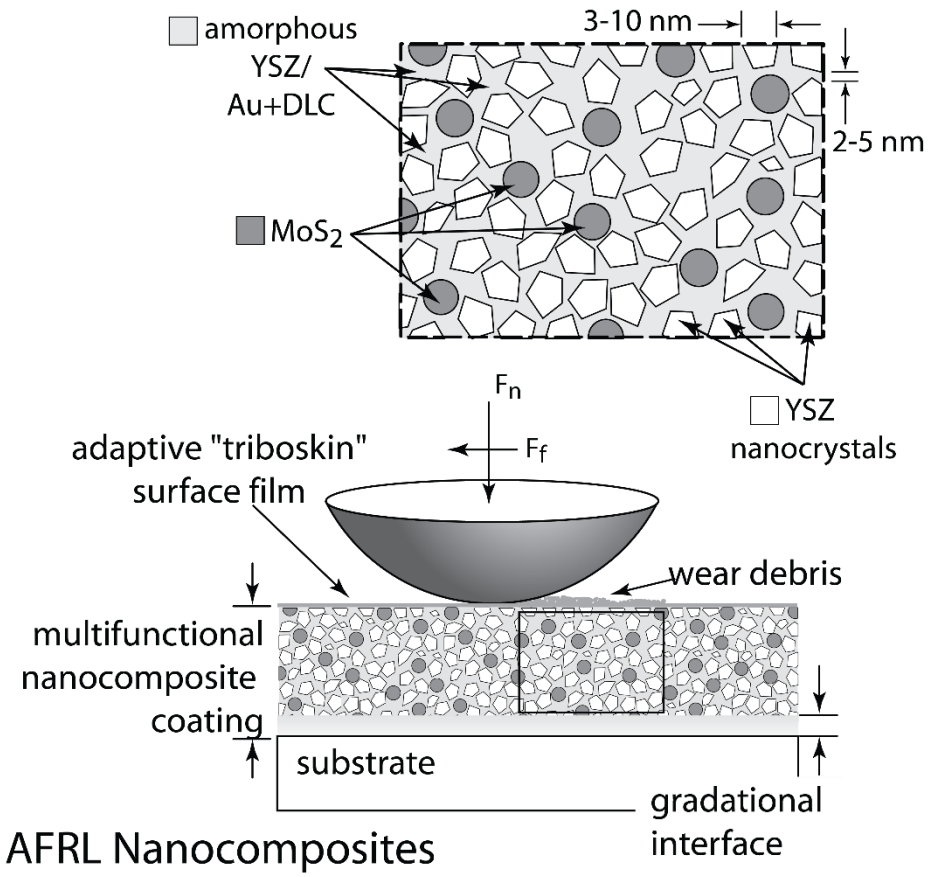

Fig. 2-6. Conceptual design of nanocomposite coating with "chameleon" like adaptation to surrounding environment [168].

coatings mentioned above are deposited via a hybrid PVD process utilizing magnetron sputtering and PLD. Seemingly, the only detractor for adaptive or chameleon coatings is the expensive and complicated deposition processes which utilize multiple targets of various components as well as multiple PVD systems at once.

2.4 Deposition Techniques

2.4.1 Burnishing, Resin-Bonded & PVD

MoS_2 coatings were initially prepared via a burnishing process in which powders are rubbed onto surfaces and kept adherent via resins or other bonding agents [39], [44], [72]–[74]. The process is known to produce coatings that have surfaces with their basal planes oriented parallel to the surface of the film which is preferential in promoting low

friction. Unfortunately, this preferential orientation is only noticed within the top few layers of burnished coatings yet not throughout the bulk of the coating which is thought to be necessary for better protection and adhesion [22]. The poor adhesion and subsequently low endurance [22], [24], poor control of thickness, and outgassing of bonding agents in vacuum [11] motivated the need for more adherent coatings with tighter tolerances.

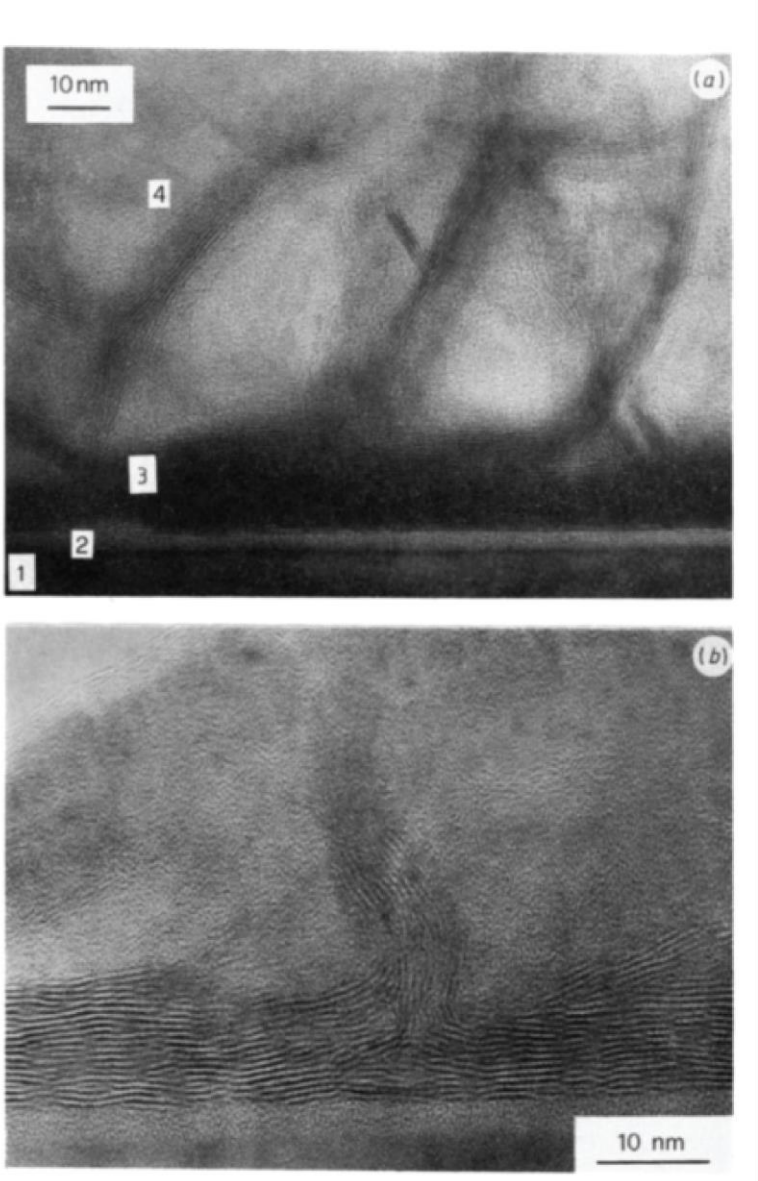

Fig. 2-7. – a) shows the long, columnar MoS_2 structure with and b) a close-up of the substrate with aligned MoS_2 [80].

In the late 1960's rf-magnetron sputtering was developed for just these purposes. The sputtering process was capable producing thick, adherent coatings in which thicknesses could be easily controlled, typically in the range of 0.2 - 1.5 um. The downside, and cause for extensive research into the sputtering process, is its crystallographic texture which often is largely amorphous and partially porous due to its columnar void structural formation. (Figure 2-7)

The nucleation of MoS_2 islands on a substrate during sputtering can either form in a basal or edge orientation (Figure 2-8). Most of the optimizations made to the sputtering processes over the years [24], [48], [75]–[79] have been focused on fine tuning conditions that promote a greater degree of basal island formation at the substrate and throughout the bulk of the coating. The problem is, basal planes as shown in Figure 2-1 are sulfur terminated and as such are very inert. Atoms deposited on the basal plane have a higher probability of being desorbed or re-sputtered before adsorption or burial by incoming target material [76]. Not to mention, any defects in the substrate [77] or lattice defects formed during deposition cause nucleation of edge oriented grains [80], [81] that preferentially propagate by bonding to active edge sites in columns perpendicular to the substrate, hence the term columnar void structures.

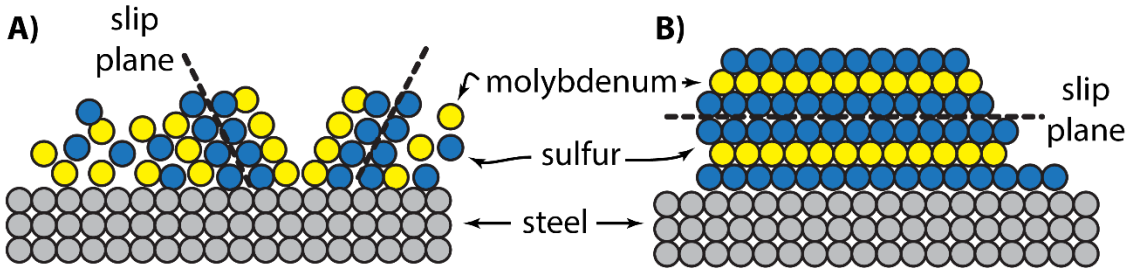

Fig. 2-8. Side view schematic of (A) films with basal planes perpendicular to substrate, with higher susceptibility to environmental contaminants and (B) films with basal planes parallel to the substrate that exhibit higher resistance to environmental degradation. [24]

The amorphous composition poses many problems in all aspects of lubrication performance. Randomly oriented, amorphous films suffer a considerable amount of crystallographic reorientation during the run-in period [24]. This shear induced reorientation is thought to be a contributing factor to the increased friction during initial sliding. Fleischauer showed that films with initially greater parallel orientation (as observed via AES) have both superior lubricating properties and substantially greater resistances to oxidation and other chemical degradation processes in storage than films with random crystallite orientations (Figure 2-8) [24]. While orientation is beneficial to lubrication, crystallite size and subsequently the ratio of accessible edge sites, is the driving reason for resistance to intrusion from environmental contaminants [22].

The columnar structure also influences the wear mechanisms of the coatings. Spalvins showed that under certain sliding conditions that the columnar bulk of the films fractures in the first few cycles as shown by investigative SEM experiments and either remains within the wear track or is ejected, losing much of the original film thickness [82], [83]. Similar experiments done by Hilton et al showed that the columnar region deforms, bends and compresses instead of fracturing but leaves a similar reduction in film thickness [57]. As such, films with large, oriented crystallites throughout their bulk are highly desirable but difficult to achieve with PVD methods such as sputtering.

2.4.2 Ion beam assisted deposition (IBAD)

Further attempts to densify MoS_2 coatings and induce surface parallel basal orientation were made by bombarding the coating with ions (such as Ar^+) during deposition [84]–[89]. This process is known as ion beam assisted deposition (IBAD) and was first explored by Mikkelsen to preferentially alter the microstructure of PVD coatings for enhanced

lubrication. The process is largely affected by the rate/intensity [84], ion-to-atom ratio and temperature[86], [87], with optimal performance and structure resulting from impingement rates on the order of 1 displaced atom per incident ion at temperatures above 423 K. It was shown that the conferred basal orientation by the IBAD process enhanced wear endurance [85], [89] yet the resulting impact on initial friction behavior and environmental resistances, however, were not discussed. Dunn further showed that the basal orientation in these films exhibited many defects and small crystallites with random in-plane orientation. IBAD deposition processes represent a very interesting sample set of MoS_2 coatings that exhibit basal orientation, yet a varying degree of defects and crystallite sizes. While of great interest, studies on IBAD coatings were not pursued in this dissertation. Extended periods of time are necessary apart from initial sputter deposition and subsequent ion bombardment making the process cost and time prohibitive.

2.4.3 Nitrogen Spray Deposited MoS_2

MoS_2 coatings have also been applied by nitrogen spray deposition, a relatively common technique in cold spray deposition systems, yet nearly absent from the literature in terms of depositing MoS_2 [90]. Commercially available MoS_2 powder stock is fed through a small circular spray nozzle via nitrogen carrier gas at high speeds impinging on the surface. This high kinetic energy deposition is able to shear the MoS_2 particulates onto the surface, resulting in film microstructures with preferential basal orientation throughout the thickness of the coating. The resulting surface parallel basal texture of these films are unique and provide many interesting comparisons that enable a better understanding of the effect of microstructure in MoS_2 films during initial sliding and in different environments

[90]. Further information on deposition parameters and the effect of microstructure on the performance of MoS_2 are detailed throughout this dissertation.

3. Hypothesis for Structurally Influenced Tribological Performance

Central to this dissertation and motivation for many of the studies conducted begin with nitrogen spray deposited MoS_2. It is thought that the spray impingement process can shear MoS_2 powder onto the substrate and impart a preferential basal orientation, due to the high kinetic energy at impact. This is motivated from what we already know about MoS_2 in the literature, where shear-induced, surface parallel reorientation of basal planes within the top 10 nm or so occurs when sliding on amorphous, PVD coated MoS_2. We hypothesize and later demonstrate that this reorientation process directly affects the initial friction evolution of MoS_2 and can be abated when using coatings developed specifically to increase the degree of preferential basal orientation.

There is also evidence suggesting water interrupts the formation of large, continuous MoS_2 crystallites, resulting in high friction and increased ejection of platelets leading to higher wear. This does not, however, poison the ability of coatings with existing long-range order to provide low friction. This runs counter to the commonly held notion that the intercalation of water increases friction between MoS_2 lamellae.

In addition to basal orientation, it is hypothesized that crystallites produced during the spray process will be relatively large in comparison to nanocrystalline (PVD Sputtered) MoS_2. This is similar to the large, continuous crystallites produced by burnished or slid upon MoS_2. As such it is not unreasonable to think that the surface has a relatively high ratio of passivated basal surfaces to the more reactive edge-sites. With minimal edge exposure, these surfaces should be less defect dense and therefore less susceptible to infiltration and reactivity with environmental contaminants such as oxygen. Less oxidation

on the surface and throughout the depth of the coating should also be reflected in the tribological response of MoS_2 coatings, likely with lower friction and less erratic behavior at the onset of sliding.

It is also hypothesized that the orientation or rotation of each basal plane relative to one another can affect friction. This concept of mis-orientation between atomic planes or commensurability is a well-known phenomenon attributing to super-lubricity in systems such as graphene and mica surfaces [91], [92]. With atomic planes, such as the crystallites of MoS_2 in perfect registry with one another, the energy barrier to sliding should be greater than in a higher energy system with surfaces already out of registry. Furthermore, this energy barrier related to the commensurability of a flake or crystallite of MoS_2 should be affected by temperature and able to be related to temperature dependencies at the macro scale. Altogether, it is hypothesized that the fundamental shear strength of MoS_2 is a function of commensurability, defect density, temperature and orientation.

Overall, it is hypothesized that a detailed characterization of the microstructural components of these coatings can reveal much about the fundamental mechanisms of friction and environmental sensitivities in MoS_2.

4. Methods & Materials

There is no one technique that can accurately describe the behavior of a coating or tribological material system. A combination of methods is used to characterize the friction and wear of various material systems to learn more about the underlying mechanisms that dictate friction and wear. Ideally these techniques are coupled with other chemical, structural and spectroscopic characterization techniques to assess internal and external film interactions at a range of length scales. The aim of this chapter is to provide the reader with a basic understanding of the techniques used and enough knowledge to process results in both tribological testing and chemical or crystallographic characterization techniques. Individual chapters to follow will build upon basics established here and further discuss intricacies of data presented in the context of the material system and purpose of the experiments.

4.1 Tribotesting

4.1.1 Friction Measurements

The ability to properly measure a friction coefficient in many different geometries and contact conditions is central to the arsenal of a tribologist. The most typically used contact geometry for macroscale experiments is that of a ball on a flat surface. The radius of the ball is usually below an inch in diameter (1/8" standard in most experiments in this dissertation), but can be changed to accommodate different contact pressures at fixed loads. For such large contacts, we define the friction coefficient (μ), as set by da Vinci and Amonton, as the ratio of the measured resistance to motion (lateral or friction force, F_f) to the applied normal load (F_N).

Equation 4-1

$$\mu = \frac{F_f}{F_N}$$

Friction coefficients typically range from $\mu \approx 0.2 – 1.0$ in many standard applications with typical materials [93], and hover around $\mu \approx 0.2$ - 0.3 for most tribological materials with $\mu \approx 0.3$ believed by Amonton to be a universal constant [4]. A handful of materials have also been shown to reach as low as $\mu = 0.01$ - 0.001, into a regime designated super-lubricious.

4.1.2 Methods for Applying & Measuring Forces

There are many ways to apply a load in testing. For certain tests that require large loads, pneumatic cylinders can be utilized to apply loads typically greater than 25N and in the current capacity at the Lehigh Tribology Laboratory, upwards of 1500N. With such high loads in normal and friction directions, high capacity six-axis load cells comprised of internal strain gauges are used to measure forces.

At lower loads in the range of 1N – 25N and depending on how the testing equipment is developed, dead weight loads are applied. In this case a well calibrated mass is loaded on the normal force applicator the sample is attached to. Load cells like those mentioned above can still be employed to measure forces near the sample interface.

Even lower loads of 10 – 1000 mN are in the range of interest for coatings in this dissertation and present several options to apply and measure loads. The technique involves a rectilinear dual cantilever assembly with finely calibrated stiffness, and the ability to carefully measure their deflection in the normal and lateral direction. This is the predominant technique used in this dissertation and outlined in the section below [94].

4.1.3 Dual Flexure Capacitance Probe Microtribometer

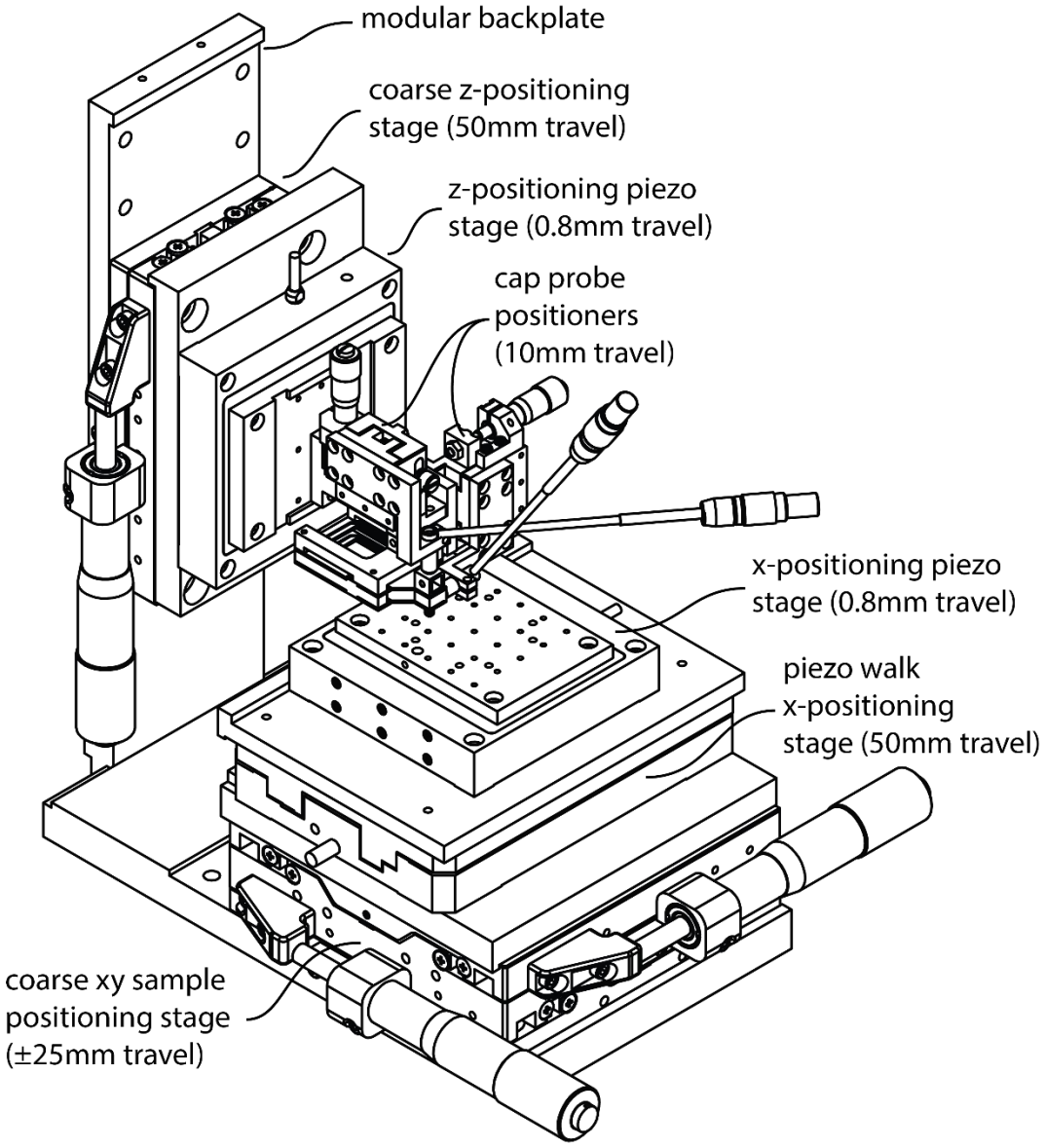

Fig. 4-1. Annotated schematic of microtribometer components

A custom-built microtribometer (Figure 4-1) was constructed to carry out friction measurements. The lower half of the instrument is responsible for holding the sample (typically steel coated MoS_2), manually re-positioning in x & y (±25mm) the sample to allow testing in new areas and reciprocating the sample during testing with a piezoelectric flexure stage of 800µm travel. While typically run at 1mm/s, the piezoelectric x stage is

capable of speeds ranging 0.1 – 100 mm/s with applications in fretting wear at higher speeds. These piezoelectric stages (both reciprocating and loading) are operated in closed-loop with a 1.8 nm resolution and repeatability of ±10 nm.

The upper portion of the tribometer held by the back plate is responsible for bringing

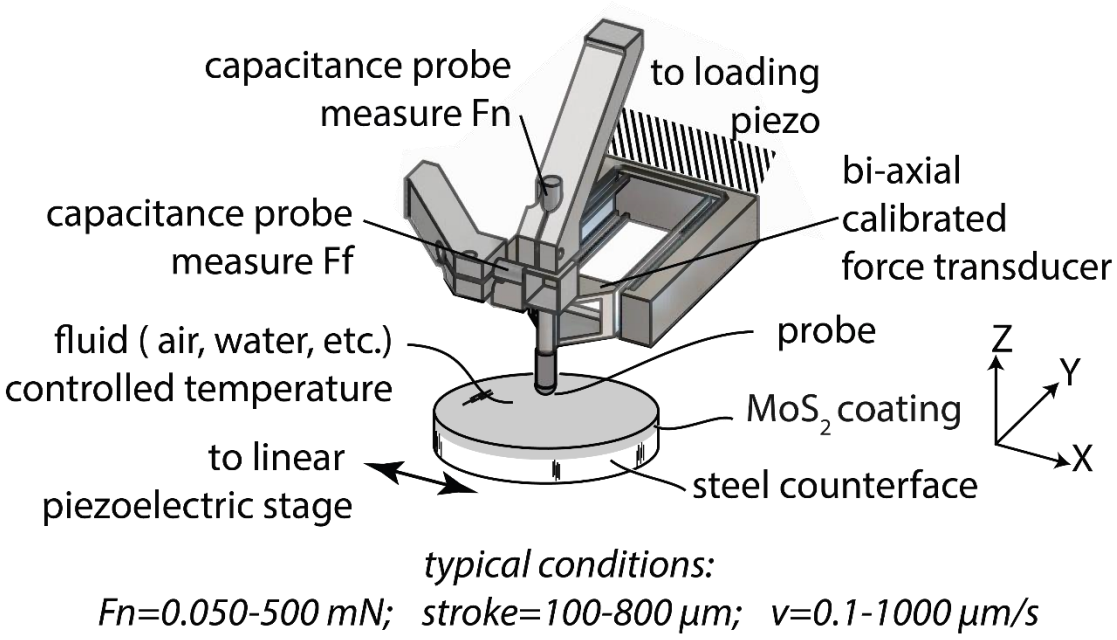

Fig. 4-2. Annotated schematic of cantilever assembly components & typical operating conditions

the cantilever assembly into proximity to the countersample. The cantilever assembly (Figure 4-2) holds the sample pin at the head of the flexure and utilizes a piezoelectric stage to bring the sample into contact with the countersample and apply a load.

Capacitance probes are positioned normal and tangential to flat, metallic portions of the cantilever head. The probes and flat metallic portions of the cantilever head operate like parallel plate capacitors, such that a change in distance between them and the cantilever head provide a change in voltage which can be calibrated as a distance. The cantilever is also calibrated by hanging masses off the head in either direction to calculate its

characteristic stiffness (N/m) in normal and tangential directions. Together, the capacitance probes and cantilever flexures give normal and tangential (friction) forces during sliding. To correct for any slope of the cantilever head during deflection, two double-leaf cantilevers and mounted in parallel so that motion of the flexures is constrained to rectilinear displacements. Without rectilinear motion of the head, proper displacements calculated assuming parallel plates would no longer hold and provide incorrect measurements [94], [95].

Cantilevers are first designed parametrically in excel and then tested in SolidWorks Simulation to get an estimate of the stiffness in normal and lateral directions. Two dimensional drawings of the cantilevers are sent to Micro Waterjet LLC where an Abrasive Waterjet Micro Machining (AWJMM®) procedure is used to cut cantilevers out of alloy Ti-6Al-4V. This customization enables a large range of attainable applied loads (50 μN – 2 N) and theoretical friction coefficients.

All load and position control and acquisition of the tribometer was done in LabView 2013 interfaced with a 16-bit analog-to-digital National Instruments Data Acquisition (NI-DAQ) device. All channels are typically sampled at 200 samples per second.

4.1.3.1 Linear Reciprocating Experiments, Friction Loops & Uncertainty

One of the challenges in accurately obtaining friction coefficients, apart from signal noise and inherent uncertainties in certain measurement techniques, is the misalignment present in the assembled microtribometer. In order to reduce misalignments, great care is taken to include alignment features such as ledges in all machined components. Even taking these precautions to provide accurately machined and aligned components, misalignments can still be present. If running a sliding experiment in a single direction, or

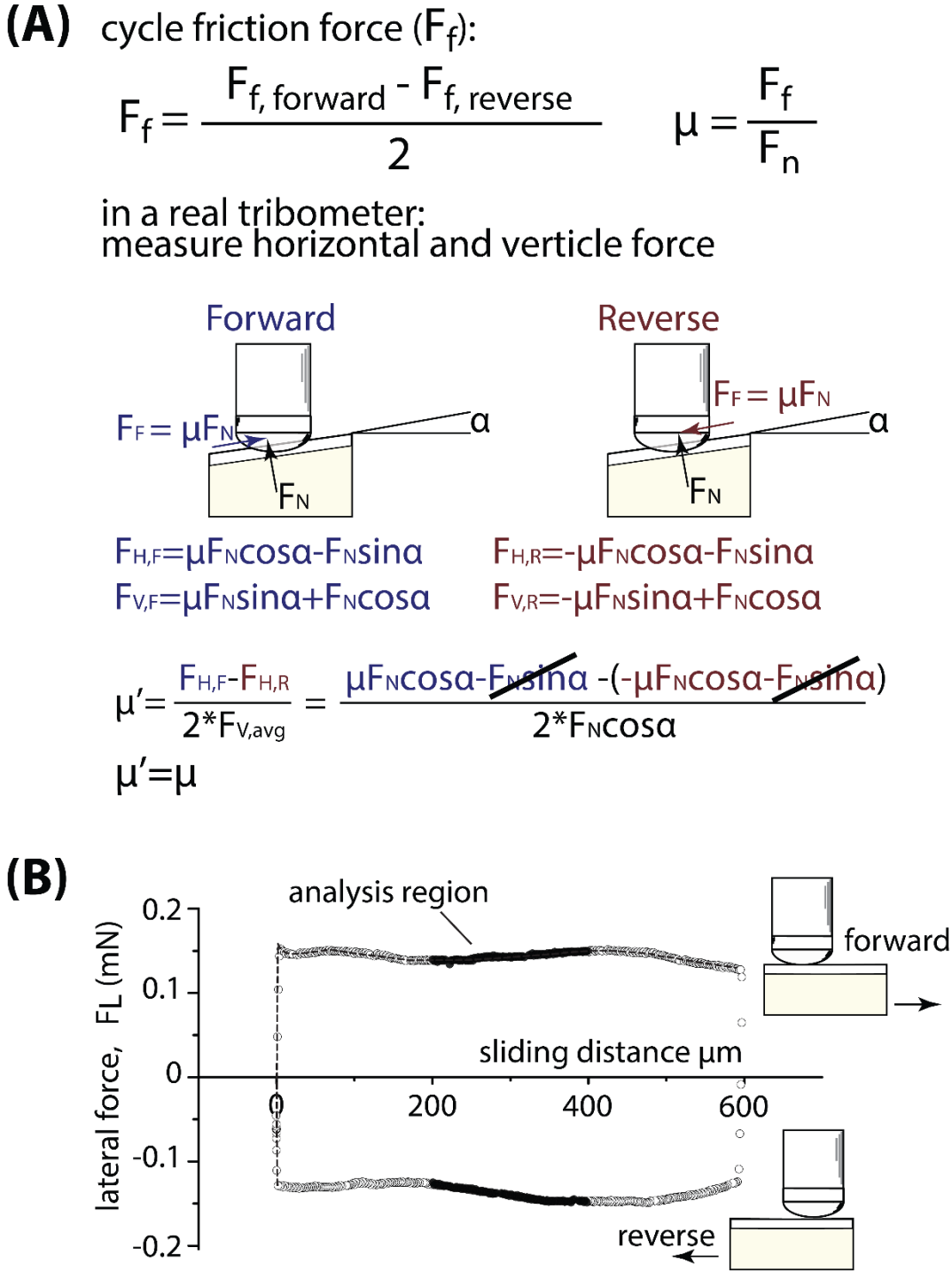

Fig. 4-3. Idealized reciprocating experiment showing possible sources of error.

uni-directional, you would have to account for the tilt of the surface and also determine the zero-load offset which can also be obscured due to tilt. The solution to this, proposed by

Burris and Sawyer [96], is to run reciprocating experiments that average the forward (positive) and reverse (negative) friction forces (Figure 4-3 A) and allow for them to be corrected by an offset fit through the middle of what is known as this friction loop (Figure 4-3 B). Typically, the coefficient of friction is calculated at every point along the track and then averaged over the middle 50% of the track for forward and reverse sliding directions. The absolute difference is taken between forward and reverse directions then divided by two to provide the cycle average friction coefficient. Uncertainty analysis can also be carried out on the functional form:

Equation 4-2

$$\mu = \frac{\overline{F}_{L,fwd} - \overline{F}_{L,bwd}}{2\overline{F}_N}$$

Using partial derivatives to assess uncertainty propagation provides the following functional forms:

Equation 4-3

$$u(\mu)^2 = \left(2\left(\frac{1}{2F_N}\right)^2 + \left(\frac{F_L}{F_N{}^2}\right)^2\right)u(F)^2$$

Equation 4-4

$$u(\mu) = \frac{u(F)}{F_N}\sqrt{\frac{1}{2} + \mu^2}$$

As such, uncertainty in friction coefficient depends on friction coefficient measured, normal load and uncertainty in measuring load. In our lab there are many difference equipment configurations, applied loads and expected friction coefficients which can all lead to different uncertainties in friction. For example, in typical use case for studies shown in this dissertation at 100 mN normal load, μ=0.1 and $u(F) \approx 1$ mN, one could expect negligible uncertainties in force measurements close to $u(\mu) \approx 0.002$.

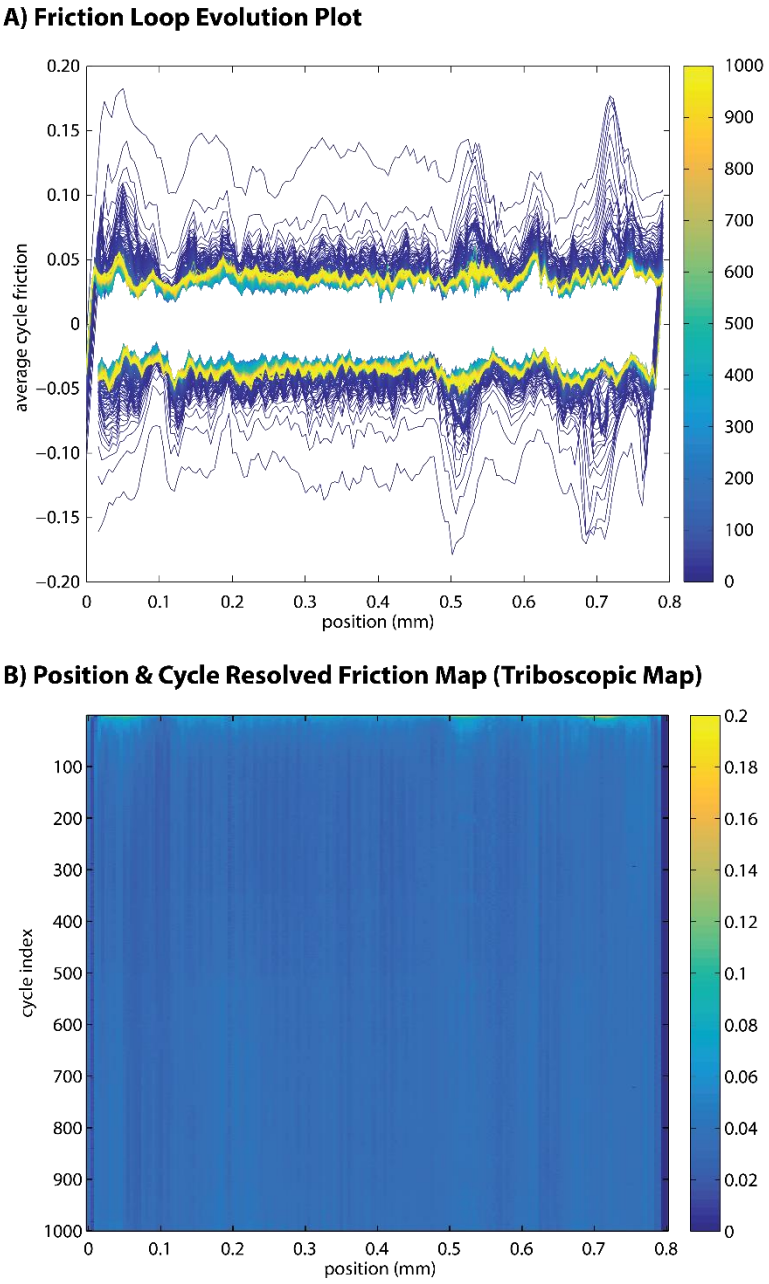

Fig. 4-4. Example friction data from *MoS2* experiment showing (A) friction loop evolution over cycles and (B) a triboscopic map of position and cycle resolved friction coefficients. Both plots provide a way to visualize the evolution of friction behavior for a test.

Recording position resolved friction coefficient in these friction loops also allows for a time and position resolved visualization of the evolution of friction coefficient (Figure 4-

4). This can be an important tool when assessing the friction behavior of a material over the course of thousands of cycles of sliding.

4.1.3.2 Spiral Orbit Experiments

Spiral orbit tribological tests are a form of uni-directional testing that allows the formation of a tightly packed spiral with equal spacing in between (Figure 4-5). To accomplish this on a microtribometer, the cantilever assembly must be attached to a linear stage that retracts as it traces out a spiral on the rotating stage below where the countersample lays. It is a difficult test to run as the retraction speed and angular speed must be matched to provide a constant circumferential speed.

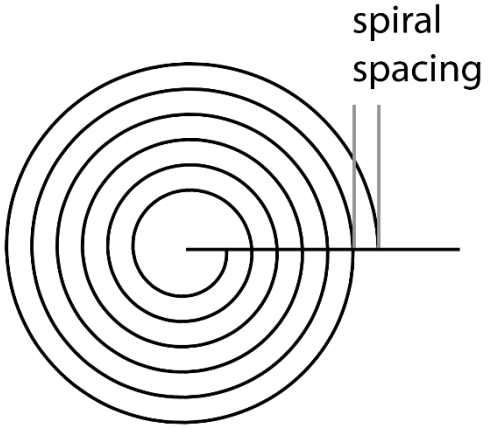

Fig. 4-5. Shape and spacing of an Archimedean spiral used in spiral orbit testing.

With a spiral orbit test, you are able to make tightly packed wear scars that can easily be used in characterization techniques with large sampling or spot sizes, such as x-ray diffraction (XRD). It also allows for sliding upon continuously new material but for very long sliding distances which is not available in reciprocating or uni-directional testing such as pin on disk. The challenge with spiral orbit testing is that maintaining a constant load over a wide range of the sample becomes difficult due to any tilt present. The further your radius becomes, the larger the difference between force can become. To account for this samples must be as flat as possible and likely supported with some form of active load metering to maintain a set load.

4.1.4 High Temperature Tribometer

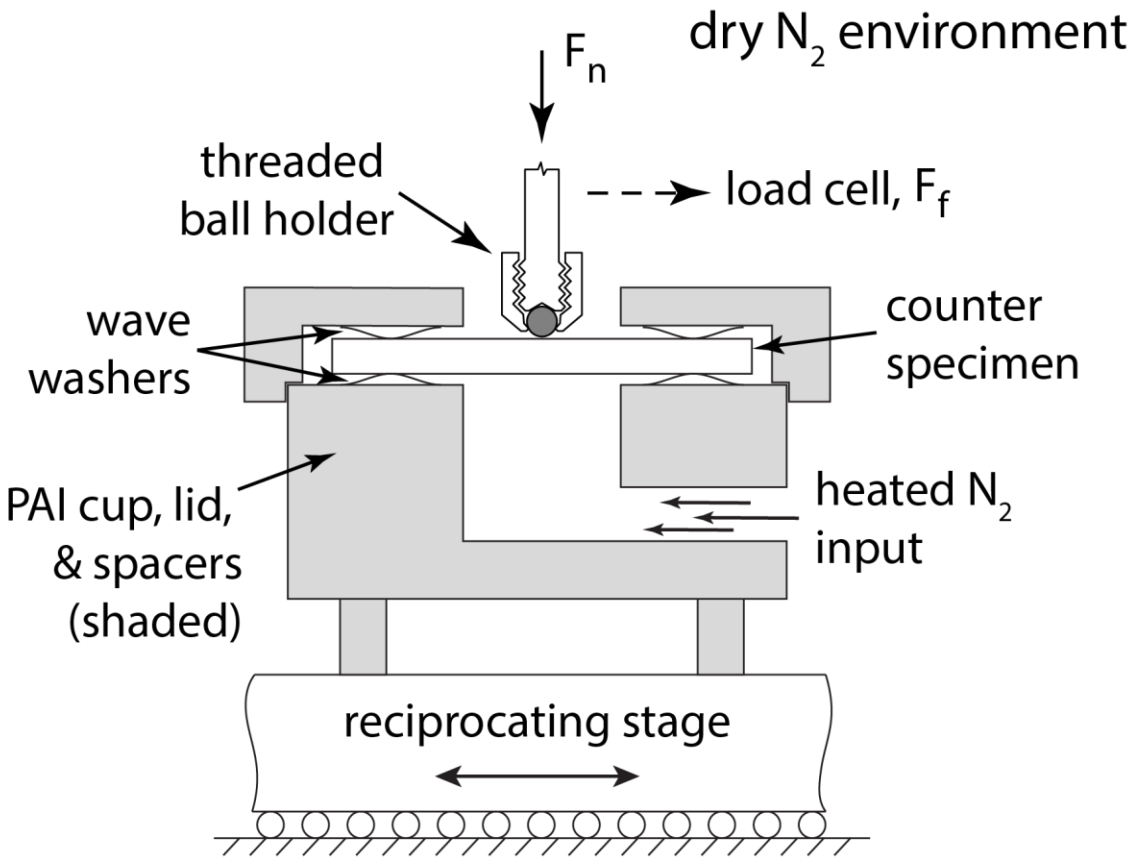

Fig. 4-6. Annotated schematic of flow cell used in high temperature tribometer.

A cam driven, dead weight load tribometer was utilized for high temperature studies. This was achievable due to the construction of a flow cell by collaborators at Sandia National Labs (Figure 4-6). The inert gas flow cell was used to help limit the amount of water molecules that could impinge upon the surface during testing. Liquid nitrogen was supplied to a dual stage heating tube assembly that enabled high (250°C) and low (-150°C) temperature gas to enter the flow cell and precisely control the temperature of the sample during testing.

4.2 Spectroscopic & Analytical Characterization Techniques

4.2.1 High-Sensitivity, Low-Energy Ion Scattering (HS-LEIS) Spectroscopy

The laws of conservation of energy and momentum directly govern the principle techniques of ion scattering spectroscopies and subsequently HS-LEIS. Elastic collisions between incident ions and the surface within the angle of detection (generally 145°) enter

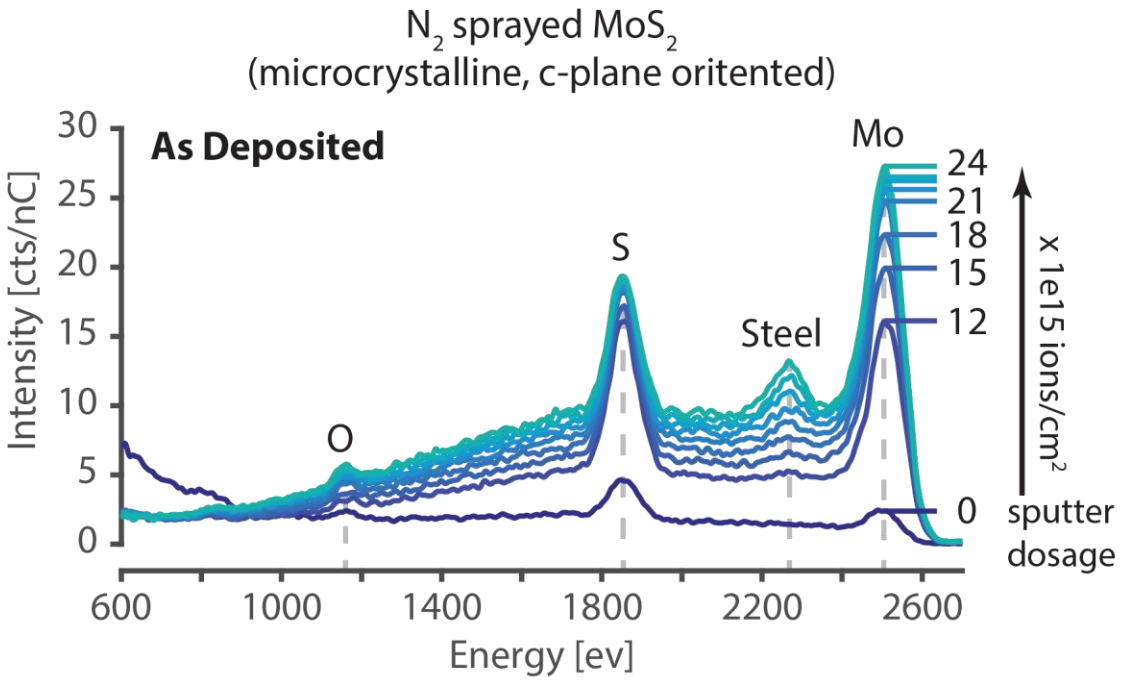

Fig. 4-7. Example LEIS spectra with each peak representing the energy level detected after the incident ion scatters off of a given target atom. In this plot, peak energies correspond to: Mo (centered ~2500 eV), S (1820 eV), O (~1150 eV), Fe (~2300 eV) and C and/or H (background contamination ~ 600-1000 eV shoulder)

an electrostatic analyzer to be detected. The scattered low energy He^+ ion energy increases with the atomic mass of the incident atom; peaks in energy (x-axis) correspond to specific elements (higher energies = higher mass elements). For this study, the relevant peaks and their energy are: Mo (centered ~2500 eV), S (1820 eV), O (~1150 eV), Fe (~2300 eV) and C and/or H (background contamination ~ 600-1000 eV shoulder) (Figure 4-7) [97]. As intensity (cts/nC) increases in the LEIS spectra for a given peak, so does the fractional coverage of that element on the surface. Broad shoulder-like features observed in the HS-

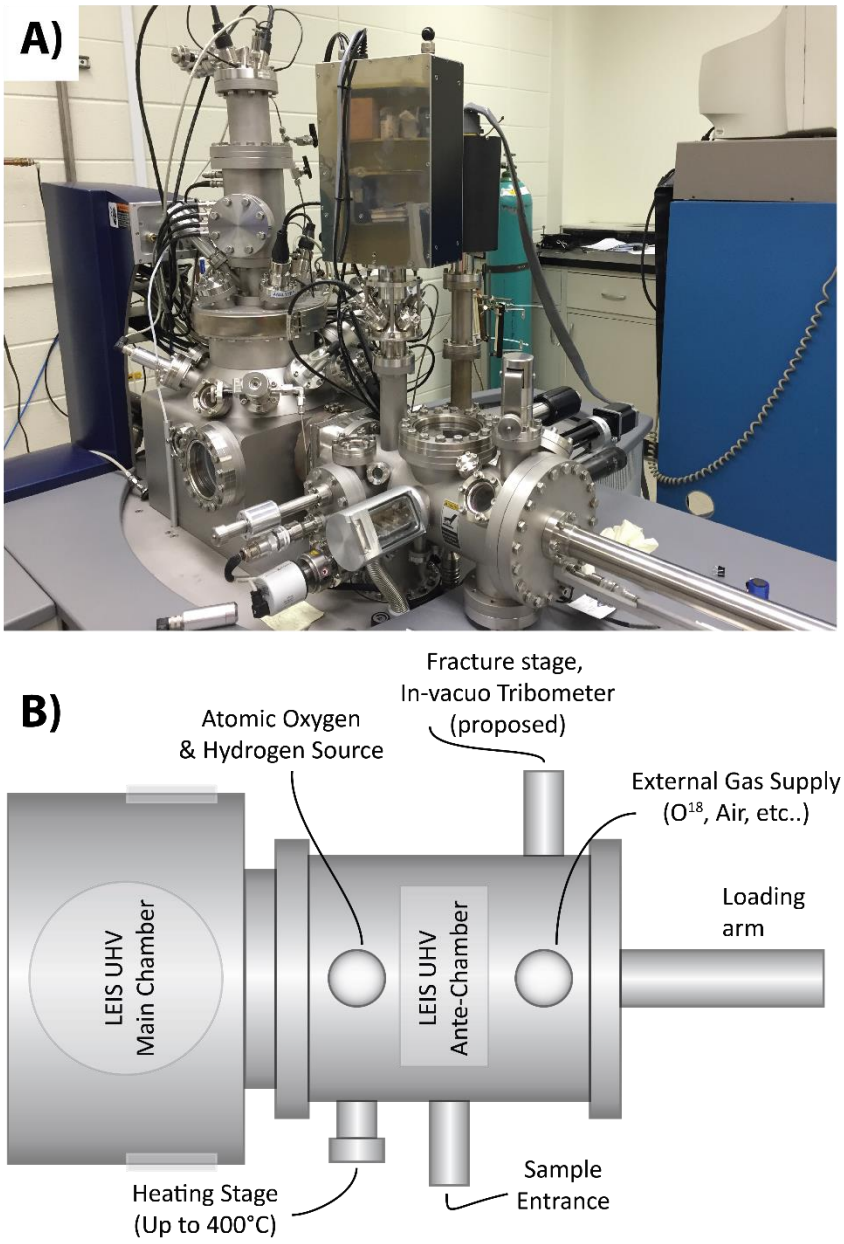

Fig. 4-8. (A) Photo of HS-LEIS and (B) Schematic of antechamber capabilities

LEIS spectra can be interpreted as a reionization event of the low energy ion off atoms directly below the surface. The length of a shoulder relative to an unobscured surface atom of the same mass is directly proportional to the approximate depth of that element below the surface, with every 150 eV of separation from the primary peak corresponding to ~1

nm of depth [98]. The instrument is also equipped with an ion sputter gun to enable destructive depth profiling as well as an antechamber with an external gas entry, heating stage and atomic oxygen source (Figure 4-8).

In order to calculate the relative amounts of each element present on the surface, surface sensitivity factors were obtained. Sulfur, molybdenum and oxygen factors were obtained via spectra taken on pure sulfur powder, pure molybdenum metal and molybdenum trioxide (MoO_3) powder samples respectively. Atomic density (**atoms/cm^2**) is approximated by the product of mass density (**ρ**), atomic diameter (**r**) and Avogadro's number ($\mathbf{N_A}$) over the molecular weight (**M**). As perfect crystal specimens were not tested, atomic diameter is chosen over crystal spacing for calculations. The product of atomic density and the ratio of raster area (**A**) to integrated peak area for the standard sample ($\mathbf{I_p}$) gives a sensitivity in terms of atoms per intensity (**nC*atoms/cts**) (Table 4-1). This sensitivity factor then converts intensity signals from LEIS spectra to counts of atoms that can be compared (Equation 6-1).

Equation 4-5

$$S = \frac{MI_P}{2\rho r A N_A}$$

Table 4-1. Calculated sensitivity factors for each elemental constituent and values used to calculate them. Oxygen density is calculated as part of MoO_3 oxide. Sensitivity for oxygen is determined from the ratio of Mo & O signals in the MoO_3 sample and from the Mo sensitivity.

Element	ρ (g/cm^3)	M (g/mol)	r (nm)	I_p (cts/nC)	S (atoms·nC/cts)
S	1.819	32.065	0.36	610	4.54×10^{11}
Mo	9.330	95.940	0.42	10,200	5.43×10^{10}
O	3.143	15.990	0.31	-	3.38×10^{11}

4.2.2 X-Ray Diffraction (XRD)

X-Ray Diffraction, specifically powder X-Ray diffraction is a technique that can be applied to thin films grown on substrates (such as sprayed or PVD MoS_2) which allows for the determination of crystalline phases present in a given sample. The technique relies on constructive interference of X-rays at a single wavelength in a crystalline sample. X-rays are produced by an x-ray tube containing a metal such as Cu, Mo or Co focused onto the surface after first passing through a set of filters and collimators. X-ray interaction with the sample produces constructive interference if a crystalline phase is present, satisfying Braggs Law ($\lambda=2d\sin\theta$). From this the diffraction angle of the detected crystallographic plane can be calculated as well as the lattice spacing for all crystalline phases detected during the 2θ detector sweep. The specific reflection geometry used for these powder diffraction studies is Bragg-Brentano with various filters and collimators to best focus the beam onto the sample [99].

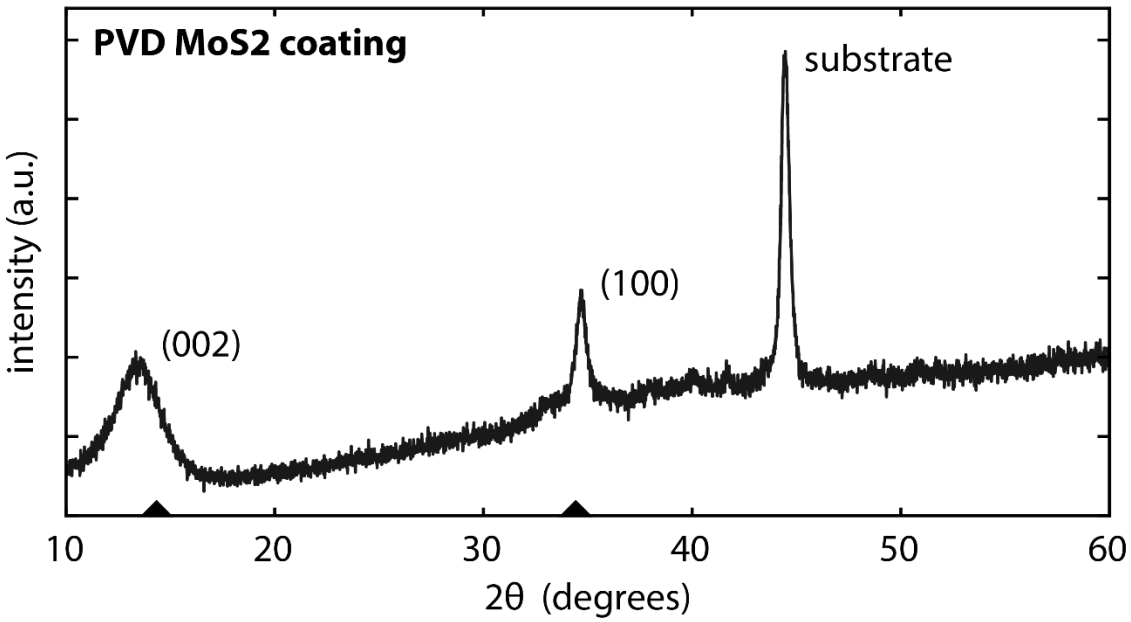

Fig. 4-9. Example diffraction pattern for a PVD *MoS_2* coating. Triangles at the bottom denote values of peak positions from literature [121].

Figure 4-9 shows an example spectra of a PVD MoS_2 coating. Two of the peaks are indicative of crystalline phases important to MoS_2 lubrication, with the (002) peak at ~ 14° indicating surface parallel basal crystal planes and the (100) peak at ~ 34° indicative of surface normal basal crystal planes. The peak close to 43° is a signal from the underlying steel substrate.

Table 4-2 shows a list of the diffraction angles for all the crystalline phases detectable over a 2θ sweep from 14 – 90 degrees, as well as the relevant miller indices and atomic spacing [100].

Table 4-2 Peak list for Molybdenite powder (reference code 96-900-7662) [100]

No.	h	k	l	d [Å]	2θ [°]	I [%]
1	0	0	3	6.12333	14.454	100.0
2	0	0	6	3.06167	29.144	1.4
3	1	0	1	2.70928	33.036	28.1
4	1	0	-2	2.62499	34.129	25.9
5	1	0	4	2.35254	38.226	34.5
6	1	0	-5	2.19605	41.068	37.2
7	0	0	9	2.04111	44.344	4.5
8	1	0	7	1.89499	47.969	23.8
9	1	0	-8	1.75974	51.919	14.3
10	1	1	0	1.58150	58.296	18.2
11	1	1	3	1.53125	60.404	12.1
12	0	0	12	1.53083	60.422	5.2
13	1	0	10	1.52568	60.648	4.5
14	1	0	-11	1.42590	65.397	3.3
15	1	1	6	1.40511	66.489	0.9
16	2	0	-1	1.36583	68.663	2.9
17	2	0	2	1.35464	69.310	2.9
18	2	0	-4	1.31250	71.874	4.7
19	2	0	5	1.28335	73.772	5.8
20	1	0	13	1.25582	75.669	2.1
21	1	1	9	1.25015	76.073	4.9
22	0	0	15	1.22467	77.951	1.0
23	2	0	-7	1.21420	78.752	5.0
24	1	0	-14	1.18338	81.224	1.7
25	2	0	8	1.17627	81.819	3.5
26	1	1	12	1.09994	88.904	10.5
27	2	0	-10	1.09802	89.100	1.5

4.2.3 X-Ray Photoelectron Spectroscopy (XPS)

A common use of XPS is to acquire the oxidation states and hybridization states of a material to understand what kind of bonds exist on the surface. XPS is a relatively surface sensitive technique with analysis depths upwards of 1-10 nm. X-ray photoelectron spectroscopy uses monochromatic x-rays to investigate the surface of a material as XRD does, but instead detects the photoemission of electrons from orbitals in the atoms of a material. The incident x-ray or photon has a kinetic energy (*hv)* based on the wavelength used and gets absorbed into an atom, leading to excitation. Energy is conserved in photon absorption such that an electron is emitted (if it does not scatter back into the material) with kinetic energy (KE) equal to the difference in photon energy and binding energy (BE) of the electron (KE = hv-BE).

4.3 Sample Preparation & Storage Procedures

4.3.1 N_2 Spray Deposition Procedure

Steel coupons were first cleaned in an ultrasonic bath water solution of Dirl-Lum 603, 26 to 34 g/L, at 60 to 70°C at 40 kHz (35-45 kHz) for 5 minutes and then rinsed in ultrasonically activated water for 15 seconds. Coupons are then dried with dry nitrogen and baked at 100 to 110°C (212 to 230°F) for 1 hour. After baking the coupons out, the entire surface is spray coated with MoS_2 through a .018” circular nozzle 2 inches away from the surface at a gas supply pressure of 88 psi with a quarter of the flow being particles of MoS_2 (Figure 4-10). Any excess powder is removed with a lower supply pressure than that of deposition. A post cleaning process involves an ultrasonic cleanse in IPA at 20 kHz for 20 seconds and then blown down again with dry nitrogen. The compressed nitrogen source

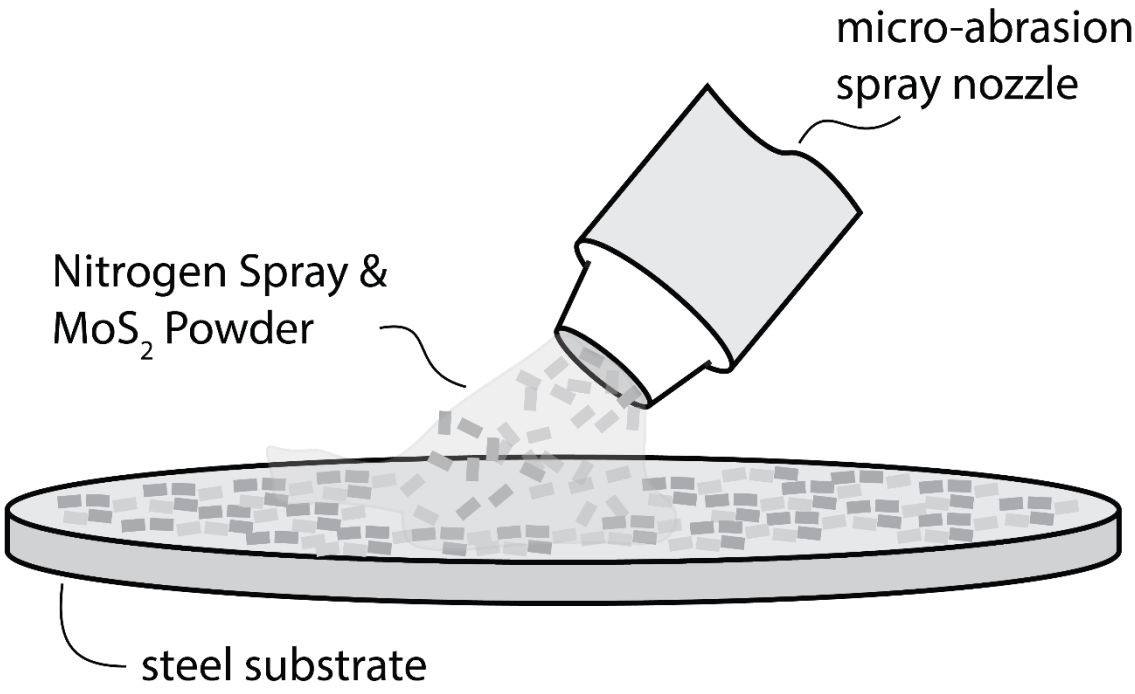

Fig. 4-10. Schematic of N_2 spray deposition process

should be fitted with a coalescing filter, and the spray tip must have a 0.01-micron absolute filter with the spray gun itself outfitted with a 0.2-micron absolute filter.

4.3.2 DC Magnetron Sputtering

A typical technique in which MoS_2 thin films are deposited involves magnetron sputtering, a physical vapor deposition technique. Essentially, target materials of Molybdenum and Sulfur are biased relative to the intended deposition substrate such that the materials are vaporized and ejected at high energies (>10 eV) [101].

For our samples prepared by Tribologix Inc, the coating chamber is pumped down to a minimum of 5E-6 torr and the bare steel coupons are ion cleaned for 20 minutes. After ion cleaning the MoS_2 is deposited by DC magnetron sputtering via argon gas bombardment. A bias voltage is maintained on the parts between -30V and -60V depending on the surface area being coated.

5. Investigating Roles of Structure: Highly Ordered MoS_2 Films

5.1 Overview of N_2 Sprayed Film Performance & Characterization

Molybdenum disulfide (MoS_2) coatings were deposited by nitrogen (N_2) spray deposition, a method capable of impinging MoS_2 particulates onto a substrate in an effort to yield preferential basal orientation. 100-to-300-nm-thick adherent and highly oriented coatings were produced by this method. Sprayed coatings exhibited lower initial friction coefficients during run-in than the more amorphous sputtered films regardless of environment (dry and humid). It is thought that the high degree of basal plane orientation throughout the thickness of the film (confirmed via XRD) owes to such reductions in initial friction. In humid air, initial friction for sprayed coatings ($\mu = 0.10$) was just under half the friction coefficient of sputtered coatings ($\mu = 0.21$), highlighting the ability of basally oriented surface films to produce low shear strength interfaces. When aged in humid nitrogen, sprayed coatings resisted poisoning of their structure which could have degraded tribological performance. These findings also support previous publications purporting that water vapor does not appreciably contribute to oxidation of MoS_2.

5.2 Motivation

Molybdenum disulfide has been and continues to be heavily researched over the past century as a phenomenal solid lubricant widely used in space applications due to its lubricating properties in dry and inert environments. The sulfur-terminated basal planes of MoS_2 are separated by weak van der Waals forces which are thought to provide low friction via easy shear between lamellae [24], [46], [59]. For the past 60-70 years, MoS_2 coatings have been made with a wide variety of deposition methods and different compositing materials to improve densification and reliability to perform in many different

environments and operating conditions [102]. Prior to more modern deposition techniques, MoS_2 was burnished onto surfaces by rubbing MoS_2 powder onto surfaces and kept adherent by various binding agents or resins [39], [44], [72], [74], [103]. The burnishing process was relatively simple and inexpensive, yet thicknesses were difficult to control and in some environments such as the vacuum of space binding agents could outgas and damage the coating or nearby components [103], [104]. Coating components with MoS_2 via RF magnetron sputtering gained widespread use in the late 1960s. This physical vapor deposition (PVD) technique enabled a finer control of coating thickness as compared to burnished coatings and high incident energies of MoS_2 onto substrates (10 eV) aided in the coating adhesion [79].

PVD methods such as radio frequency (RF) and direct current (DC) magnetron sputtering are the go to deposition technique for coating critical interfaces in aerospace mechanisms today. The morphology and crystallographic textures of these films can vary greatly due to the wide range of deposition parameters available during deposition [24], [48], [75]–[79]. As such, many commercially available magnetron-sputtered MoS_2 coatings are produced in either an amorphous state [25], [80] or mixed textures [80] in which a thin region of basally oriented MoS_2 ({001} texture with c-plane parallel to substrate) forms (~ 5-20 nm) at the coating substrate interface proceeded by a basal columns growing normal to the surface. This unfavorable growth of surface normal basal columns occurs because it is more energetically favorable during deposition when incident ions of MoS_2 bind to edge sites that have begun to grow upwards as compared to the relatively passive basal surface [76]. Many attempts to better understand and control the sputtering process to induce this basal orientation have been made [24], [48], [75]–[79] but

consistently producing thick, highly crystalline basally oriented films has proven to be difficult. Sputter deposition with many different metal dopants and additives has also been attempted to increase coating density and in turn improve oxidation resistance and other processes that may interfere with transfer film formation [60], [61], [105]. During the first few cycles of sliding, a transition occurs in which crystallites of MoS_2 on the surface of the wear track undergo shear-induced reorientation [24]. This initial friction behavior or run-in process orders the basal planes of these MoS_2 crystallites parallel to the substrate which allows for easy shear between lamellae. It has been shown that this reorientation typically occurs within the top 10 nm of the coating surface [25]. It is also thought that the run-in process is affected by the ability of a transfer film to form on the mating surface and the presence of contaminants [106]. Minor increases in friction during the start of sliding can be very detrimental when there is such a small amount of power available to motors and actuators in aerospace mechanisms [11], [102].

MoS_2 lubrication falters when applied in terrestrial environments [42], [43], [46]–[48], [54], [65], [107]–[110]. It has also been shown recently that water vapor does not alter coating composition due to oxidation. Khare et al. demonstrated this on sputter deposited MoS_2 in humid and oxygen containing environments [108]. They also suggested that the rate of formation and depth of a highly surface localized oxide layer would increase over time and be proportional to increasing temperature and O_2 concentration. Holinski & Gänsheimer put forth the hypothesis that the strong polarity of the sulfur-terminated MoS_2 basal planes was another factor in the absorption of water and high friction in MoS_2 run in humid environments [46]. Absorption isotherms of water into/onto the surface of MoS_2 have also been observed [24], [42], [74]. As such, the combined effect of water and oxygen

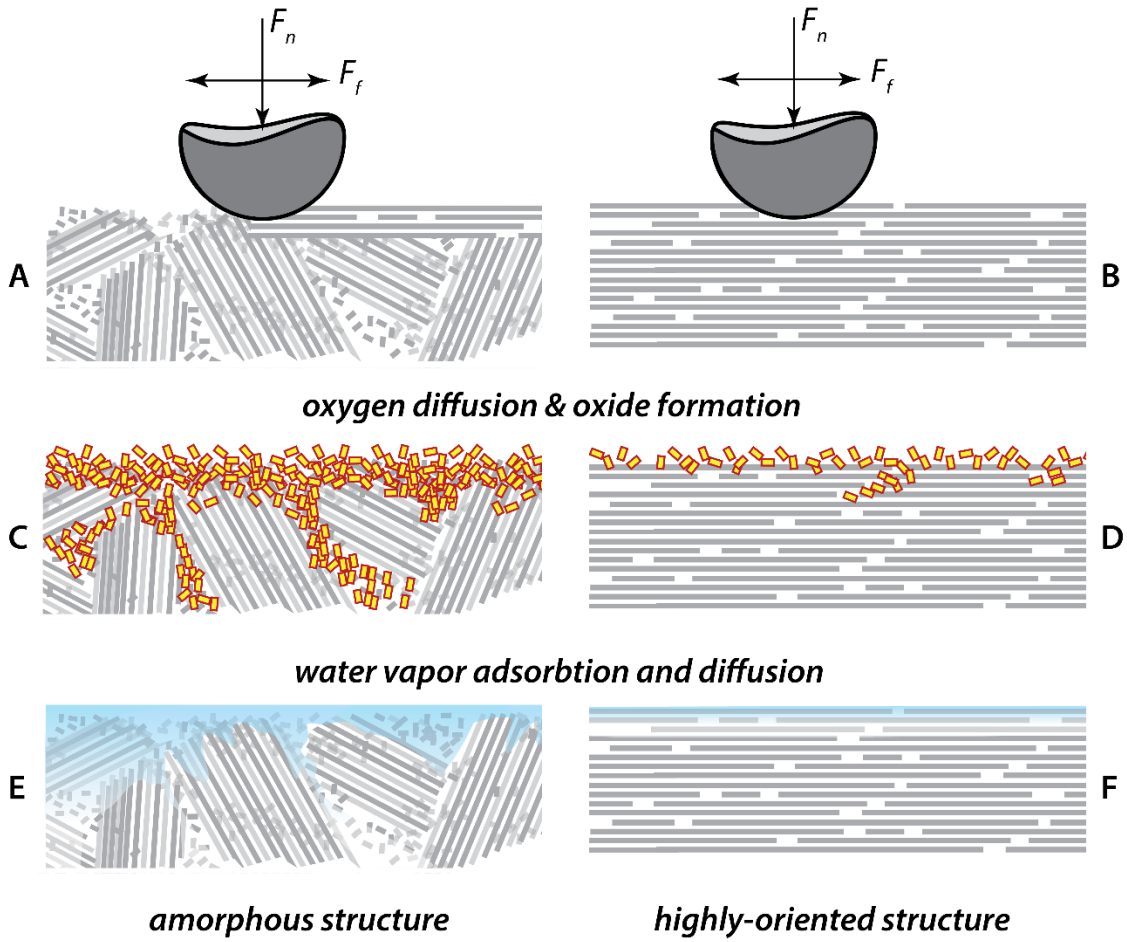

Fig. 5-1. Hypothesized mechanisms for sprayed film microstructure. Higher surface parallel basal orientation should help mitigate shear induced re-orientation and reduce intrusion of environmental contaminants

present on or throughout the surface of MoS_2 coatings presents challenges that can occur during sliding and after storage in humid or oxygen containing environments [24].

5.3 Hypothesis

Utilizing deposition methods that can deliberately reduce the density of edge sites present on the surface and induce preferential orientation of lamellae are hypothesized reduce the friction during run-in and mitigate effects of environmental contaminants [22], [57], [102]. Deposition processes control many structural aspects of coatings such as orientation, density, crystallite size and adhesion to the substrate. Further research efforts

into deposition processes must be driven with the intent to reduce effects of run-in and protect against degradation from environmental contaminants [66], [67], [69], [86], [102], [111]–[114]. A basally oriented film with minimal edge sites on the surface should help not only reduce initial friction but improve coating integrity during storage [22], [24], [56]–[59] (Figure 5-1). To obtain coatings with a higher degree of basal orientation, N_2 spray deposition was employed. To our knowledge, this is the first utilization of such an impingement technique to apply MoS_2 in the literature. Such impingement velocities helped to shear the MoS_2 powder in the nitrogen feed into the surface of the steel coupons and create a higher degree of basally oriented MoS_2 throughout the thickness of the film. The ability of these sprayed coatings to mitigate high initial friction during run-in is investigated via tribological testing in humid air and dry nitrogen. These results are accompanied by TEM, SEM and XRD analyses to view the structure, morphology and crystallographic orientation of the films. The effect of aging in high temperature humid nitrogen environments, effect of roughness and wear properties of these films are also investigated.

5.4 Materials & Procedures

Stainless steel coupons (13-8 PH and 17-4 PH) were coated with MoS_2 powder by N_2 spray deposition. Coupons with 20 nm and 200 nm average roughness (R_a) were coated and tested against grade 5 (~40nm R_a) 3.2-mm-diameter 440C stainless steel pins (counter samples) purchased from McMaster-Carr used in all experiments. To serve as a point of comparison, pure MoS_2 coatings were sputter deposited onto 440C substrates by Tribologix Inc. (Golden, CO) at a nominal thickness of 2 μm (per manufacturer specifications).

5.4.1 Friction & Wear Testing

The custom built linear reciprocating microtribometer [94], [96], [115], [116] as described in the §4.1.3 was used to assess the friction behavior of both N_2 sprayed and sputter deposited MoS_2 films. Experiments were carried out on both smooth and rough samples in dry nitrogen (<10 PPM O_2 and <10 PPM H_2O) and humid air (20 % RH). Reciprocating experiments were run for 1000 cycles each under the same contact conditions: 100 mN normal load (450 MPa Hertz contact pressure), 1 mm/s sliding speed, 0.8 mm stroke. Wear rates for the samples were difficult to quantify given the variability in coating thickness for N_2 sprayed coatings. The samples coated on rough substrates also exhibited asperities with heights on the same order as the thickness of sprayed films in some cases which made profilometric wear measurements infeasible. Due to this, coating life was compared based on the number of cycles til failure when a sharp transition to high friction ($\mu > 0.15$) was observed.

5.4.2 Coating Thickness, Coverage & Orientation

Scanning electron microscopy (SEM) and energy-dispersive spectroscopy (EDS) were used to assess the coverage of N_2 sprayed coatings on smooth and rough substrates. Thickness and morphology were investigated via cross-sectional views of the coating prepared by a dual-beam scanning electron microscope-focused ion beam (SEM-FIB, FEI Helios). The thin, electron transparent wafer produced from this process was then imaged on a transmission electron microscope (TEM) in a TEM/scanning-TEM (STEM, FEI Tecnai F30-ST) with a field-emission source operated at 300 kV. STEM mode was employed with a high-angle annular dark-field detector that gave primarily Z-contrast in images. To study the crystallographic orientations of the sprayed and sputtered films, X-

ray diffraction (XRD, Panalytical Empyrean) was used. X-ray diffraction analysis was done with a Cu Kα radiation source and symmetric scan with a Pixcel 3D detector in scanning line (1D) mode and Bragg-Brentano HD incident beam optic.

5.4.3 Aging of MoS_2

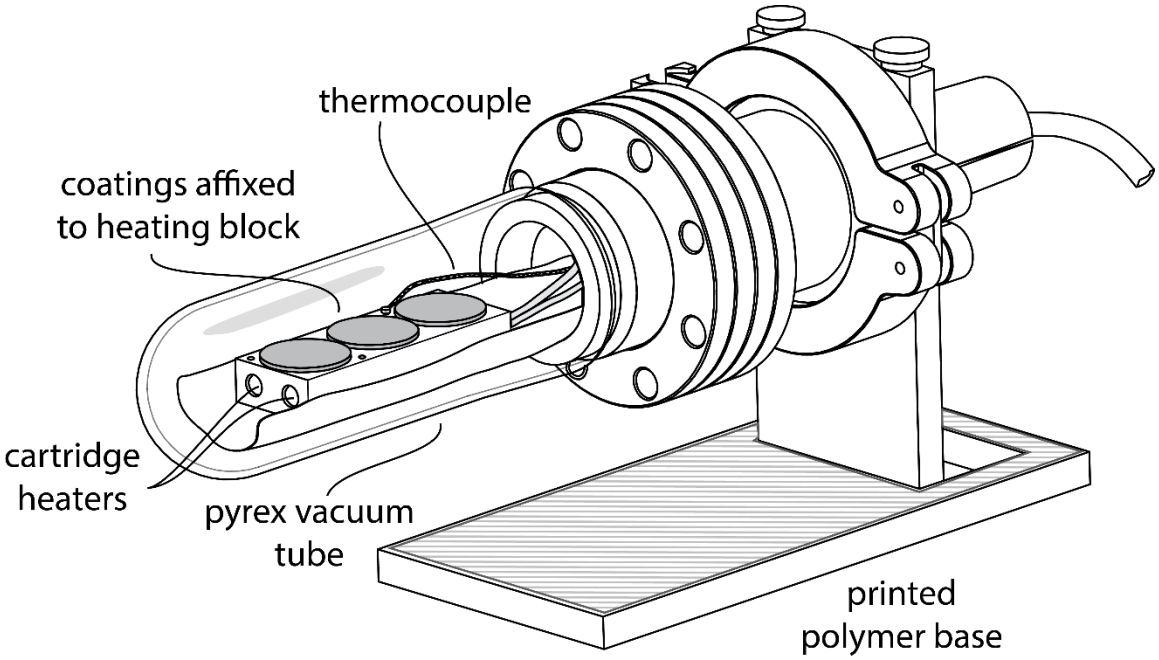

Fig. 5-2. Annotated photograph of vacuum flange aging vessel

High temperature aging experiments carried out in humid nitrogen on the sprayed samples was done in a custom-built tube furnace assembly. Components for the furnace were easily acquired, commercially available, off-the-shelf vacuum chamber components (Figure 5-2). A 50-mm-diameter, 125-mm-long glass-to-metal tube fitting was sealed with a blank flange consisting of Swagelok feedthroughs for gas flow and electrical connections that supplied a pair of cartridge heaters and thermocouples. During testing, coupons were affixed to the heater block and the chamber was flushed with nitrogen (<10 ppm O_2) at 50% relative humidity at room temperature (~ 1.1 kPa H_2O). The chamber was then sealed shut to preserve the humid nitrogen environment and heated to 150°C and kept at

temperature for 10 days, after which the chamber was cooled and coupons removed for friction testing in a dry nitrogen environment.

5.5 Results

5.5.1 Coating Thickness, Coverage & Orientation

The coverage of N_2 sprayed MoS_2 coatings differed between rough and smooth substrates as shown by SEM (Figure 5-3). By comparing the topological and elemental information from the SE and BSD detector, respectively, it appears as if the coverage is dictated by the roughness of the coating. Despite the similarity in coverage, the thickness of the coatings in a few representative locations were comparable between different roughness' (Figure 5-4) varying from 100 – 300 nm. As such, it may be that roughness only serves to limit the coverage of the MoS_2 sprayed coupons. The variation in thickness of the coatings as well as the partial coverage are some of the largest drawbacks of the N_2 spray deposition of MoS_2 and may limit applicability. Optimization of the spray technique may help in developing more uniform and thicker coatings.

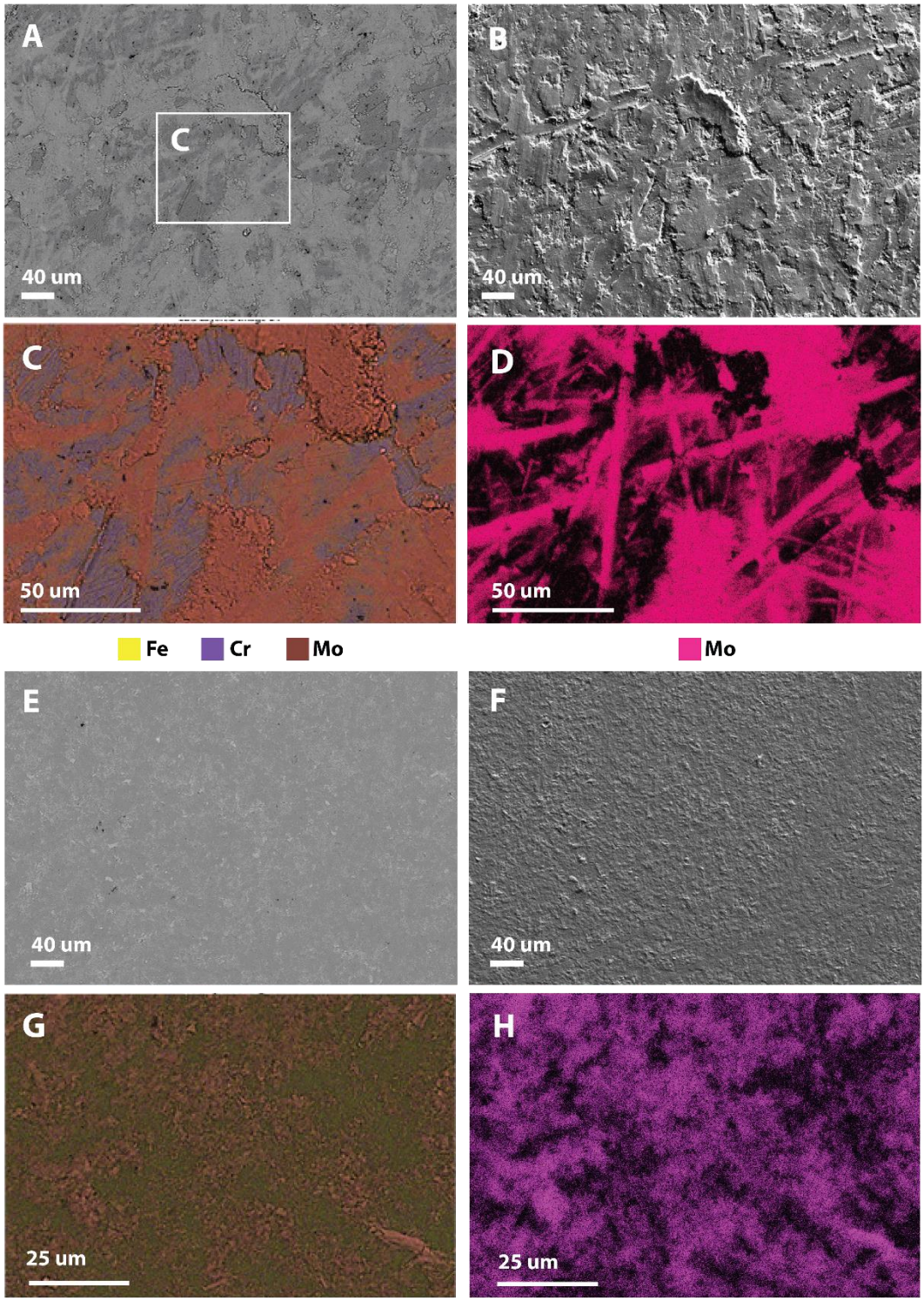

Fig. 5-3. SEM images of a N_2 sprayed MoS_2 sample with a rough (Ra ~ 200 nm) substrate. **(A,E)** Backscatter detector (BSD) images showing elemental contrast, **(B,F)** secondary electron (SE) detector showing topographical contrast, **(C,G)** energy dispersive spectroscopy (EDS) highlights primary species (Fe, S, Cr, O) and MoS_2, and **(D,H)** showing intensity maps of the EDS signal were Mo (pink/purple)

TEM cross sections reveal a highly ordered structure and morphology for N_2 sprayed coatings that persists throughout the thickness of the film, a trait that is not typically found in physical vapor deposited (e.g. sputtered) coatings. Large, continuous crystallites of MoS_2 in surface parallel basal orientation can be found in the cross-section from 200 nm to 1 μm in length and as thick as 50 nm. It appears as if a majority of the large and oriented crystallites are in proximity to the surface of the coating as show in the inset of Figure 5-

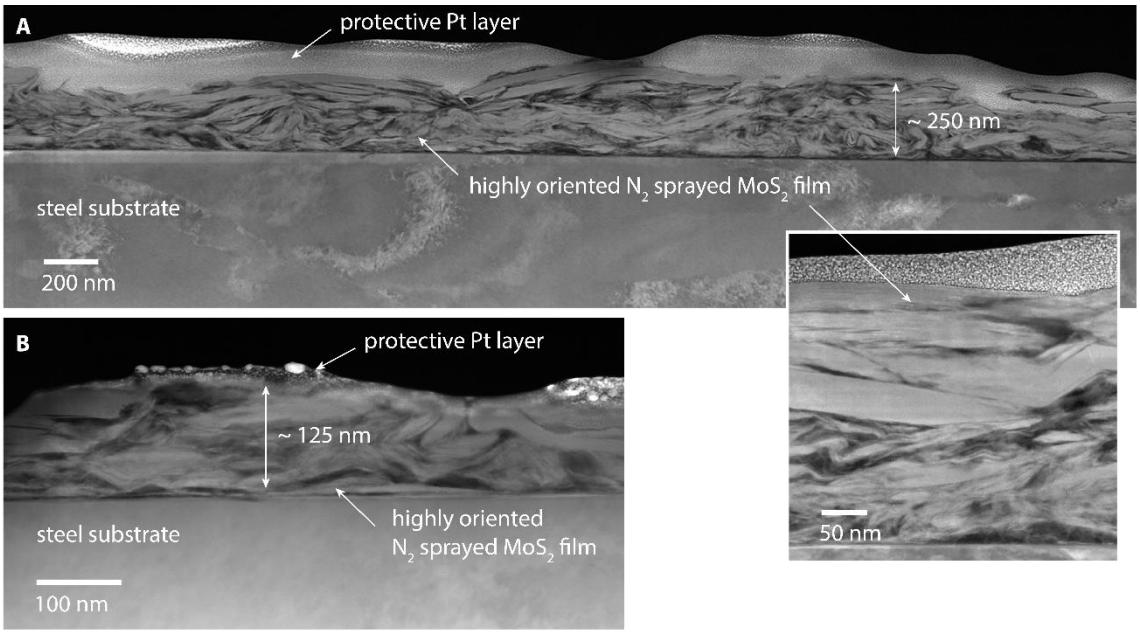

Fig. 5-4. Annular dark-field TEM images of *N_2* sprayed *MoS_2* cross-sectional views from coated (A) smooth and (B) rough steel coupons; inset is a higher magnification view of a smooth coupon cross-section.

4. Below this region and continuing to the substrate, the MoS_2 appears to bend and twist to greater degrees, most likely due to the turbulence during initial spray impingement.

XRD was used to validate the presence of basal orientation in sprayed films. Diffraction patterns for sprayed and sputtered films were taken and revealed a dramatic difference in (002) plane reflection intensity found at $2\theta \approx 14.45°$, indicative of basal orientation of MoS_2 crystallites in sprayed films (Figure 5-5) [59]. These results agree well

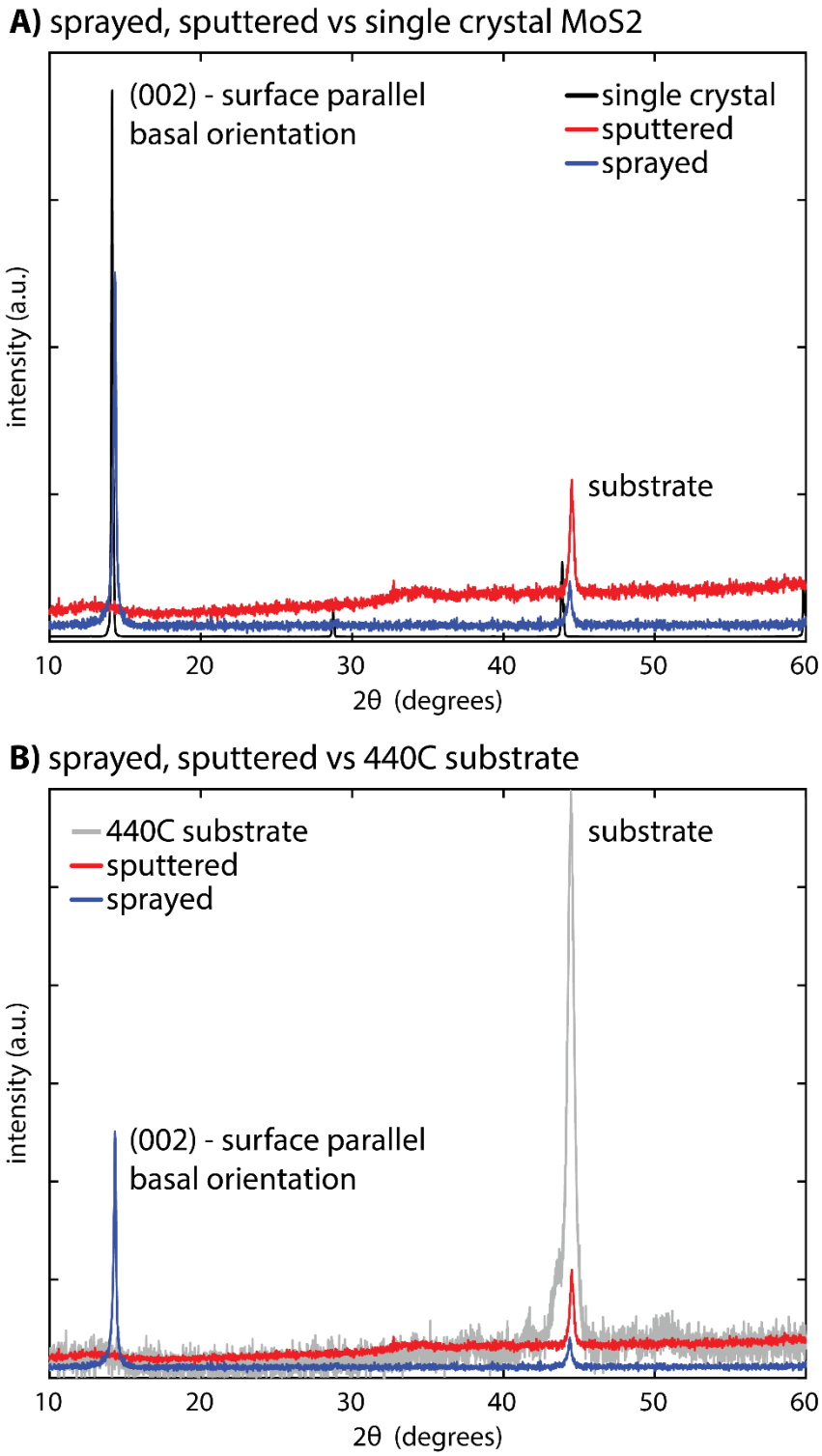

Fig. 5-5. XRD patterns for N_2 sprayed and sputtered MoS_2 vs (A) a single crystal of synthetic molybdenite and (B) the 440C substrate. Sprayed coatings exhibit a much higher presence of (002) peak denoting greater basal plane orientation.

with findings from TEM and support the hypothesis that N_2 spray deposition is capable of

creating highly ordered films of MoS_2 with a dominant basal orientation parallel to the surface. Scans taken to compare against a single crystal MoS_2 sample showed a similarly intense peak at $2\theta \approx 14.45$ (Figure 5-5 A). A secondary symmetry peak of (002) at $2\theta \approx 44.34°$ is shown in the single crystal sample but should not be confused with the peak just to the right of it at $2\theta \approx 45°$ [100]. The peak at $2\theta \approx 45°$ is most likely indicative of the steel substrate below (Figure 5-5 B). The general absence of any distinct peaks and broad features in the sputtered sample (apart from the substrate) indicates a predominantly amorphous structure.

5.5.2 Tribological Behavior of N_2 sprayed MoS_2 coatings

Friction coefficients were acquired for N_2 sprayed MoS_2 coatings in both dry nitrogen and 20% relative humidity (RH) laboratory air (Figure 5-6). It is important to comment here that the low loads (100 mN) and subsequently low contact pressures (450 MPa) are used in this study with the intent of prolonging run-in processes. It is well known that MoS_2 exhibits an inverse relationship between friction and contact pressure [63], [117]. As such the loads shown for 100 mN experiments may appear higher than typically reported values of friction coefficients for MoS_2 (e.g. $\mu \sim 0.05$ at contact pressures >1 GPa) [118]. The load dependence and how it relates to run-in are explored further in §7.

In general, sprayed coatings deposited on rough substrates (Ra ~ 200 nm) reached lower steady state friction coefficients with steadier transient performance than smooth, highly polished (Ra ~ 20 nm) coatings. Sputtered coatings exhibited a similar dependence of performance on roughness but with less erratic transient behavior overall. Results for the rough sprayed samples show that initial friction is reduced by ~0.03 in dry nitrogen and ~0.1 in humid air when compared to their sputter deposited counterparts. These findings

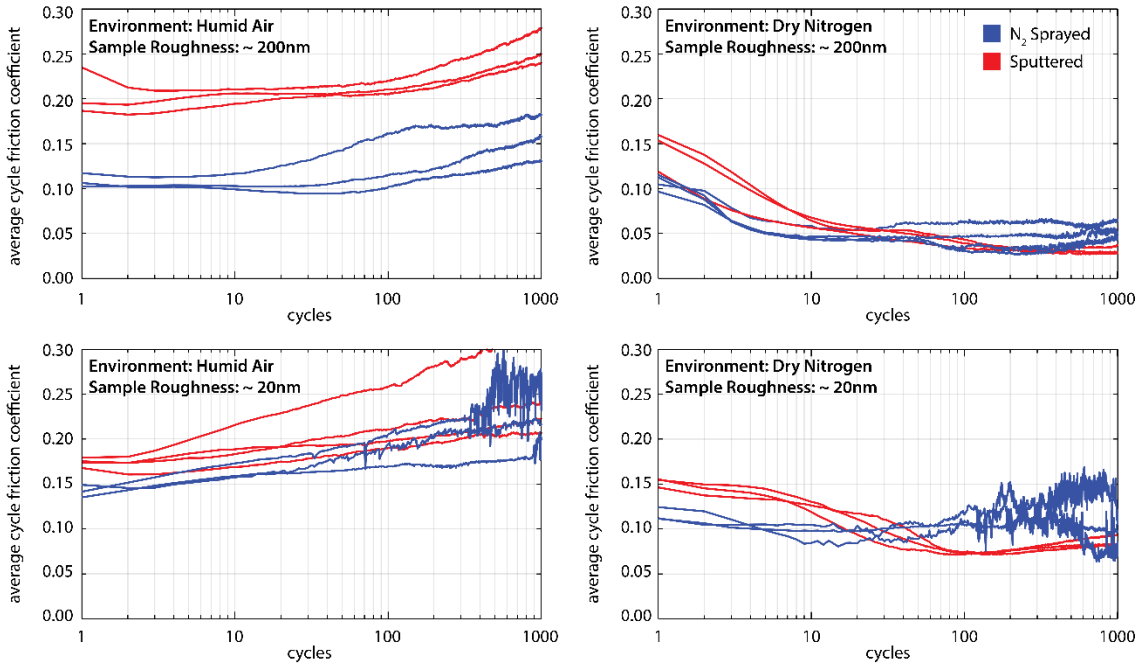

Fig. 5-6. Representative average cycle friction coefficient data for "smooth" (Ra ~ 20 nm) and "rough" (Ra ~ 200 nm) *N_2* sprayed and sputtered *MoS_2* coupons in humid (20% RH) laboratory air and dry *N_2* (< 10 ppm *O_2*, dew point < -60°C) at 20°C; bi-directional linear sliding at 1 mm/s, 0.8 mm long wear track, 1/8" diameter 440C ball, 100 mN normal force.

are consistent with the hypothesis that the higher degree of basal orientation in the film is able to mitigate higher initial friction in amorphous or sputtered coatings (see Discussion).

Interestingly, initial friction and steady-state friction for sprayed coatings was half that of sputtered coatings on rough substrates in humid air. For sprayed MoS_2 coatings on rough substrates, friction coefficient did not change, with $\mu \approx 0.1$ for dry nitrogen and humid air. The sputter deposited MoS_2 coatings with a higher degree of amorphous texture had higher initial friction coefficients in dry nitrogen $\mu \approx 0.15$ which rose even higher in humid air to $\mu \approx .21$. The reasons for this difference are also discussed further in the discussion.

No measurable differences were observed in friction behavior of sprayed MoS_2 coatings aged in humid nitrogen at 150°C as compared to unaged results (Figure 5-7) tested in a dry nitrogen environment at room temperature. These aging studies were intended to

assess previous findings that claimed water alone was not able to alter the surface composition of MoS_2 films via oxidation as explored by Khare et al. [107], [108]. It should also be noted here that the general friction behavior (run-in and steady state friction) is lower than friction traces shown in Figure 5-6 due to the difference in load. It is not unreasonable that loads an order of magnitude higher (1000 mN vs 100 mN) would cause a drop in friction of μ= 0.03 - 0.04 [117].

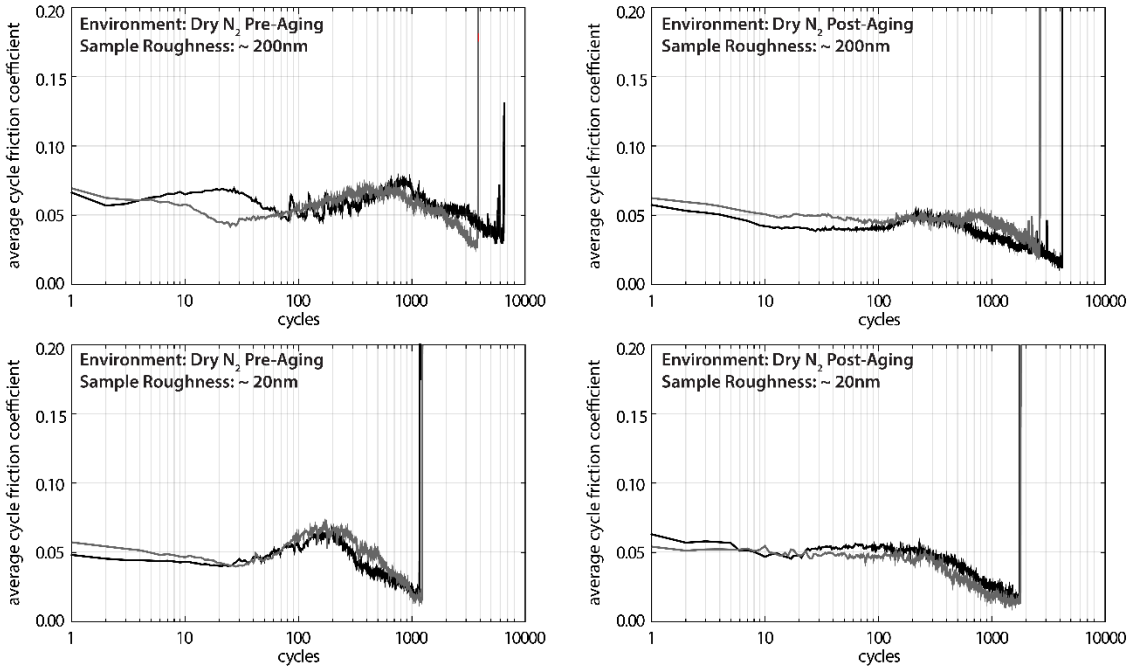

Fig. 5-7. Friction data in dry N_2 for pre- and post-aging N_2 sprayed MoS_2 coatings on smooth and rough coupons; all tests performed at 1 N normal force with all other conditions equivalent to those described in the caption of Fig. 6; each plot shows two overlaid data sets from separate experiments with freshly cleaned and prepared 440C balls; coating failure was observed as a sharp increase in friction coefficient in all cases shown here.

Wear life of the sprayed films varied with both load and roughness of the substrate (Figure 5-8). Coatings deposited on rough substrates (200 nm) exhibited lower friction coefficients and lasted ~ 3-4 times longer than MoS_2 spray deposited on smooth coatings. Roughness of the substrates made comparisons via profilometric measurements infeasible so wear was assessed by comparing cycles til failure. Slopes of linear regression best fit

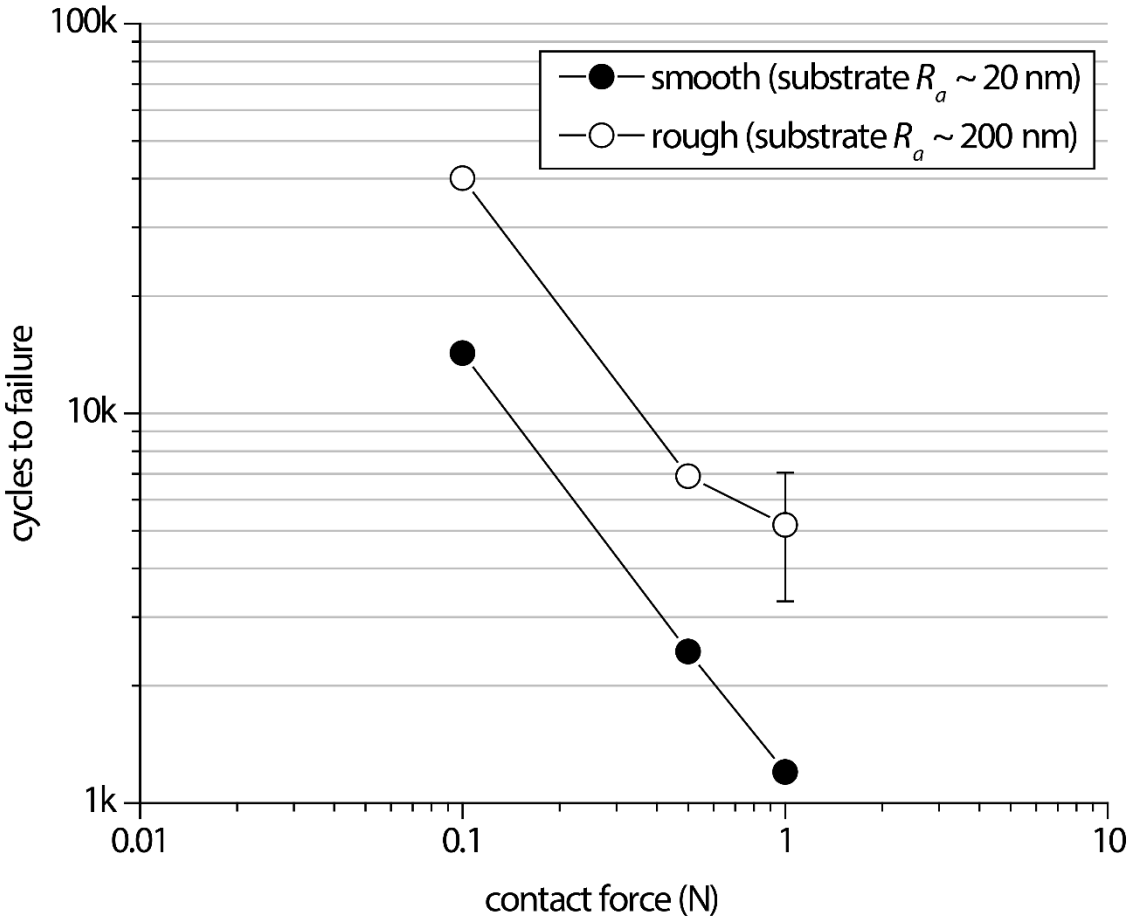

Fig. 5-8. Coating life measured by evidence of a sharp transition in friction coefficient associated with metal-on-metal contact; experiments performed in dry nitrogen using the same conditions as listed in the caption of Fig. 5; only the rough coupon showed significant variability in cycles-to-failure at 1 N normal force, where the error bars represent the standard deviation throughout six separate experiments.

lines of cycles to failure versus contact force (for both rough and smooth samples) suggest wear is inversely proportional to contact force and sliding distance, as is shown in Archard wear theory [119]. Also, sprayed coatings deposited on rough substrates were able to last 40k cycles until a "soft" failure at only μ=0.25 that persisted for over 200k cycles as compared to coatings on smooth substrates which only lasted upwards of 5k cycles before failure at μ=0.10 (Figure 5-9). Overall, MoS_2 spray deposited onto smooth substrates

showed inferior friction and wear performance as compared to rougher substrates, in agreement with previous reports in the literature [38], [39], [46], [74], [120].

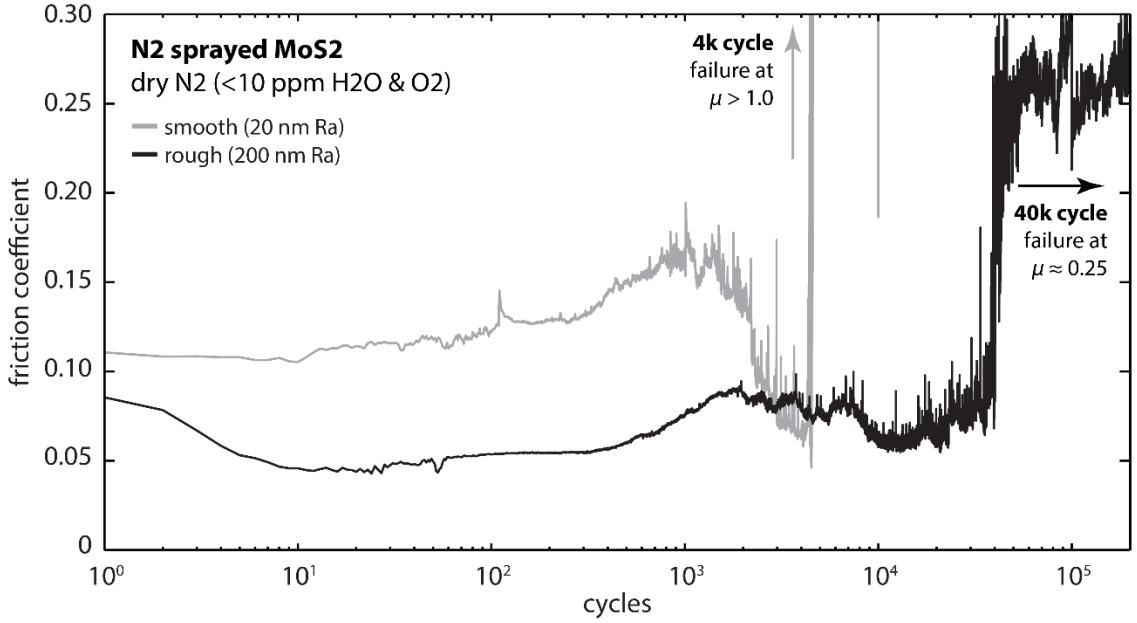

Fig. 5-9. Example friction traces for long cycle tests run on sprayed *MoS_2* coatings with 20 nm and 200 nm Ra. See Figure 5-6 for contact and loading conditions.

5.6 Discussion

As hypothesized, the nitrogen spray process was able to produce highly oriented MoS_2 coatings with surface parallel basal orientation throughout the thickness of the film. It is thought that the kinetic energy imparted during impingement enables the shear of MoS_2 powder onto the substrate in such a manner that develops with additional spraying into the highly ordered texture. This texture allows for the low shear strength direction of MoS_2 basal planes to be parallel to the imposed shear stress, enabling low friction earlier on in the sliding history of the coating. Amorphous coatings, on the other hand, must first re-orient and form cohesive crystallites in the wear track with basal orientation, leading to higher friction until the basally oriented MoS_2 is formed. Sprayed films are also similar to burnished films in that they are applied through a method of shearing MoS_2 onto the

counterface. Burnished films [74] and even run-in sputtered films [25], however, do not exhibit orientation through the thickness of the film as sprayed coatings appear to exhibit as shown by TEM cross-sections. Burnished films are also known to exhibit relatively poor adhesion to the substrate and blister easily [38], [55]. This poor adhesion is likely due to weak bonding to the substrate from loosely adhered particles which may also create the need for bonding resins and other supportive matrix components. As touched upon in §5.2, sputter deposited MoS_2 films can be produced with a wide variety of microstructures, from amorphous to highly crystalline but with basal planes normal to the surface [24], [59], [82], [83], [118], [121]. This chapter serves to demonstrate the impact MoS_2 films with an established crystallinity upon deposition can have on the initial friction behavior and environmental sensitivities known to cause increased friction in MoS_2.

Results from friction tests in dry nitrogen and humid air environments showed initial friction coefficients of basally oriented sprayed coatings was the same ($\mu = 0.1$). Amorphous MoS_2 films on the other hand exhibited higher initial friction in dry environments ($\mu \approx 0.15$) and even higher in humid air ($\mu \approx 0.21$). The trends noticed are largely seen on rougher coating substrates as compared to smooth which exhibit overall worse performance for sprayed coatings and sputtered especially in dry nitrogen environments. This effect is also see in the wear performance (Figure 5-8). Differences are attributed to the fractional coverage of the sprayed coatings and how the coverage is formed. For rough substrates, EDS reveals larger crystallites while smooth substrates exhibit uniformly patchy or speckled MoS_2 surfaces with likely smaller crystallites. This would explain the difference in performance in humid environments which should initially be governed by the ratio of sulfur terminated MoS_2 surfaces to the reactive edge sites. In

terms of wear, it has been observed in the literature that rough surfaces last longer than smoother ones. The difference here is due to the capability of rough surfaces to hold lubricant within the roughness better and replenish the coating longer than that of smooth surfaces [28], [39], [122]–[125].

It is thought that the presence of an initially basally oriented surface parallel to the direction of sliding is a primary contributor to such a large difference in initial friction between the oriented and amorphous coatings. Further, such a difference may suggest that the presence of contaminants on the surface such as adventitious carbon, water and oxygen only appreciably impacted the films with an amorphous structure while unable to have an effect on films with an ordered surface. This suggests that, even in the presence of water, MoS_2 films with an established ordered surface (such as sprayed coatings) can still generate low friction at the onset.

During prolonged sliding, it is well known that the presence of oxygen and water can increase the friction in MoS_2 coatings. Experiments done by Fleischauer et al showed that sputter deposited films with varying degrees of basal orientation, as indicated by XRD, responded differently to aging. Films with slightly more surface parallel basal orientation oxidized to depths of ~ 1nm while those with more surface normal basal orientation oxidized to depths greater than 10 nm [24], suggesting films with ratios of surface to edge sites on the surface would provide greater resistance to oxidation. If we assume that a 200-nm thick (Figure 5-4) is representative and the coating must last at least 1000 cycles (Figure 5-8) then the average wear rate would be ~ 0.2 nm/cycle or a monolayer of contaminants removed per pass. For the sprayed films during run-in in dry nitrogen (Figure 5-6), the reduction in friction during run-in may also be due in part to removal of contaminants at

the surface which do not likely reform in dry nitrogen and both coatings are able to attain low steady state friction coefficients. In humid air, however, increases in friction past initial values for either coating type are likely due to prolonged contact with latent contaminants that continually form, pile up and interfere with formation of a low friction basally oriented interface. This is also accentuated at the start of testing for amorphous sputtered MoS_2 on rough substrates, where the presence of moisture had a much greater impact on the initial friction behavior and subsequent formation of basally oriented crystalline surface layers which already existed in ordered sprayed films.

Performance of sprayed films during run-in are also remarkably different than what is reported for sputtered films in similar environments. Water is a known contributor to increased friction in MoS_2 coatings [118]. As shown by Khare [108] and corroborated with out own experiments (Figure 5-7), water did not lead to oxide formation in sprayed films, even at high temperatures (150°C). Pritchard and Midgley also demonstrated that the initial friction behavior of burnished MoS_2 films increased with increasing RH [109]. Our observations that initial friction did not change for sprayed films between environments on rough coatings does not agree with Pritchard and Midgley's findings, yet results for our sputtered films did.

Many mechanistic factors governing friction, wear and run-in of ordered MoS_2 coatings and all other forms of MoS_2 coatings are still likely unexplored.

5.7 Concluding Remarks

Tribological performance and environmental stability of N_2 sprayed MoS_2 coatings were assessed in this chapter to better understand their unique as-deposited microstructure which closely mimics that of surface parallel basally oriented MoS_2 lamellae. The N_2 spray

deposition technique was shown to be able to effectively produce coatings with this microstructure throughout the thickness of the films. This structure was first confirmed by cross-sectional TEM and XRD measurements as well as coverage and morphology of the sprayed coatings shown via SEM/EDS.

The highly ordered sprayed films consistently showed low initial friction in dry nitrogen and humid air as opposed to amorphous sputter deposited MoS_2 films which exhibited higher initial friction in every environment, especially humid environments. The reduction in friction for sprayed films is attributed to a highly crystalline structure that reduces the energy and the need to re-produce this structure during sliding as amorphous sputtered films do.

The impact of water vapor on friction in MoS_2 is also reinterpreted and it is proposed that the presence of water restricts the growth and formation of ordered tribofilms on the surface, instead of serving to reduce the shear strength of established films. This theory was formed due to the large difference in run-in behavior for ordered and amorphous films when compared between dry nitrogen and humid air environments. Artificial aging experiments on the sprayed coatings in humid nitrogen at 150°C also confirmed the films are resistance to oxidation in the absence of molecular oxygen. Overall, this work demonstrates the remarkable improvements in friction behavior and environmental resistances by simply modifying the microstructure of pure MoS_2.

6. Effect of Microstructure on the Oxidation of MoS_2

6.1 Overview of Oxidation Focus Study

As demonstrated in the previous chapter, §5, microstructure plays a critical role in the initial friction behavior and environmental sensitivities of MoS_2 films. This chapter further investigates the role of microstructure on the friction behavior and oxidation resistance of MoS_2. A systematic investigation is carried out on planar/highly ordered sprayed MoS_2 and amorphous sputtered MoS_2 coatings before and after treatment in aggressive atomic oxygen and high temperature (250°) molecular oxygen environments. Multiple techniques were employed such as friction tests, molecular dynamics (MD) simulations, X-Ray photoelectron spectroscopy (XPS) and high-sensitivity low-energy ion scattering (HS-LEIS) to better understand the link between structure and oxidative resistance. After either oxidative treatment, initially ordered films showed a remarkable resistance to oxidation with minimal increases in friction. Samples exposed to atomic oxygen showed similar amounts of oxidation via XPS; however, when combined with monolayer resolved elemental depth profiles from HS-LEIS, oxidation was shown to be limited to the first atomic layer for ordered MoS_2 and throughout the depth for amorphous MoS_2 films.

6.2 Motivation

Molybdenum disulfide (MoS_2) is a widely applied 2D material, with applications in catalysis [126], solid lubrication [118], semiconductor materials in transistors [127]–[129] and photodetectors [130], [131]. As explained in previous sections, MoS_2 is a layered material in which lamellae interact via weak van der Waals forces between basal planes that translates to low friction in vacuum and inert environments. As such, MoS_2 is widely used as a solid lubricant in satellites and other moving mechanical assemblies employed in

extraterrestrial environments such as low earth orbit (LEO) space [11], [33], [37], [102], [132]. Still, exposure to and operation in environments that contain molecular (O_2) and/or atomic (O) oxygen [33], [108], [133] and water vapor [24], [39]–[41], [108] is known to oxidize or alter the properties of MoS_2 enough to significantly affect desired performance in semiconductor and tribological applications [134], [135].

Oxidation of the articulating joints in solar wings or even simple ball bearings in satellites can be a catastrophic failure during deployment [11]. Oxidation or exposure to molecular oxygen (O_2) can occur at multiple points during the lifetime of a part such as: initial assembly, testing in a terrestrial environment prior to service [53] and most importantly during deployment in LEO where atomic oxygen (AO) exists [32]. Composite films have been developed to combat the problem of oxidation [69], [70], yet the mechanism that enables composites to provide more stable low friction in these environments is unclear.

6.3 Hypothesis

The systematic investigation detailed in this chapter suggests that the degree of ordering and availability of defect sites in the first few layers of MoS_2 is a primary mechanism for the microstructural impact on oxidation. Edge sites present at the surface of MoS_2 coatings enable molecular oxygen to preferentially interact and form oxides at high enough temperatures (250 - 350°C) that can impeded lamellar shear which can increase friction and wear [39], [136]. As such, MoS_2 coating development has historically focused on densifying films with a preference for a small edge/defect density ratio on the surface. A best-case scenario would have the surface of the MoS_2 coating relatively free of defects with the passive basal planes exposed to help prevent interactions with

contaminants and also provide a low shear strength interface. Even if this scenario were attainable, atomic oxygen is very reactive and can easily oxidize even an inert, defect free basal plane of MoS_2 [137], [138].

It is hypothesized that oxidation of MoS_2 by atomic oxygen exposure is limited only by the proximity of an atomic oxygen species to a reaction site that in turn oxidizes and prevents further penetration and reaction of AO throughout the depth of the coating. Oxidation and diffusion of oxygen into the surface of amorphous/nanocrystalline and highly ordered crystalline MoS_2 films (i.e. from the surface to ~ 4 nm depth) is assessed. The composition of the outermost atomic layer and composition through the depth by sequential sputtering steps is studied via HS-LEIS and supported by XPS, MD and tribological experiments in order to test this hypothesis.

6.4 Experimental Procedures

6.4.1 Materials Synthesis and Oxidation

Basally oriented (*i.e.* basal (0001) planes parallel to surface), crystalline MoS_2 films (~200 nm thick) were deposited on 17-4 PH stainless steel coupons with R_a 200 nm (0.8 µin -- mirror finish) via N_2 spray deposition, as shown in the previous chapter [90]; these are referred to as "ordered MoS_2". Further details on the spray deposition process can be found in §4. Amorphous/nanocrystalline MoS_2 films (~2 µm thick) were deposited via DC magnetron physical vapor deposition (PVD) by Tribologix, Inc. on 440C substrates with similar roughness values to those tested for sprayed coatings; these are referred to as "amorphous MoS_2". Further details on the PVD sputter deposition process can be found in §4.

For comparison, MoS_2 samples underwent two separate aging treatments as well as a control environment without oxygen exposure:

1) as-deposited in which coatings were baked for 30 minutes at 250ºC in high vacuum (10^{-5} mbar)

2) after exposure to an atomic oxygen source (thermal atomic oxygen, molecular oxygen and ozone [98] – referred to as "atomic oxygen" or "AO"), in high vacuum (10^{-5} mbar) at room temperature for 30 minutes

3) after exposure to O_2 at atmospheric pressure at 250ºC for 30 minutes (referred to as "high temperature oxygen" or "HT O_2").

Comparisons are predominantly made between sample types and not exposures due to the fact that each oxidative treatment is intentionally different with different pressures and temperatures to serve as analogues to commonly experienced degradative environmental conditions.

6.4.1.1 Atomic Oxygen Source

As mentioned in previous sections, atomic oxygen is a readily encountered species in low earth orbit applications that can oxidize MoS_2 and greatly enhance friction and wear. To simulate conditions in orbit, the atomic oxygen source mounted to the HS-LEIS antechamber was utilized.

An atomic oxygen source is typically used to clean or modify a surface of impurities by reaction with oxygen in vacuum. In principal, an oxygen gas plasma discharge is used to produce oxygen in all forms (O, O_3 and various forms of oxygen ions). Prior to reaching the surface of the sample, the particles are filtered out based on charge such that only neutral particles such as monatomic oxygen and ozone pass through. The neutral particles

also pass through with a reduced kinetic energy such that they are on par with the thermal energy of the chamber. As such the highly chemically reactive monatomic oxygen species impinge on the surface and readily react with organic surface contamination such as adventitious carbon or hydrocarbons. It is also expected to react readily with any spot on the surface of MoS_2, passivated sulfur basal surfaces or edge sites.

6.4.1.2 High Temperature Oxygen Gas

High temperature oxygen gas was also employed in experiments to emulate high temperature air environments coatings may experience during testing prior to launch. Temperatures upwards of 250 – 350°C are also known ranges in which MoS_2 begins to oxidize in the presence of oxygen gas [53].

Generally, the polarity present in the bonding for a sulfide should prevent oxygen gas molecules from adsorbing and reacting with a sulfur terminated surface of MoS_2 such as the basal planes. However, on edge sites that are terminated with readily accessible Mo metal, reactions can easily take place to form various oxides of Molybdenum (MoO_2, MoO_3). All of this is exacerbated at higher temperatures, upwards of 250 -350°C when the sulfur surfaces begin to react with the impinging O_2 molecules and desorb as SO_2 gas, providing Mo metal for additional reactions to produce oxides.

To emulate this environment for testing, samples were attached to a custom-built adapter for use with ION-ToF ceramic button heaters in the HS-LEIS. The samples were first transferred into the antechamber and heated to 250°C. After reaching temperature, the antechamber which was originally under high vacuum was gradually brought up to near ambient pressure with oxygen gas and left at temperature for 30 minutes.

6.4.2 Tribological Experiments

After treatments in the HS-LEIS antechamber, samples were quickly moved to an inert glovebox backfilled with dry nitrogen. The glovebox also houses a custom-built linear reciprocating microtribometer [93], [115], [116], [139] which is used to assess friction behavior of the coatings. Friction tests were done three times at different locations on the sample. Each test lasted for 1000 cycles at 1 mm/s speed, 0.8mm stroke and 100 mN normal load (450 MPa). Grade 5 1/8" 440C stainless steel bearings (R_a ~ 40 nm) from McMaster-Carr were used as pins (countersamples) in all sliding experiments.

6.4.3 High-sensitivity low-energy ion scattering (HS-LEIS)

After oxidative treatments, elemental composition of the first 3-4 nm was investigated with high-sensitivity, low-energy ion scattering spectroscopy (ION-TOF Qtac 100). Elemental composition of the outermost atomic layer can be determined with HS-LEIS and was chosen for this astounding feature [140]–[142]. Most other surface characterization techniques such as X-Ray photoelectron spectroscopy (XPS), time-of-flight secondary ion mass spectroscopy (ToF-SIMS) and auger electron spectroscopy (AES) are not able to reach such a resolution and typically probe much larger depths, obscuring potentially useful information about the first few atomic layers like the presence of thin oxides on the surface.

In this study, a 3 keV He^+ ion source primary ion beam with an ion fluence of 2 x 10^{14} ions/cm^2 and 3 keV pass energy was rastered over a 1.5 mm x 1.5 mm area. After each scan with the primary beam, approximately a monolayer of material over a 2mm x 2mm area was removed by the sputtering gun (1.0 keV Ar^+ ion source) to avoid edge effects when sensing with the primary ion beam. Total sputtering dosage (or depth) varies by experiment and is listed in each figure caption, but the main study profiled to a depth at

minimum 18 x 10^{15} ions/cm^2 in approximately 2.5 x 10^{15} ions/cm^2 steps. This resulted in a total depth of 3-4 nm with 1 x 10^{15} ions/cm^2 corresponding approximately to 0.2 nm.

6.4.4 X-ray photoelectron spectroscopy (XPS)

XPS was done on a separate sample with the same environmental treatments on a Scienta ESCA-300 HR-XPS with a high power, rotating-anode Al Kα X-ray source with an excitation energy of 1486.6 eV. An offset was used on all spectra with a reference C 1s signal at a binding energy of 284.60 eV to account for minor residual electrostatic charging effects. The less intense Mo 3p photoelectron signal was used for quantification to avoid interference between the dominant Mo 3d features and that of S 2s. A 70% Gaussian – 30% Lorentzian function was used to fit each set of peaks. When applicable, the width (FWHM) of peaks corresponding to a given atomic orbital are set to be equal. Also, peaks of spin-orbit doublets (e.g., Mo (3p3/2 and 3p1/2)) are set to have an area ratio in accordance with quantum degeneracy values (i.e. 2:1 for p3/2 and p1/2 orbitals and 3:2 for d5/2 and d3/2 orbitals.).

6.5 Results & Discussion

6.5.1 Preliminary HS-LEIS Powder Studies

The very first studies on the HS-LEIS were carried out on pelletized powder samples of commercially available McLube MoS_2-100 Moly Powder®. The powder is a research grade product with ~ 0.65 – 0.8 µm sized particles and minimal MoO_3 content (< 0.05%). These samples were used as a basis to better help understand the spectra to follow for additional experiments. Sputter-etching of the as deposited powder (Figure 6-1 A) shows S and Mo features growing while secondary ion background signals decrease. This is because much of the ambient contaminants are removed with every sputter dosage, but a

tail of low energy contaminants always persists. It is not unexpected that contamination would be found throughout the depth for loosely packed powder MoS_2, as hydrocarbons are likely surrounding each individual particle.

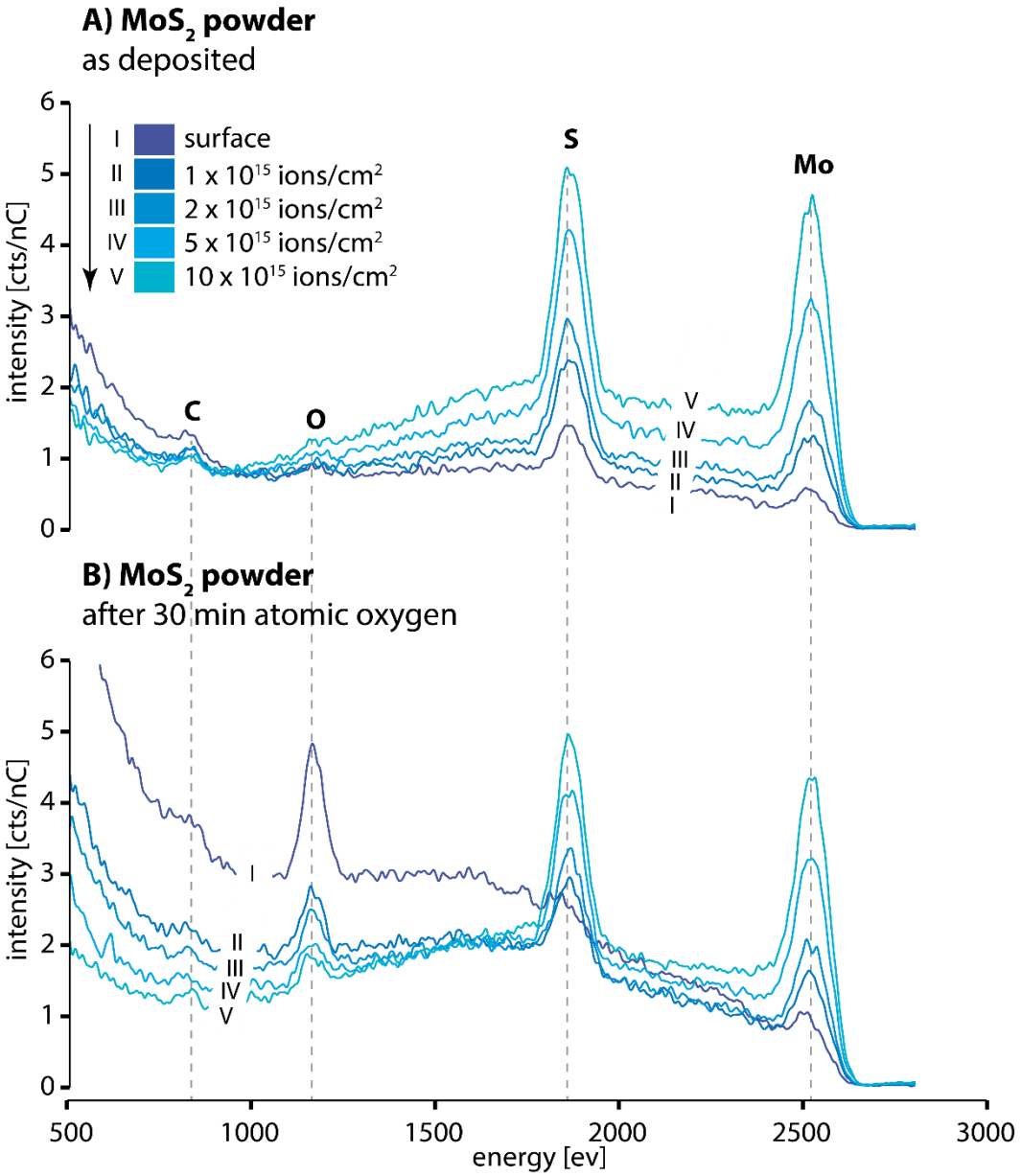

Fig. 6-1. Energy spectra for MoS_2 powder (A) as deposited and (B) after AO exposure for 30 minutes. Sputter doses (2.0 keV Ar^+ beam over 2x2 mm^2) extended to $10x10^{15}$ ions/cm^2 (2 nm) For the 3 keV He^+ probe, peaks are assigned: Mo (2500 eV), S (1820 eV), O (1150 eV).

Background signal from in between elemental peaks is most likely due to He^+ ions recoiling from atoms below the sample surface. Typically, one would expect that any He^+ that managed to penetrate the surface become buried and neutralize, yet some are still capable of escaping. The He atom would experience a similar energy loss as striking an atom on the surface, but would experience further losses from any collisions while traversing below the surface and back out. These events would show as a signal in the LEIS spectrum with energies lower than that of the surface peak. It is important not to forget, though, that the He atom must be re-ionized upon exiting the material to be detected in the LEIS. There are many factors that could influence the probability or reionization for He. A likely culprit is the electronegativity of the surface, with a higher electronegativity increasing the probability for the He atom to lose an electron. The background signal shown in Figure 6-1 between peaks increases with further sputter-etching. It is thought that by sequentially removing hydrocarbons on the surface, the emerging and more electronegative sulfur can increase the probability of He reionization. This is an interesting feature that can be seen on many of the spectra in this chapter.

After surveying the powder as provided, the entire sample was exposed to an oxygen atom (AO) source and depth profiled again in the same area surveyed prior to exposure (Figure 6-1 B). A prominent O peak is now visible with little to no surface S peak and a slight reduction in Mo. It can also be seen that the secondary ion background signal is greatly enhanced, as well as in between O and S surface peaks. A shoulder is present left of where the S peak would be, indicating sulfur is present below the surface and the highly electronegative O is enhancing the probability of He reionization. It is thought that after such a chemically reactive treatment with AO, sulfur on the surface readily reacts and

desorbs as SO_2. Use of a residual gas analyzer in these experiments would enable confirmation of SO_2 formation and desorption. After sputtering past the initial surface, oxygen decreases and sulfur emerges with a noticeable drop in background signal between O and S peaks due to less O presence on the surface causing reionization events. As expected for a powder sample of MoS_2, oxygen remains throughout the depth of the first few nm surveyed.

6.5.2 Heavy Oxygen (O^{18}) Study

Prior to a full suite of oxidative aging experiments, tests were done to see if heavy oxygen or O^{18} was detectable in the HS-LEIS. If so, the use of O^{18} gas instead of regular O^{16} would help separate latent oxygen, oxides or water within a coating to isolate the contribution from oxidative processes [143]. Prior to any spectra taken, the sample was baked out at 250°C in UHV for 30 minutes to drive any latent water (Figure 6-2 A). Depth profiling via Ar^+ sputter-etching of the surface was carried out every 1 x 10^{15} ions/cm^2 (~ 0.2 nm). To better resolve a separation of 2 atomic mass units (O^{16} vs O^{18}), a higher energy 5 keV primary ion beam, compared to typical 3 keV, was used. As such, lower energy adsorbates such as hydrocarbons cannot be seen in the any of the spectra (Figure 6-2). A lecture bottle of O^{18} was connected to a pressure regulator and attached to the LEIS antechamber. Samples were brought to 250°C again, then exposed to O^{18} gas at a chamber pressure of ~ 50 mbar and left to age in the environment for 1 hour. The resulting depth profile showed both O^{16} and O^{18} at similar concentrations throughout the depth of the coating. Even after approximately 17.3 nm (89x10^{15} ions/cm^2), concentrations did not appear to change much relative to one another. From this study, we learned that simply baking coatings at 250°C for 30 minutes was sufficient to alleviate concerns over latent

oxygen signal in LEIS. Utilizing isotopes of oxygen was also shown to be easily done in the LEIS for future experiments. Most importantly, these early findings showed that even

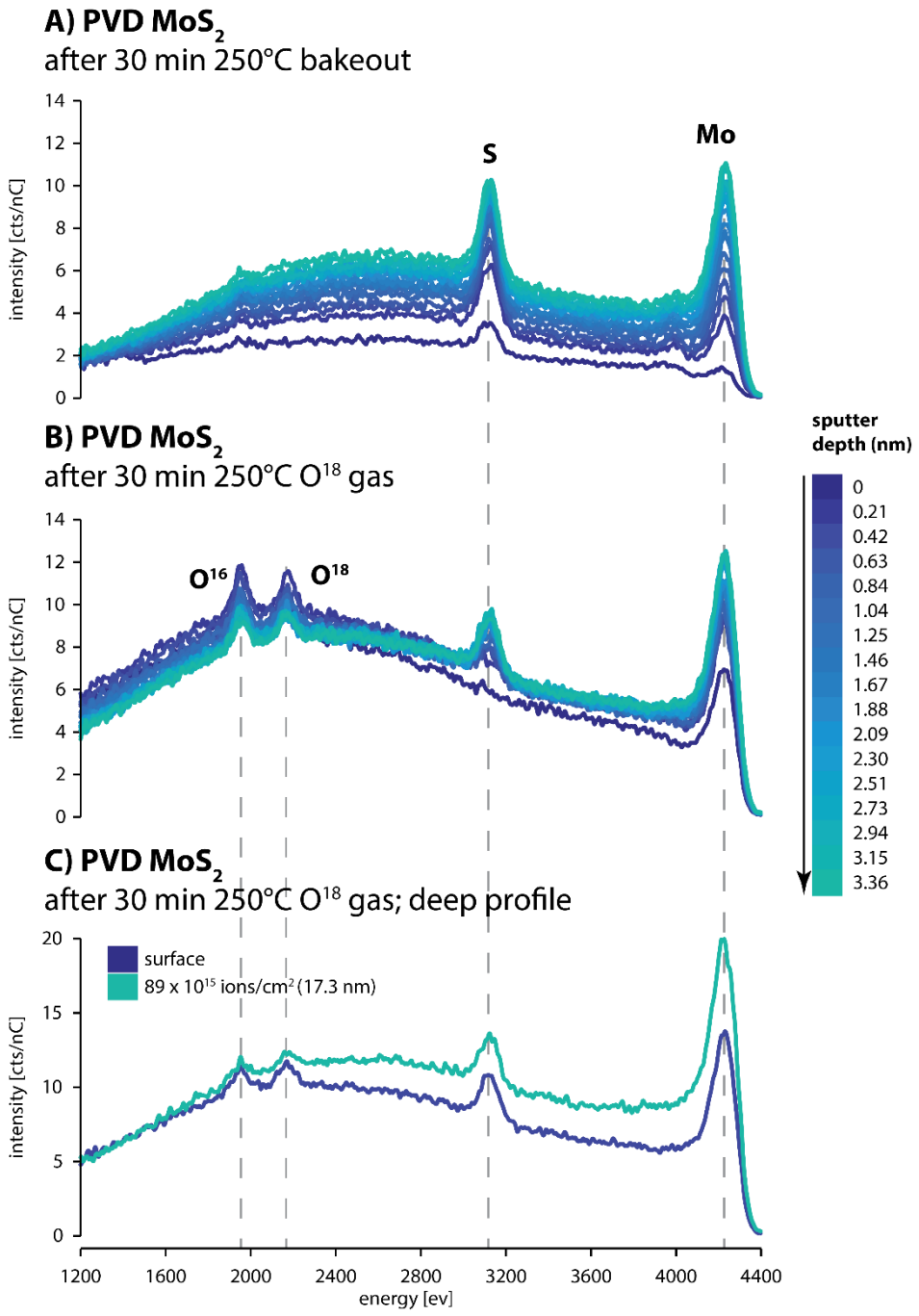

Fig. 6-2. Energy spectra for PVD MoS_2 powder (A) after 30 min at 250°C in UHV (B) and after O^{18} gas exposure for 30 minutes at 250°C. Sputter doses (2.0 keV Ar^+ beam over 2x2 mm^2) extended to (A,B)16x10^{15} ions/cm^2 (2 nm) and (C) 89 x10^{15} ions/cm^2. For the 5 keV He^+ probe, peaks are assigned: Mo (4226 eV), S (3117 eV), O^{16} (1955 eV), O^{18} (2167 eV).

in relatively low chamber pressures (50 mbar), presence of oxygen was extensive, as deep as the 17.3 nm sampled for this PVD amorphous MoS_2 coating.

6.5.3 HS-LEIS Depth Profiling

As-deposited spectra for MoS_2 (Figure 6-3 A, D for the sprayed and PVD samples, respectively) and exposed samples are all shown together in Figure 6-3. Almost all room

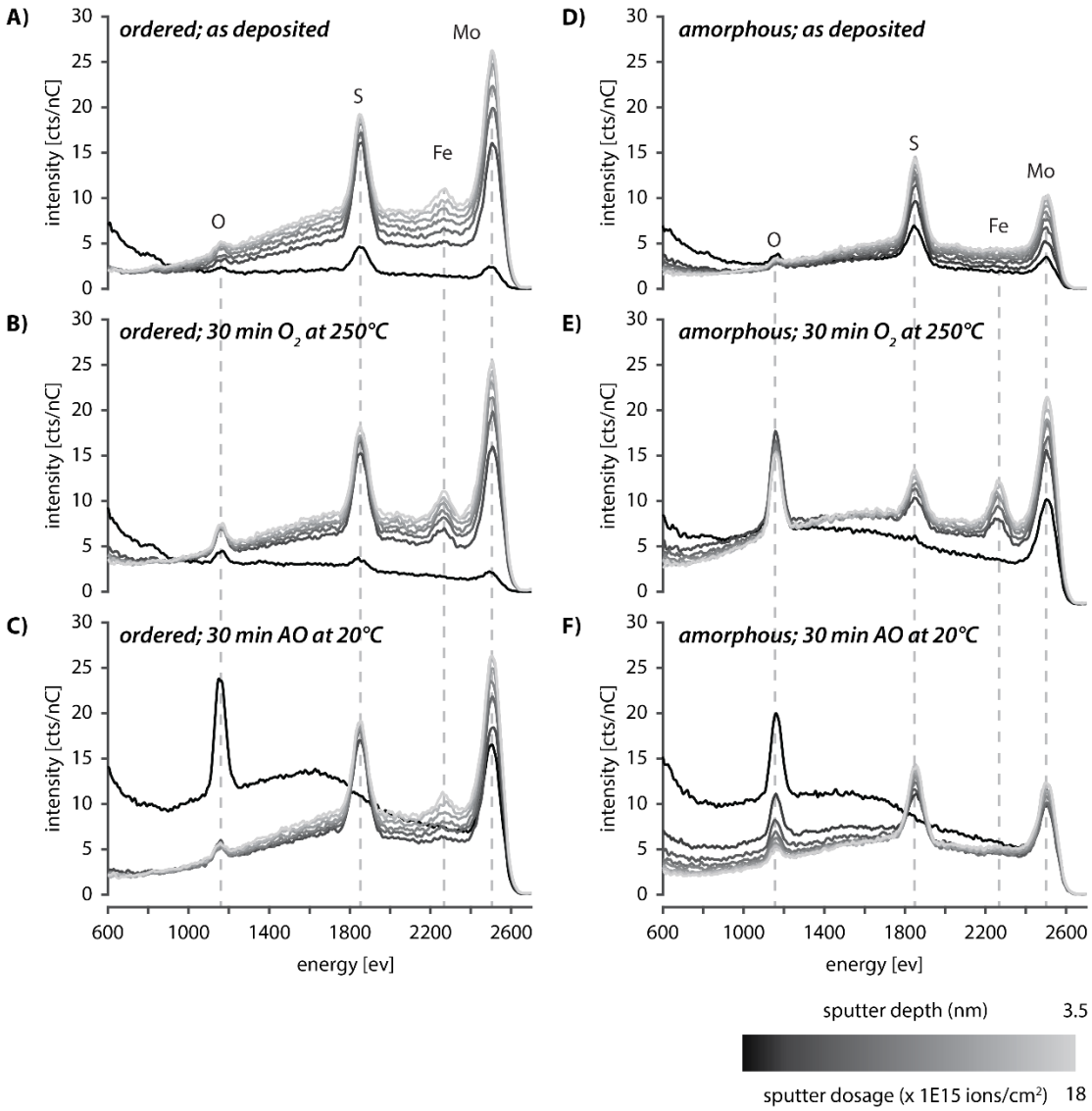

Fig. 6-3. Low energy ion scattering spectra for ordered (A,B,C) and amorphous (D,E,F) MoS_2 films. Sputter doses (1.0 keV Ar^+ beam over 2x2 mm^2) extended to $18x10^{15}$ ions/cm^2 (3.5 nm) for films as-deposited (A,D), after 30 min O_2 gas @ 250°C (B,E) and after 30 min AO @ 20°C (C,F). For the 3 keV He^+ probe, peaks are assigned: Mo (2500 eV), S (1820 eV), O (1150 eV), Fe (2300 eV).

temperature AO (Figure 6-3 C, F) and high temperature (HT) (250°C) exposed O_2 (Figure 6-3 B, E) samples exhibited strong oxygen signals at the surface (shown as a black line) for both types of coatings relative to the as-deposited case. The surface LEIS spectra of HT O_2 treated sprayed MoS_2 (Figure 6-3 B) did not experience any significant increase in oxygen on the surface but was also very similar to the as deposited sprayed MoS_2 spectra (Figure 6-3 A), with a large signal from low energy contaminants such as hydrocarbons and a reduced sulfur signal. This suggests that the HT O_2 was unable to react with organics present on the surface but still able to interact with the MoS_2 and either chemisorb or physisorb, possibly to dangling sulfurs at edge sites. A crucial misstep in this study was neglecting to include lower energy signals that could better show the extent of low-Z contamination. This is assumed to be the source of unseen mass conservation that could help explain cases where all signals increase without a decrease somewhere else in the spectra to uphold conservation of mass. High surface concentrations of low-Z contaminants on the surface may be a possible explanation for the reduced intensity signal for the as-deposited amorphous coating (Figure 6-3 D). HT O_2 treated amorphous MoS_2 (Figure 6-3 E) showed negligible amounts of sulfur on the surface and a high intensity of oxygen present throughout the depth. It is also interesting to note in Figure 6-3 E that, the background signal increases as more sulfur is uncovered through the depth, likely due to oxygen and sulfur (both highly electronegative) increasing likelihood of re-ionization events of the He atom probe. Sulfur is undetectable on the surface of either films exposed to AO (Figures 6-3 C and F) which suggests AO reacts with all sites in proximity on the MoS_2 surface, regardless of crystallinity. A tail of intensity still exists for the lower energy elements after the treatment, extending from low energies up to 800 eV. After a single

sputter dose to expose the first subsurface layer (3 x 10^{15} ions/cm^2, ~0.5 nm), the sprayed film (Figure 6-3 C) returns to a spectrum very similar to the as-deposited composition, indicating mostly surface limited oxidation. In contrast, the oxygen content of the AO-treated amorphous MoS_2 gradually reduced with increasing sputter depth. Both of the AO

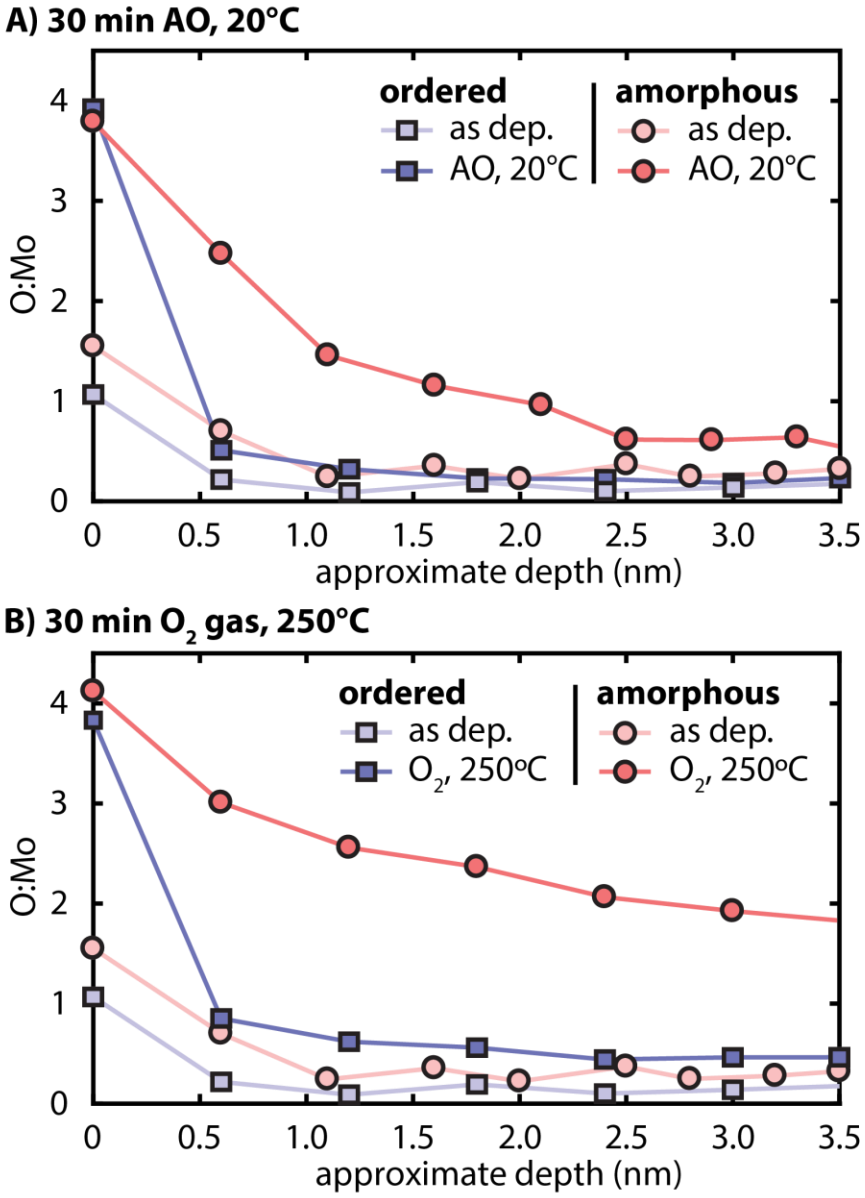

Fig. 6-4. Plots of O:Mo ratios calculated from HS-LEIS data for ordered and amorphous MoS_2 films in A) 30 min AO at 20°C and B) 30 min O_2 gas at 250°C over depths of 3.5 nm or ~ 6 monolayers of MoS_2. As-deposited profiles are also included in each plot for comparison.

treated spectra (Figure 6-3 C and F) also exhibit broad, high background energy shoulders that are indicative of a highly electronegative surface due to a strong presence of oxygen as well as a wealth of buried sulfur beneath the surface.

This relationships demonstrated in the LEIS spectra are further visualized by the relative elemental composition of O:Mo as a function of depth as shown in Figure 6-4. The O:Mo ratio of the surface layer was ~ 4:1 regardless of coating type or form of oxygen treatment (Figure 6-4). While accurate for this data set, it is also slightly misleading due to the relatively large presence of low energy, low mass signal in the spectra for ordered films exposed to HT O_2 (Figure 6-3 B). It is also important to state here that the relative error in signal for each element was not taken to account when calculating these ratios. The O:Mo ratio also shows that oxygen persists throughout the depth of the amorphous film when exposed to both AO and HT O_2 with oxygen levels nearly returning to as-deposited compositions after a sputter depth of 3-4 nm for AO exposed samples. Due to differences in the oxygen treatments, it would be unfair to assess the diffusion characteristics of a given coating between environments. Sprayed coatings, on the other hand, show that oxygen is limited to the first atomic layer in either exposure type. At depths beyond one sputter dose (3×10^{15} ions/cm^2, ~0.5 nm), the sprayed film has a nearly constant Mo:S ratio (Figure 6-3 A, B and C). These results clearly show that the nanocrystalline/amorphous microstructure of PVD films provides pathways for oxygen to penetrate, find edge sites in the MoS_2 and react to form oxides throughout the depth. The large, basally-oriented – *i.e.* (0001) surface normal -- sprayed films have very few edge sites and pathways for further reactivity with oxygen below the initial surface and prevent oxidation throughout the depth. Further studies to better understand oxidative resistances at higher temperature and

prolonged exposures would also help in understanding to what extent microstructure is able to protect the surface of MoS_2.

6.5.4 XPS Oxidation Results

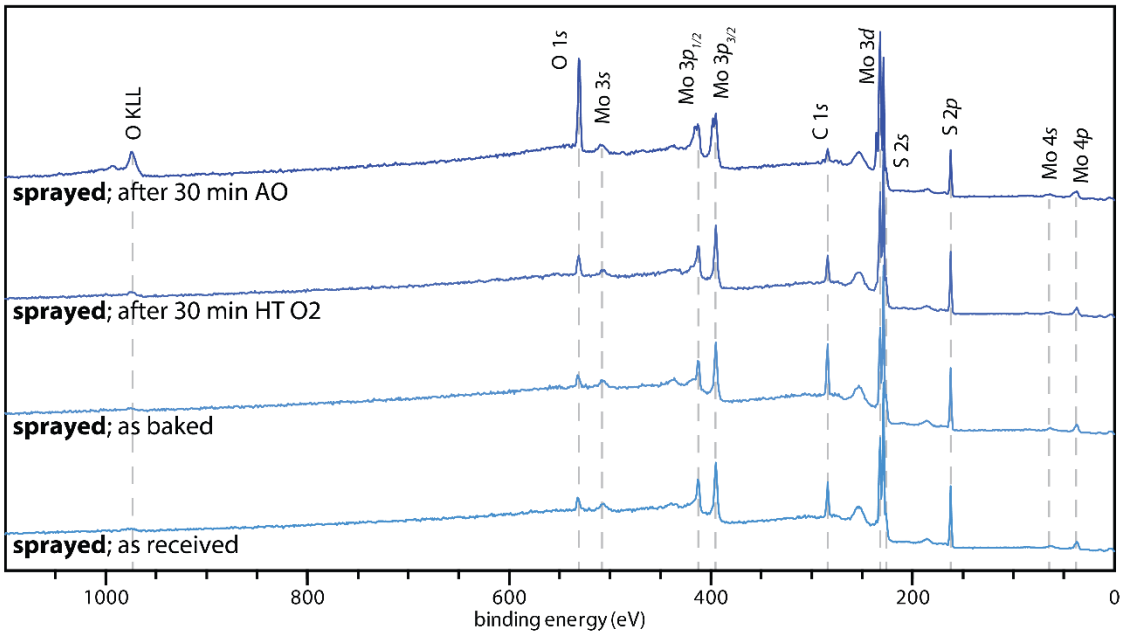

Fig. 6-6. Sprayed MoS_2 XPS survey spectra.

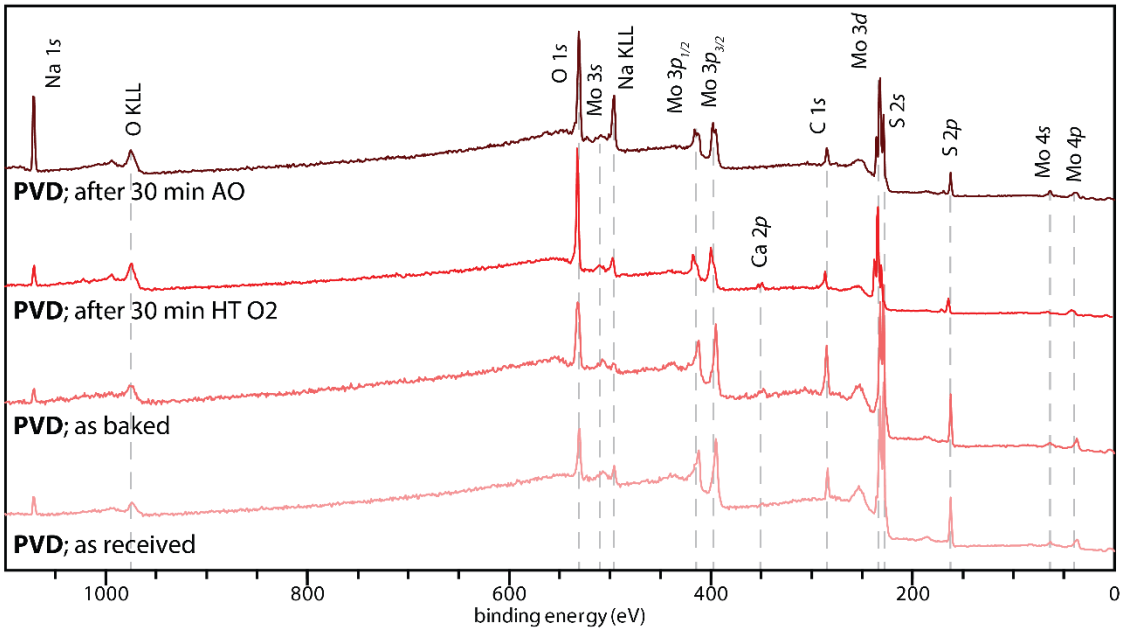

Fig. 6-5. PVD MoS_2 XPS survey spectra.

Photoelectron spectra from the XPS are shown (Figure 6-5 & 6-6) to complement depth profiles from the HS-LEIS, providing information on bonding states over a similar

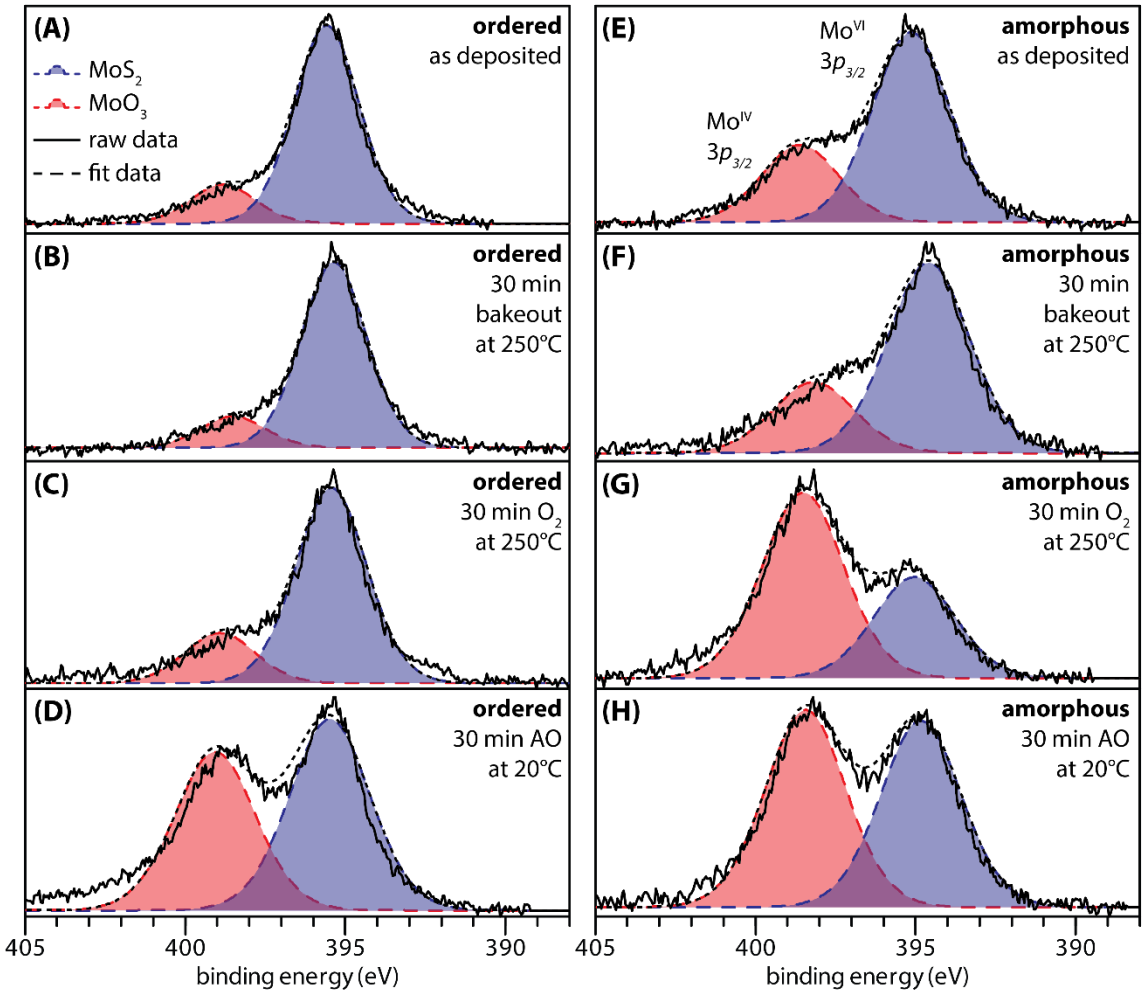

Fig. 6-7. Mo (3p) photoelectron signals for sprayed (**A-D**) and PVD (**E-H**) MoS_2 films after each type of exposure. The blue peak centered at 395.1 eV represents the Mo^{VI} $3p_{3/2}$ MoS_2 bond and the red peak centered at 398.5 eV represents the Mo^{IV} $3p_{3/2}$ MoO_3 bond. The photoelectron signal is shown as a solid black line with the fitted envelope as an overlaid dotted line.

depth (3-5 nm) from the surface. Interestingly, PVD samples exhibit a small, yet noticeable amount of Na and Ca contamination. It is thought that due to only a presence on PVD sputtered samples, the deposition process may be the source. It is also evident from the survey spectra that all PVD films exhibit a higher intensity of oxygen species on the surface as compared to sprayed films.

Further inspection of the deconvoluted photoelectron signal for Mo $3p_{3/2}$ (MoS_2 ~ 395.1 eV; MoO_3 ~ 398.5 eV) [144] confirms these observations (Figure 6-7). The higher binding energy Mo $3p_{5/2}$ part of the doublet is omitted as it was constrained to be directly proportional to the Mo $3p_{3/2}$ as mentioned in the methods section of this chapter. Figure 6-8 shows best the differences in oxidation behaviors between amorphous and ordered MoS_2 coatings. Fractions of the each peak area used to calculate the ratios of MoO_3:MoS_2 for the Mo 3p signal are also given in Table 6-2. Ordered MoS_2 in the as-deposited state and after baking out (Figure 6-3 A & B) exhibited a ratio of MoO_3:MoS_2 two to three times lower than the amorphous MoS_2 (Figure 6-3 E and F); the MoO_3:MoS_2 ratio for ordered MoS_2

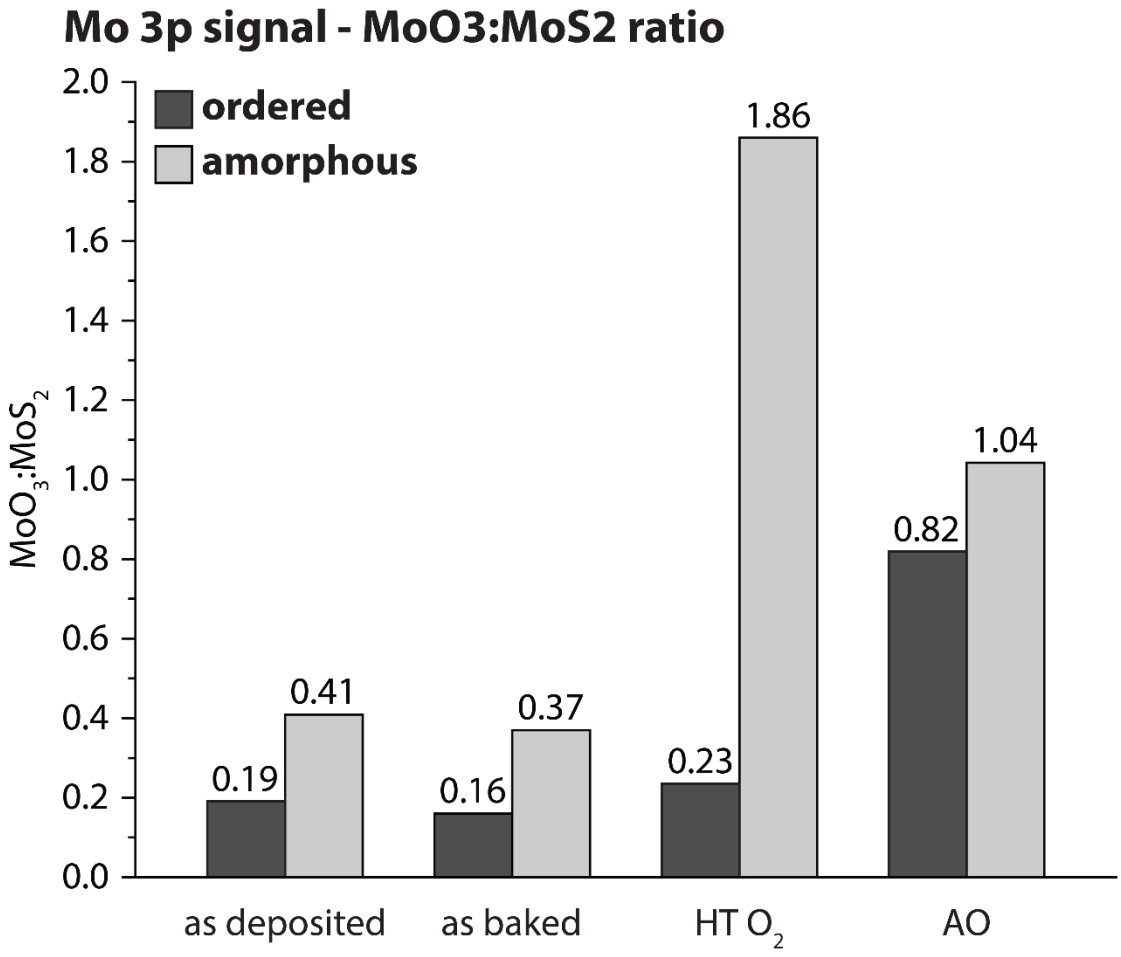

Fig. 6-8. MoO_3:MoS_2 ratios for Mo 3p signal.

was 0.16 as-deposited and 0.19 baked out while the MoO_3:MoS_2 ratio for amorphous MoS_2 was 0.37 as-deposited and 0.41 baked out (see Table 6-1 & Figure 6-8). Within possible errors of the peak fits, it appeared that the bake out process (30 min at 250°C in high vacuum) did not have any appreciable effect on oxide content of the coatings.

Table 6-1 % fraction of Molybdenum compounds for Mo 3p & Mo 3d signals

		% fraction per element (Molybdenum)							
		as deposited		**as baked**		**HT O_2**		**AO**	
		PVD	**spray**	**PVD**	**spray**	**PVD**	**spray**	**PVD**	**spray**
Mo ($3d_{5/2}$)	**Mo-S_2**	78	93	80	93	37	91	51	55
	Mo-O_3	22	7	20	7	63	9	49	45
	MoO_3: MoS_2	0.28	0.08	0.25	0.08	1.70	0.10	0.96	0.82
Mo ($3p_{3/2}$)	**Mo-S_2**	71	84	73	86	35	81	49	55
	Mo-O_3	29	16	27	14	65	19	51	45
	MoO_3: MoS_2	0.41	0.19	0.37	0.16	1.86	0.23	1.04	0.82

The most significant increase of any exposure and coating combination was for amorphous films after O_2 gas at 250°C for 30 min where the ratio of MoO_3:MoS_2 for the amorphous MoS_2 increased significantly more than the ordered MoS_2 (1.86 vs 0.23 respectively). In contrast, the MoO_3:MoS_2 ratio after atomic oxygen exposure is high for both the ordered (0.82) and amorphous (1.04) films.

As expected, the same trends in percent fractions of molybdenum compounds are seen in Mo 3d signals as in Mo 3p signals (Figure 6-9 & Figure 6-10). Across the board, Mo 3d signals tend to give between 2 – 10% higher signals for the presence of MoS_2 than MoO_3 (Table 6-1). While the differences are minimal, it is still intriguing to think of what may cause such discrepancies. One reason may be due to the close proximity of the S 2s peak to the Mo 3d which could be altering the outcome of the peak fits for either signal.

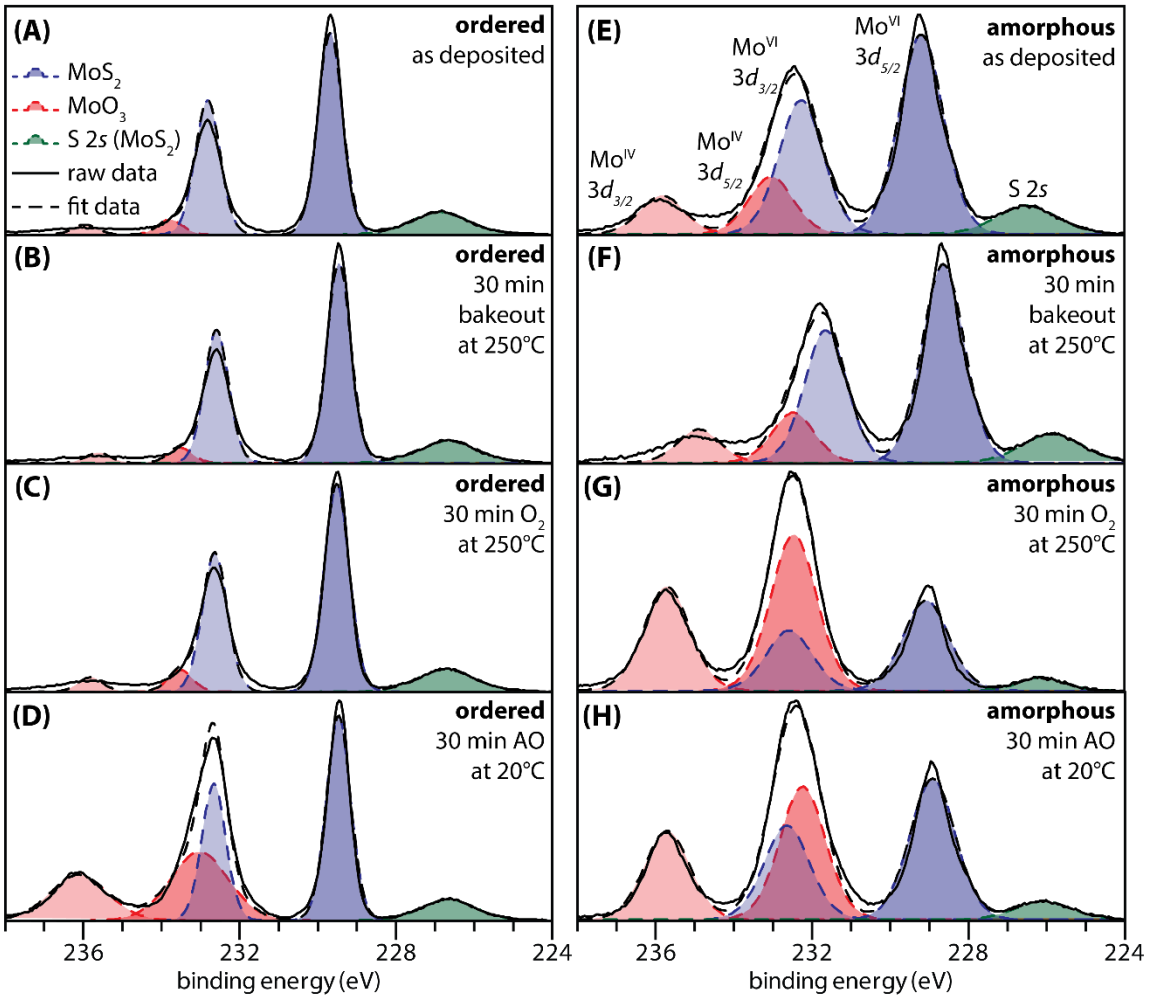

Fig. 6-9. Mo (3d) and S (2s) photoelectron signals for sprayed (**A-D**) and PVD (**E-H**) MoS_2 films after each type of exposure. Blue doublet peaks represent the Mo^{VI} $3d_{5/2}$ (XX eV) & $3d_{3/2}$ (XX eV) MoS_2, red doublet peaks represent Mo^{IV} $3d_{5/2}$ (XX eV) & $3d_{3/2}$ MoO_3 and a green peak centered at ~226.3 eV for S 2*s*. The photoelectron signal is shown as a solid black line with the fitted envelope as an overlaid dotted line.

Baltrusaitis et al have also shown that there is a possibility of shake-up satellite peaks forming associated with MoO_2 and an interstitial state of Mo^V that can overlap with MoO_3 peaks in the Mo 3p signal, giving relatively less MoO_3 signal for Mo 3d [145]. This may be more feasible as Mo 3d signals across the board exhibited lower signals from MoS_2 and higher signals from MoO_3. One last possible cause for the differences which would also make sense for all signals changing similarly would be the surface sensitivity of each

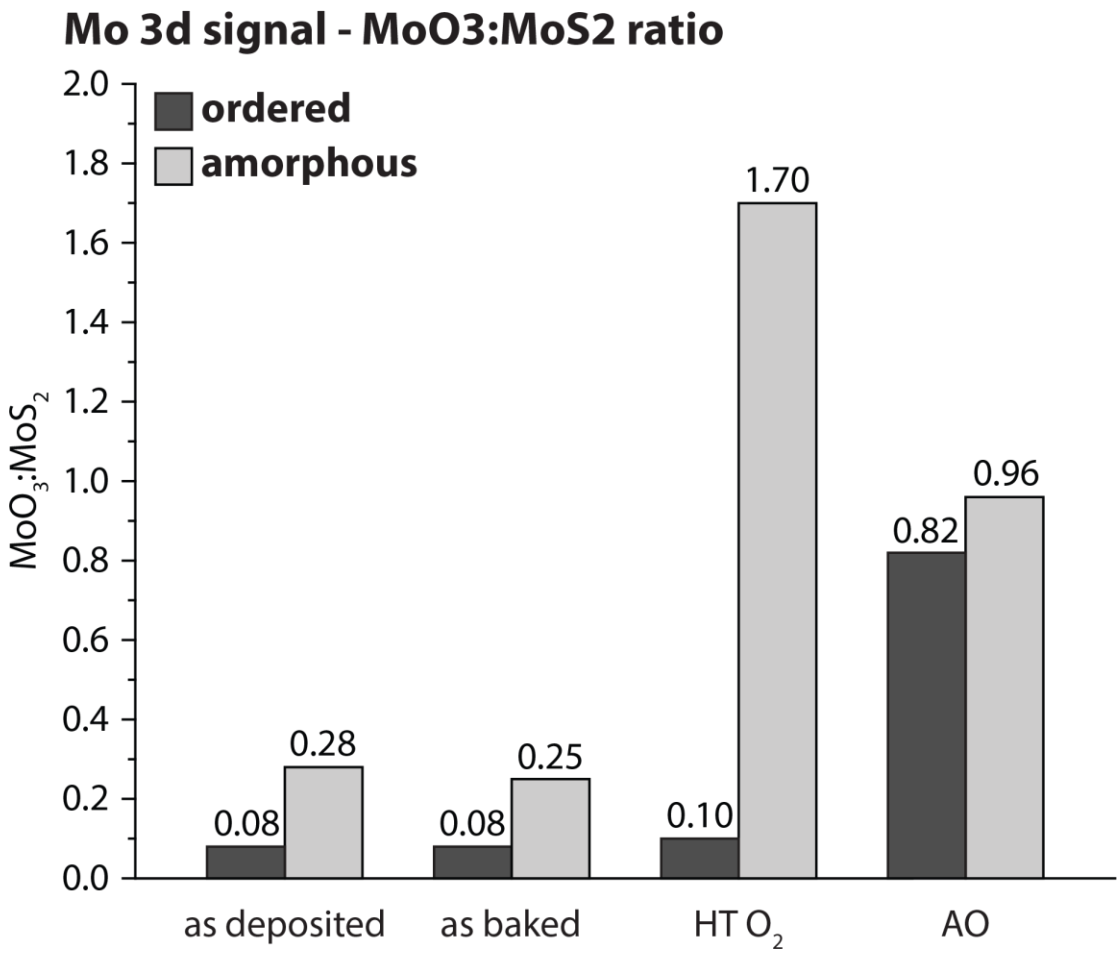

Fig. 6-10. MoO_3:MoS_2 ratios for Mo 3d signal.

signal. Lower binding energy signals denote high kinetic energy electrons which come from deeper in the substrate. This would mean that Mo 3d signals should be giving signal from greater depths where more MoS_2 is present if the oxidation is largely limited to the first 3-4 nm in any situation. It is still interesting to see that the ratio for ordered films exposed to atomic oxygen do not change between Mo 3p and Mo 3d signals. Nonetheless, the results for either doublet show the same trend and agree well with previous results in the HS-LEIS.

These results support findings from the HS-LEIS, showing that sprayed, ordered films of MoS_2 are more resistant in general to oxidative environments. XPS confirms the

presence of oxidation via MoO_3 formation in these films and shows that over similar sampling depths between XPS and the full LEIS depth profile, more MoO_3 is present in amorphous films. High temperature (250°C) O_2 gas treatment revealed the largest gap in oxidation between ordered and amorphous films with amorphous microstructures likely allowing for greater diffusion of oxygen gas into the PVD MoS_2 film (as confirmed by the HS-LEIS and tested by MD – see below). Ordered coatings on the other hand limited the effects of molecular oxygen to the first atomic layer for the sprayed MoS_2 films (Figure 6-4). This limitation of oxygen to the first atomic layer was also seen for ordered films exposed to AO, while both coatings showed substantial amounts of oxide present through the surface via XPS (Figure 6-8). The highly ordered initial structure of the sprayed coatings appears to significantly inhibit oxidation (beyond what was present in the as-deposited structure), and all oxidation is limited to the first atomic layer. Amorphous films, however, show significant oxidation in similar conditions. Oxygen composition is higher in the high temperature O_2 aging than the AO, likely because the significantly higher exposure of O_2 (1 atm) than the AO (10-5 mbar).

6.5.5 Molecular Dynamics

To better understand oxygen penetration in to MoS_2 coatings, molecular dynamics (MD) simulations were used to gain an atomistic viewpoint of the system. Specifically, reactive force field (ReaxFF) atomistic molecular dynamic (MD) simulations were utilized to probe the interaction of AO and O_2 with MoS_2. These simulations allows for detailed comparisons of oxidation to those measured experimentally with HS-LEIS and XPS. It is difficult to perfectly recreate or even know exactly what these structures look and behave like at atomistic scales. As such, analog configurations were created to help compare the

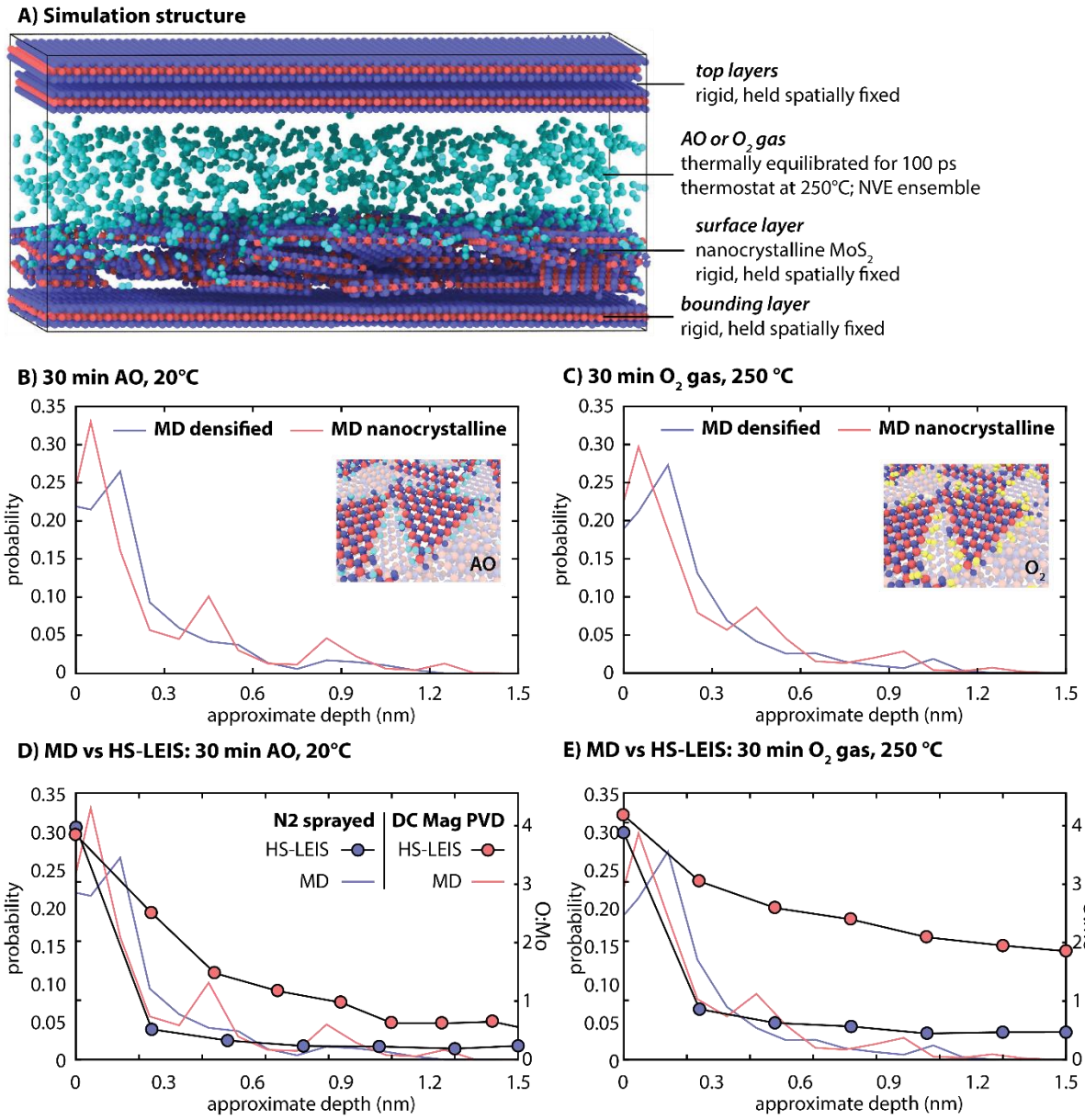

Fig. 6-11. (A) Structure of MD simulation using a reactive force field (ReaxFF) for the interaction between MoS_2 and atomic oxygen and O_2 gas. Normalized probability of oxygen locations as a function of depth into the film for (B) 30 min AO at 20°C and (C) 30 min O_2 gas at 250°C. A top-down view of the nanocrystalline MoS_2 bonded at the edge sites for both exposures are shown in the insets. Comparisons MD & HS-LEIS shown for (D) AO exposed and (E) HT O_2 exposed samples.

experimentally measured nanocrystalline/amorphous PVD and the low-defect, crystalline sprayed films. Amorphous film (referred to as "MD nanocrystalline") were made

consisting of three equally spaced layers of randomly rotated crystallites. Sprayed coatings were difficult to approximate computationally, as it would be computationally expensive to simulate and effectively capture the low defect density in sprayed/ordered coatings. The average flake size would be 100's of times larger than those able to be simulated and result in much less than one defect per simulation volume on average [90]. To approximate the low defect density of the sprayed coating structure, we instead modeled a densified film in by applying a load of 400 nN (normal pressure ~2.3 GPa) over the entire MoS_2 film (referred to as "MD densified"). The MoS_2 - oxygen systems, from the bottom up, consisted of a rigidly held MoS_2 lamella, rigid nanocrystalline MoS_2, gas (AO or O_2, thermally equilibrated for 100ps) and another rigidly held MoS_2 lamella (see Figure 6-11 A). Simulations times were 200 ps at relatively high gas pressures (100 atm) in order to improve observed statistics for both spatial and temporal scales.

Results from the molecular dynamics simulations enabled calculation of the probability of oxygen's presence throughout the depth of each coating analog for both AO and O_2 exposures (Figure 6-11 B and C). Similar to what was seen experimentally in the HS-LEIS, a trend of decreasing oxygen with depth into the MoS_2 was noticed for the MD simulations (Figure 6-11 D and E). The simulations were also able to confirm that room temperature AO can readily react with the outer surface of the coatings as first shown with HS-LEIS and even at MD timescales. It was also found that higher oxygen concentration were present at the surface but also at intervals through the depth corresponding to the spacing between lamellae (i.e. S-S) for MoS_2 of ~0.3 nm [146]. Additionally, the concentration of oxygen on the surface and in between the layers of MoS_2 is reduced by about 10% when a relatively small compressive stress of ~2.3 GPa is applied. This is

comparable to the HS-LEIS experiment, which shows higher concentration of oxygen for amorphous MoS_2 films throughout. Compression, which has the effect of increasing bonding between crystallites and therefore reducing the number of potentially active edge sites, strongly affects the ability of oxygen to diffusion into the film.

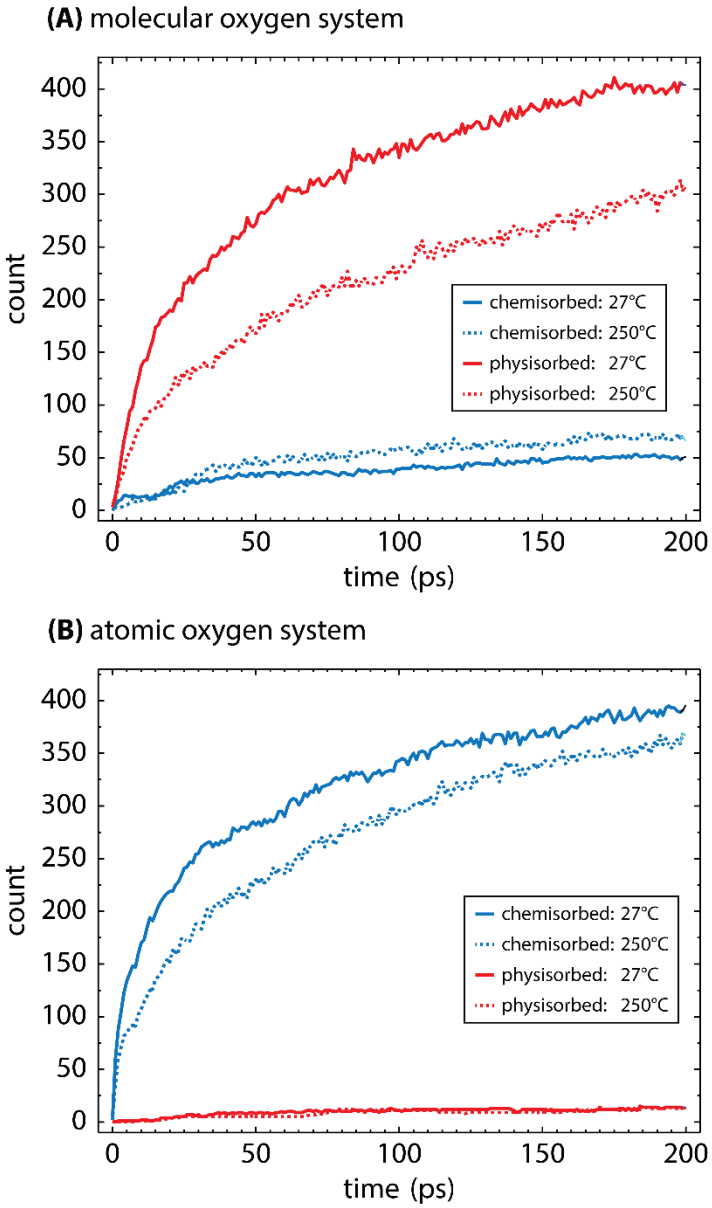

Fig. 6-12. Total bond counts of chemisorbed and physisorbed species in the MD nanocrystalline structured simulation at 27°C and 250°C for (A) molecular oxygen and (B) atomic oxygen

Chemisorbed and physisorbed species could also be calculated by defining a physisorbed species as O_2 or O that does not change electronic structure upon absorption. Chemisorbed species were defined as O_2 or O that underwent an ionic bond with Mo or O. Unreacted O_2 and O as well as dissociated or reacted O_2 are not included in these calculations as they are far higher in bonding counts. Upon initial inspection of the data it is immediately evident that molecular oxygen species are far more likely to be physisorbed (Figure 6-12 A) than atomic oxygen which predominantly chemisorbs to other species in the simulations (Figure 6-12 B). It is also interesting to see that with increased temperature, more oxygen becomes dissociated and some is able to then chemisorb. For atomic oxygen, it also appears that at higher temperatures it more readily reacts with itself and reduces chemisorption to other species.

6.5.6 Friction Tests

6.5.6.1 Steady State Behavior Post Aging

To relate the interaction of these different MoS_2 samples and oxygen species to interfacial mechanical properties, friction was measured on the ordered MoS_2 and amorphous MoS_2 films in their as-deposited and environmentally aged states (Figure 6-13 & Figure 6-14). It is important to reiterate here that comparisons are not intended to be made between O_2 and AO (as there are very different amounts of oxygen in the two aging environments); instead, we are comparing microstructures in the same environment. Typical friction behavior for MoS_2 coatings, as previous studies have shown, begins with initially high friction coefficients and then "runs-in" to a low steady-state friction coefficient [24], [106]. Steady-state friction is an important metric for the long-term performance of a tribological system. The steady-

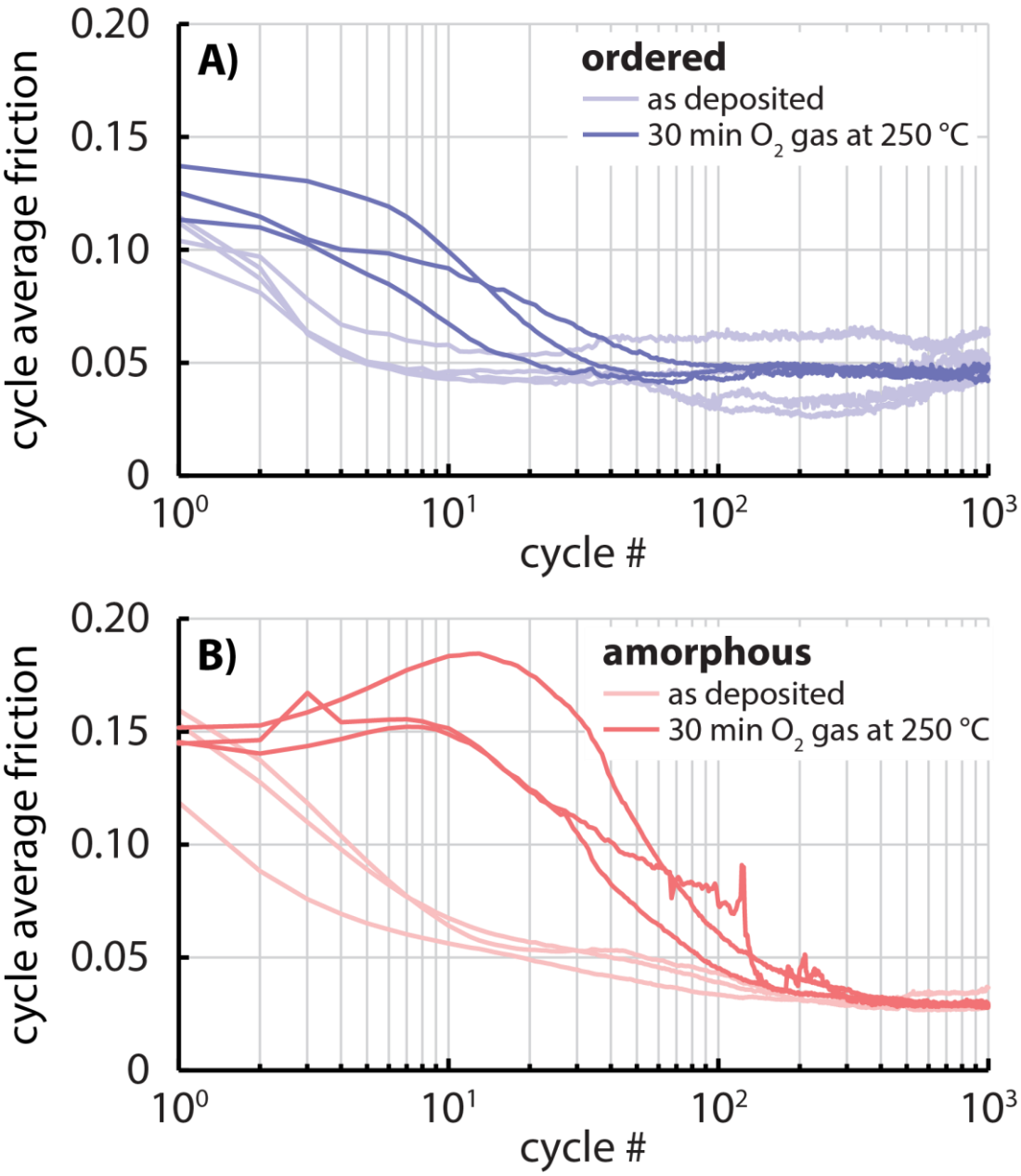

Fig. 6-13. Cycle average friction coefficients are plotted for ordered (A) and amorphous (B) MoS_2 films after treatment for 30 minutes in O_2 at 250°C. In each case, the as-deposited coating is plotted for comparison.

state friction coefficient, μ, is ~ 0.05 – 0.06 for sprayed MoS_2 and is not significantly impacted by aging. Amorphous MoS_2 has generally lower steady-state friction than sprayed MoS_2, likely because of better coverage and increased thickness of the amorphous

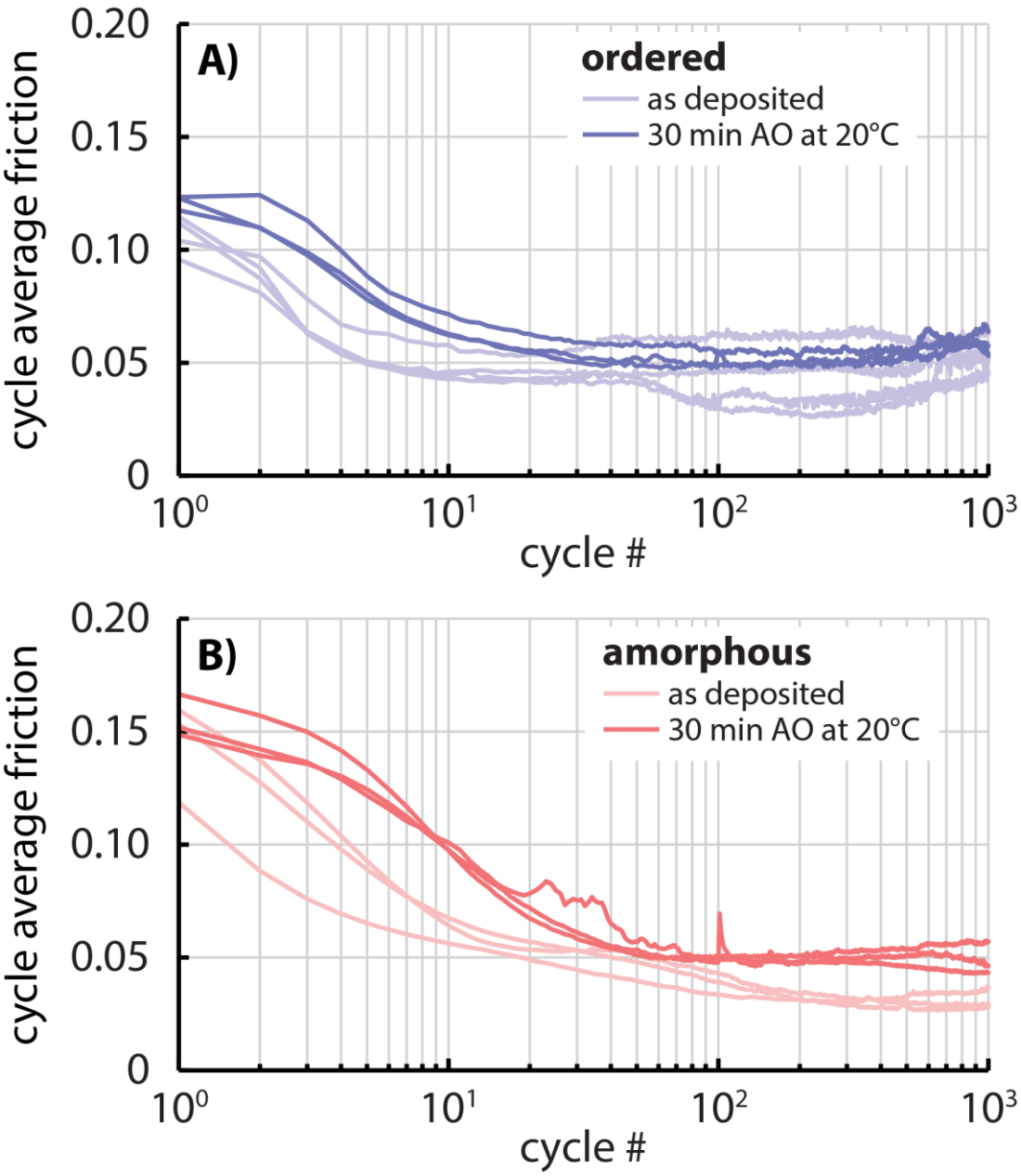

Fig. 6-14. Cycle average friction coefficients are plotted for ordered (A) and amorphous (B) MoS_2 films after treatment for 30 minutes in AO at 20°C. In each case, the as-deposited coating is plotted for comparison.

PVD films (~2 µm compared to ~200 nm) [147]. The steady-state friction coefficient for the AO exposed amorphous MoS_2 was ~0.055, approximately 2 times higher than as-deposited or HT O_2 amorphous MoS_2 (even though there was orders of magnitude more oxygen in the HT O_2 exposure). We hypothesize that although O_2 penetrates more than

AO, the penetrated AO is highly reactive and forms oxides, while O_2 is more likely to be physisorbed as shown by MD simulations.

6.5.6.2 Initial friction Behavior Post Aging

Previous studies showed that initial friction of highly ordered MoS_2 is lower than amorphous MoS_2 [90]. This extends to AO and HT O_2 treated MoS_2, as initial friction coefficients (first sliding cycle) are consistently lower for sprayed coatings (Figures 6-13 & 6-14). The environmental aging resulted in a slight increase in initial friction (~20%) for both AO and HT O_2. Friction is affected for the sprayed coatings aged with AO or HT O_2, even though oxygen is limited to the first atomic layer (Figure 6-4).

The run-in time it takes for the coatings to reach low friction ($\mu < 0.06$) also varies between coating and aging types. Similar to initial friction, highly ordered sprayed coatings consistently ran in faster than the amorphous PVD in every environment. Samples aged in oxygen gas at 250°C for 30 minutes exhibited the largest differences in time til run-in with amorphous coatings taking hundreds of cycles prior to reaching close to steady state values

of friction. These amorphous HT O_2 samples also exhibited the greater amount of oxidation in XPS, nearly 8 times that of its sprayed/ordered counterpart.

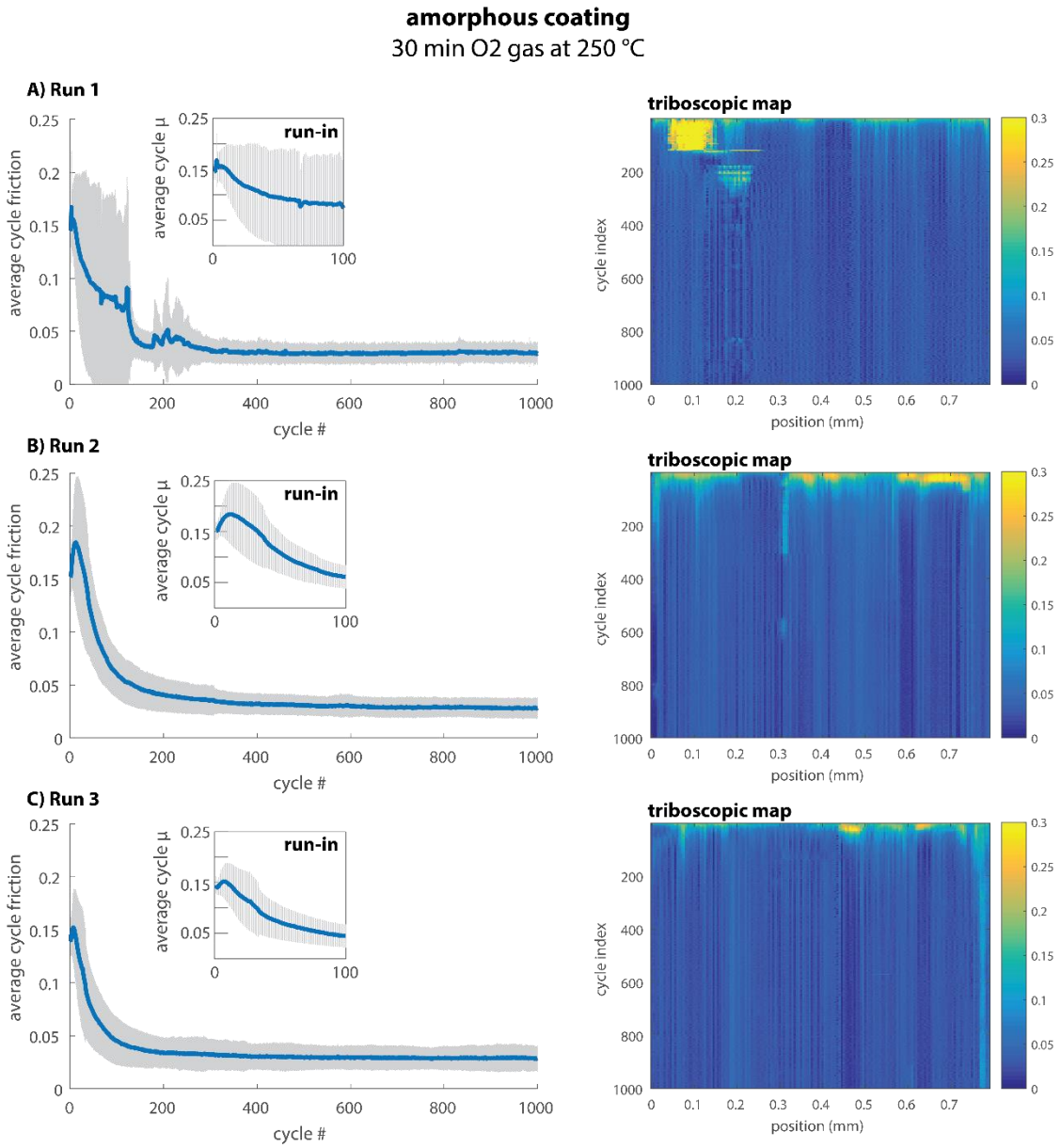

Fig. 6-15. (A-C) All three 1000 cycle friction tests are shown for the amorphous coating exposed to 30 min O_2 gas at 250 °C. Inset depicting the run-in during first 100 cycles is shown alongside the representative friction map showing time and space resolved friction coefficient

Figures 6-15 through 6-18 show the three tests for each coating under each environmental exposure in linear scale with standard deviation bounds as well as friction

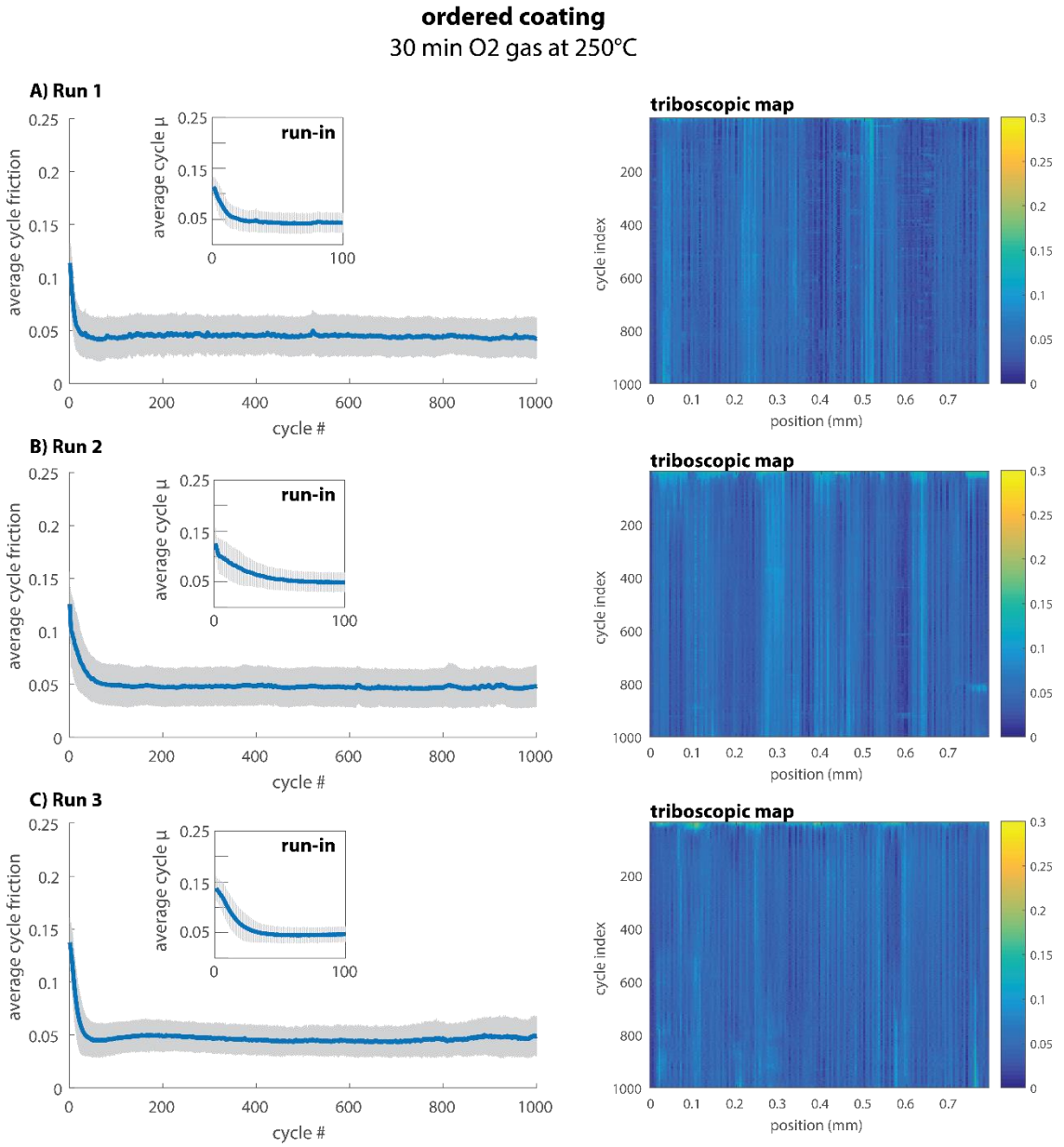

Fig. 6-16. (A-C) All three 1000 cycle friction tests are shown for the ordered coating exposed to 30 min O_2 gas at 250 °C. Inset depicting the run-in during first 100 cycles is shown alongside the representative friction map showing time and space resolved friction coefficient

maps to help visualize the evolution of friction coefficient over time and across the wear track. From the friction maps for the amorphous HT O_2 it can be seen that there are many erratic high friction events that occur across the wear track in these first 100 cycles. Such high friction events due to oxidation could be very problematic for many single actuation

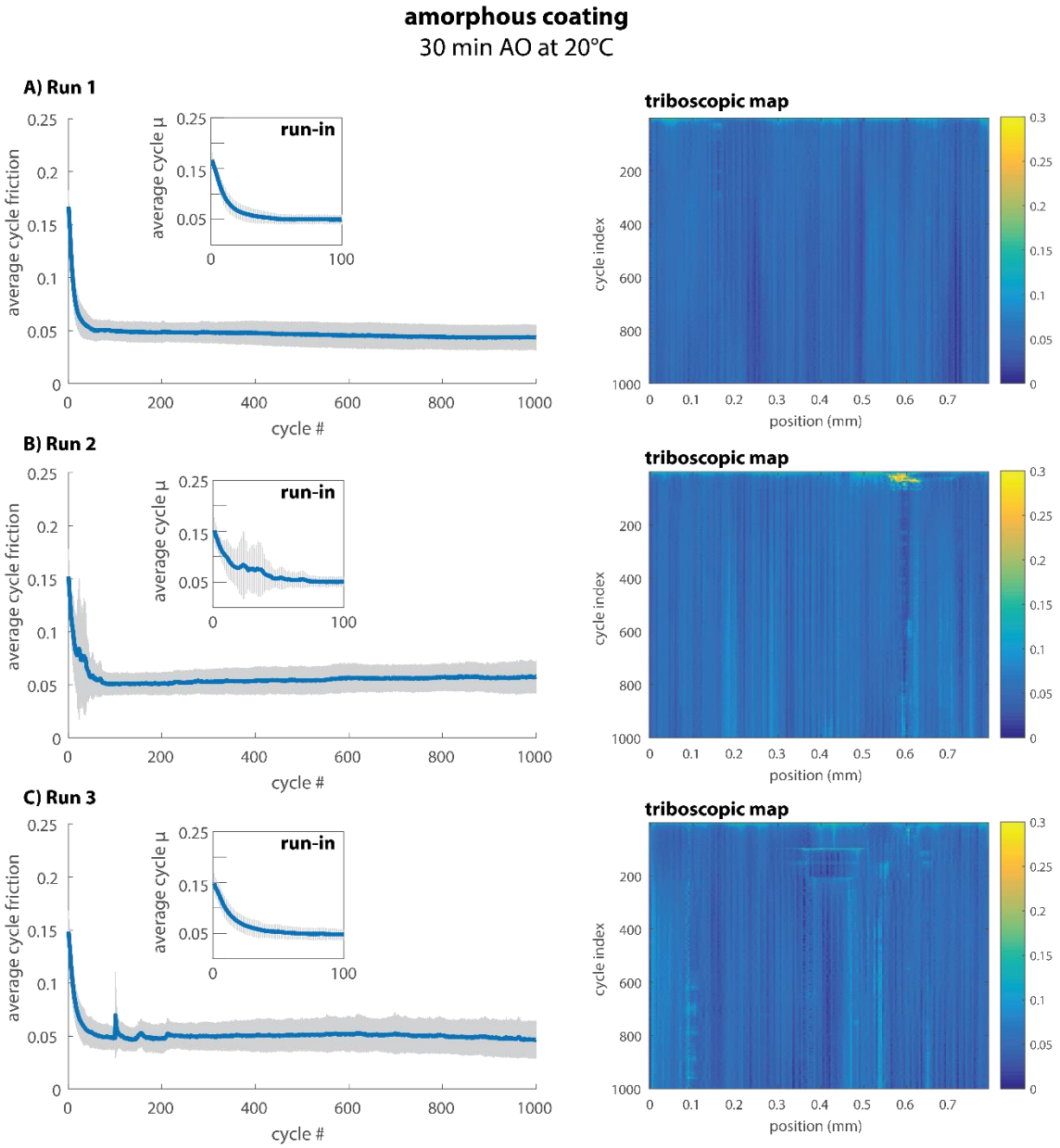

Fig. 6-17. (A-C) All three 1000 cycle friction tests are shown for the amorphous coating exposed to 30 min AO 20 °C. Inset depicting the run-in during first 100 cycles is shown alongside the representative friction map showing time and space resolved friction coefficient

devices. Initial friction and run-in is important for devices that are stored and aged for long periods of time before deploying (*e.g.* satellites) [11], [102], [148]. The effects of aging time were not studied, but will be a topic of future work.

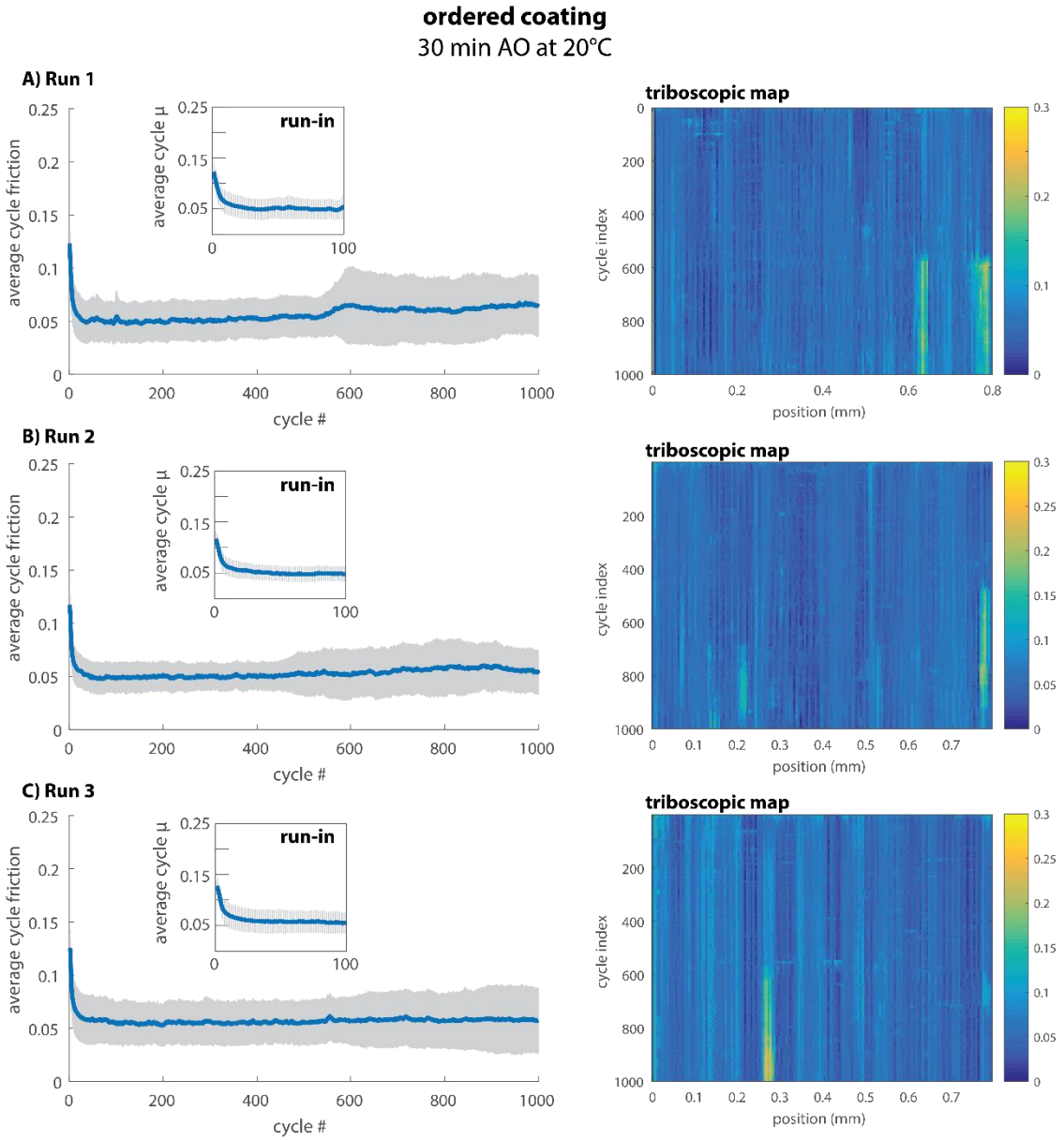

Fig. 6-18. (A-C) All three 1000 cycle friction tests are shown for the ordered coating exposed to 30 min AO 20 °C. Inset depicting the run-in during first 100 cycles is shown alongside the representative friction map showing time and space resolved friction coefficient

6.6 Summary of Chapter Findings

In this chapter, we conclude that by simply altering the microstructure of MoS_2 films, oxidative resistance can be greatly amplified. We used HS-LEIS and XPS to provide new insights regarding the surface composition of thin MoS_2 films after exposure to oxygen at various temperatures. Highly ordered MoS_2 films with surface-parallel basal orientation

are significantly more resistant to oxidation than amorphous (sputtered) MoS_2 films. Amorphous microstructures were very susceptible to oxidation throughout the depth of the film in either type of environment tested. In ordered microstructures, high temperature oxygen gas appeared to mostly physisorb to the surface of ordered coatings and likely interact with any available edge sites while atomic oxygen exposures were able to oxidize the entire surface of the ordered coating (Figure 6-19). More importantly, these sprayed/ordered coatings limited oxidation to the first atomic layer in either case (as revealed by HS-LEIS and XPS), which enables consistently lower friction on initial sliding and substantially shorter time until reaching steady state friction performance. This result can impact numerous applications for MoS_2 in oxidative environments, including lubrication for space machines and mechanisms with implications regarding the role of filler species in MoS_2-based nanocomposites, a controversial topic of ongoing investigations.

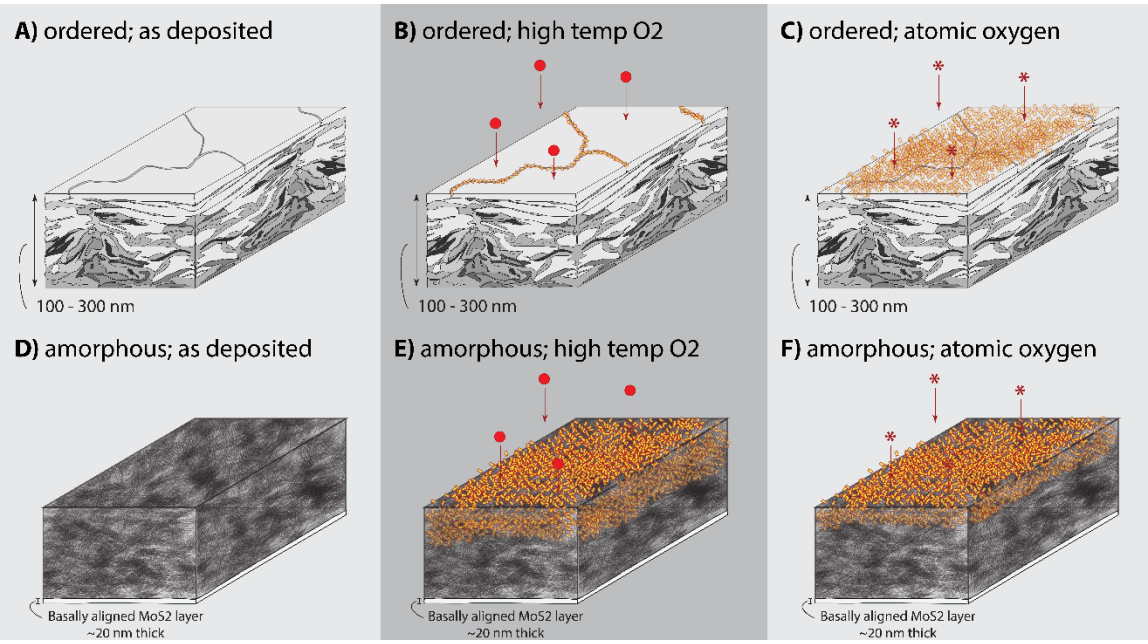

Fig. 6-19. Hypothesized model for the effect of microstructure on oxidation resistance of (A-C) ordered and (D-F) MoS_2 coatings.

7. Run-In, Commensurability and Other Factors Affecting Friction

7.1 Overview & Motivation

In this chapter, we delve further into the mechanisms behind initial friction behavior, or run-in, of MoS_2 films. A better understanding the internal processes and external factors that dictate the evolution of friction behavior is a unique challenge and incredibly valuable to engineering applications. Many moving mechanical assemblies in space and aerospace components must be specifically designed to account for weight, power consumption and reliability. Generally, MoS_2 coatings experience increased friction for the first 10's of cycles from a variety of internal and external factors. If unaccounted for, initial high friction transients could be harmful in many ways such as an undue burden on the mechanical reliability of assemblies, increased power consumption upon component startup and interference from spikes in torque from motor systems to name a few [11], [102], [149].

Run-in of MoS_2 films poses a unique challenge, as there are likely many contributing factors. Shear induced re-orientation is thought to be a contributor to increased friction during run-in [18]–[20], especially in amorphous coatings as shown in Chapter 1. This can be seen as a microstructural evolution process in which MoS_2 crystallites transition to a surface normal (basal planes parallel to sliding surface) orientation in an attempt to minimize edge exposed sites and maximize basal surface area (and possibly joining and increasing in crystallite size) [150]. Formation of a transfer film in the first few sliding cycles is also thought to be a requirement in achieving low friction behavior of MoS_2 films [21]–[23]. It is important to mention here that the ability of MoS_2 to transfer to

a counterface is well documented [21]–[23], but isolating the ability of transferred MoS_2 to provide lubrication has not yet been studied. Presence of contaminants on the surface such as water, oxides and hydrocarbons are also thought to contribute to increased friction upon first sliding [27]–[30].

To account for these factors and prevent possible failure, it is common practice to first run the coatings in prior to service[151]**.** As such, a previously run-in coating should be able to provide low friction from the onset but this, unfortunately, is not entirely true. Johnson and Vaugh were some of the first to show that if a MoS_2 coating is left to sit after run-in, upon restarting a test in the same spot friction once again increases[27]. There are only a handful of additional studies on these friction transients and most attribute the phenomenon to adsorption of water or contaminants[28]–[30]. It has also been shown that cleaved MoS_2 surfaces are extremely inert, with a very low sticking probability for water on basal planes and moderate probability on edge sites[152]. As such, there is much confusion as to what the mechanisms responsible for increased friction during run-in are, how they all affect one another, and what more we can do to learn about them and apply this knowledge to develop better coatings. In this chapter, we propose additional mechanisms that may contribute to the increased initial friction behavior of MoS_2 films.

7.2 Hypothesis

It is hypothesized that initial friction in MoS_2 films, and transient increases after dwell times, is not solely affected by the presence of contaminants such as water, oxygen and hydrocarbons, but a variety of factors, some intrinsic to the microstructure of MoS_2. It is also postulated that the degree of commensurability between flakes of MoS_2 is a factor that determines the friction behavior in MoS_2, specifically in relation to increased friction

during run-in and transients after dwell periods. Many have demonstrated or postulated that superlubricity via incommensurate contact is relevant in MoS_2 [106], [153]–[156] as it was shown for graphene [92], [157], [158]. In this case, we believe that over time and depending on temperature, flakes of MoS_2 will settle into commensurate contact and contribute to initial friction upon sliding. Initial friction is recorded after various dwell times following run-in of MoS_2 coatings at different temperatures to explore this hypothesis. Supplementary studies on the dependence of friction on temperature are also carried out. The temperature resolved friction studies are also quite interesting on their own as the thermal behavior of friction in MoS_2 is hotly debated. Molecular dynamics simulations are also included on the effect of temperature from collaborators to better understand this behavior.

Apart from temperature and commensurability, load dependencies were also assessed, with various substrates acting as the pin material. It is a known factor that MoS_2 exhibits stress dependent behavior, yet the role of substrates on this behavior is not well known and how these substrates influence initial friction is also poorly understood. It is postulated that materials of differing elastic moduli will affect friction via increased contact area up until a point where the substrate begins to yield and plastic deformation will prevent a further decrease in friction with load. Preliminary experiments were also conducted to assess the link between load and environment on the run-in of MoS_2 via a combined spiral orbit tribology and XRD study. These studies were done with the intent of monitoring the evolution of basal orientation in the first few cycles of sliding and how this changes due to increased load or the presence of water. It is expected that higher loads will cause a film to run in faster and show a greater degree of basal orientation in the XRD pattern. The

presence of water is thought to disrupt the formation of crystallite formation, but this does not necessarily translate to a change in basal orientation.

7.3 Experimental Methods

7.3.1 Tribological Testing

7.3.1.1 High Temperature Friction Tests & Stop Time Study

Friction measurements were made on a custom-built cam-driven microtribometer over a range of temperatures. Like previous studies by Babuska et al, a temperature ramp from room temperature (25°C) to cryogenic temperatures (-150°C) and back again was conducted during sliding in a dry nitrogen environment (<10 ppm O_2; <10 ppm H_2O) to assess any thermal dependence on friction [159]. Pure MoS_2 coatings were magnetron sputter deposited by Tribologix Inc. on 440C stainless steel coupons to a target thickness of 300 nm. Tests were run at 1 N dead weight load against 440C stainless steel pins at an average speed of 3 mm/s.

Additional testing was done in the cam-driven tester to assess the change in friction after stopping and resuming sliding after certain time intervals. A friction test was first run to approximately 200 cycles which was enough time for the MoS_2 to reach a low steady state friction of $\mu \approx 0.04$ - 0.05. The tester was then left to sit for 10s, 30s, 1 min, 5 min, 30 min or 2 hours before running another test in the same spot. Tests were run in a dry nitrogen environment (<10 ppm O_2; <10 ppm H_2O) at room temperature (25°C) and at -50°C to see if lower temperatures would be able to freeze out re-orientation of MoS_2 flakes hypothesized as a cause for increased friction during run-in.

7.3.1.2 Stop-Time Environmental Reversals

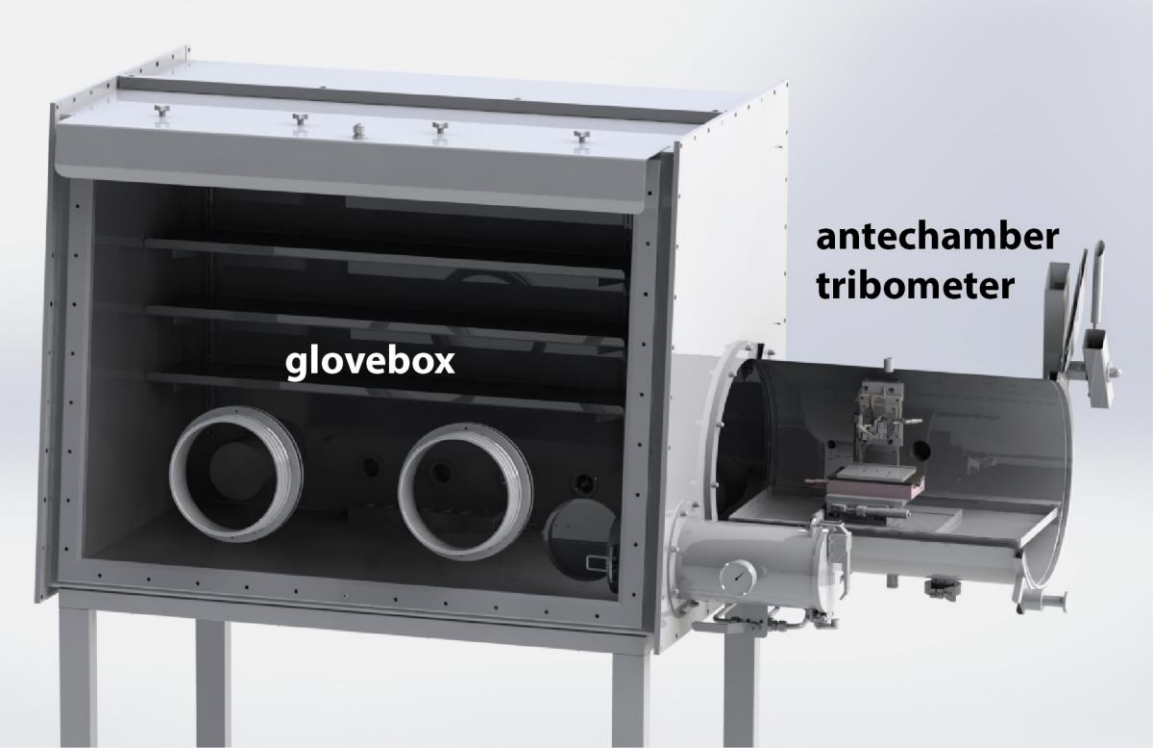

Fig. 7-1. Annotated schematic of the environmental reversal experiments. Testing was done inside the glovebox and quickly brought outside via the antechamber and back in to assess intermittent poisoning on dwell time studies.

To ensure the observed increase in friction is not due to buildup of contaminants or adsorbed water, environmental reversals were conducted. The intent was to run a friction test and expose the entire tribometer to the air outside the glovebox via the antechamber quickly enough such that if increased friction were noticed at wait times that otherwise show less friction increase in a dry run, it would mean that the affect observed is not strictly due to the presence of contaminants (Figure 7-1). This process resulted in three successive tests run on the same wear scar: 1) Run a friction test in a dry environment, 2) Expose the instrument and sample to outside air and return to dry nitrogen environment for a second test until fully run-in, 3) Run a third and final test in dry nitrogen. The increase in friction from the steady state portion of stage 1 as compared to stage 2 is considered the

contaminated stop time value. The increase in friction from the steady state portion of stage 2 as compared to stage 3 is recorded as the dry stop time value for comparison.

The amount of time it took to pump down and flush the antechamber enough times to ensure cleanliness of the main chamber initially limited our wait time in between tests to 10 minutes. Replacement of the provided Edwards RV12 vacuum roughing pump for our glovebox with a higher displacement rate Varian dry scroll vacuum pump enabled lower pump down times and subsequently quicker reversals down to 5 mins while keeping the glovebox under 10 ppm H_2O.

7.3.2 Molecular Dynamics Simulations

Molecular Dynamics simulations were carried out by collaborators to confirm two hypotheses: 1) Friction exhibited a thermal dependence and 2) MoS_2 exhibited bimodal energy barriers to sliding based on the commensurability of atomic planes. The first experiment was built to simulate many small, triangular nanocrystalline flakes held in between rigid sheets of perfect MoS_2 similar to the MD shown in the previous chapter (Figure 7-2). Friction coefficients were calculated over a range of temperatures. The second experiment utilized nudged elastic band (NEB) models to calculate energy barriers to sliding. These calculations do not consider the speed, load or dissipation in the system, they

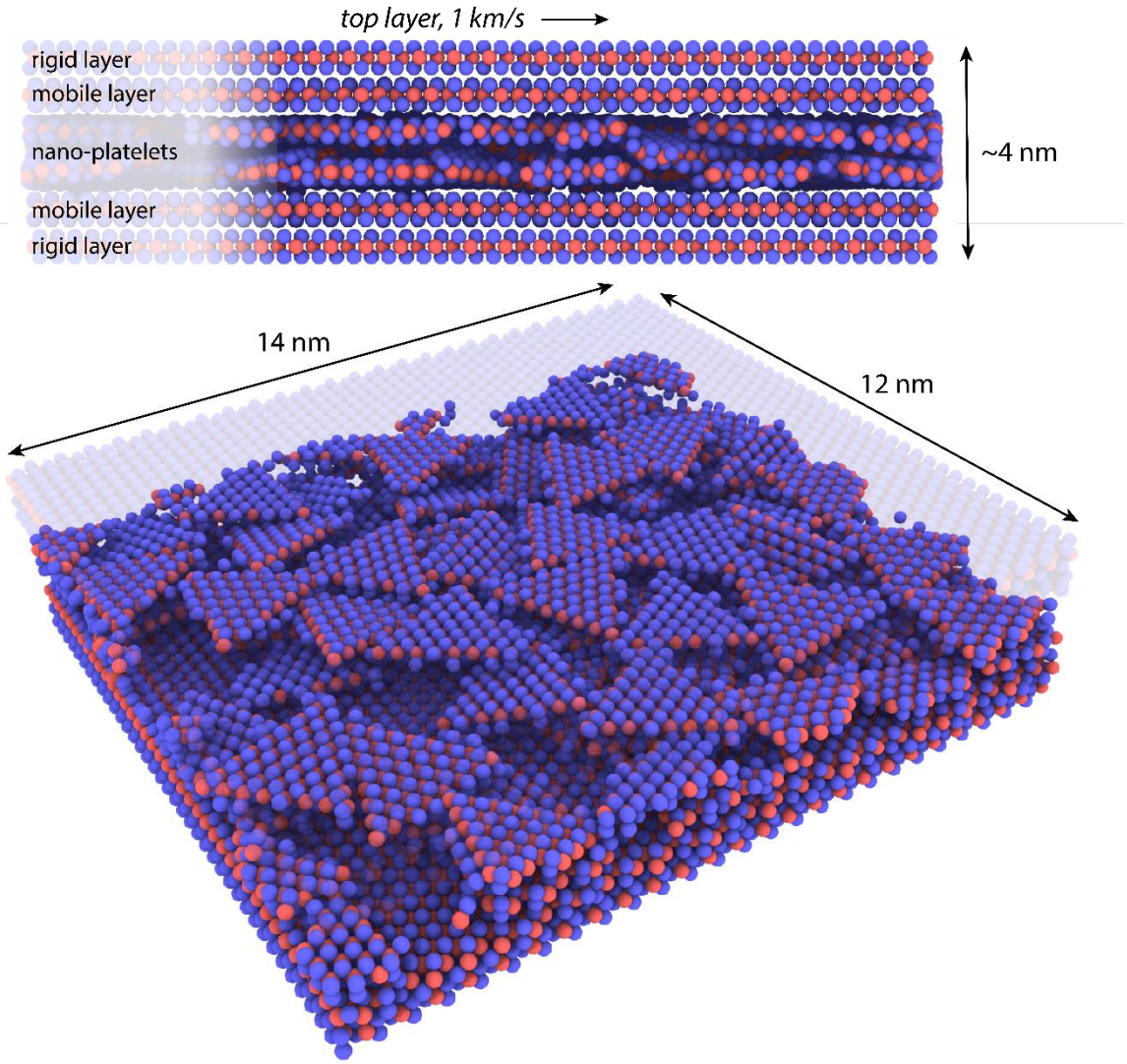

Fig. 7-2. Schematic of MD simulation relating temperature to friction. The system is bound top and bottom by rigid *MoS2* layers with mobile layers sandwiching two lamellae of randomly oriented nanocrystalline flakes of *MoS2*.

simply force (in this case) a unit cell of MoS_2 to sit at various locations sliding along a perfect sheet of MoS_2 and calculate the energies at these locations no matter how unfavorable.

7.3.3 Load & Substrate Dependence

A study was also done to assess the effect of load and substrate on the shear strength of MoS_2, similar to studies done by Singer [117]. Experiments were run on a CSM flexure based microtribometer similar to the custom built one described in the methods section.

Tests were run at 1 mm/s with a 2mm stroke at 100 – 1000 mN in 100 mN steps and 10 – 100 mN in 10 mN steps. Copper, nickel and 440C steel pins were used as well to understand how materials with different hardness and modulus affected friction as a function of contact pressure.

7.3.4 Spiral Orbit Run-In & XRD

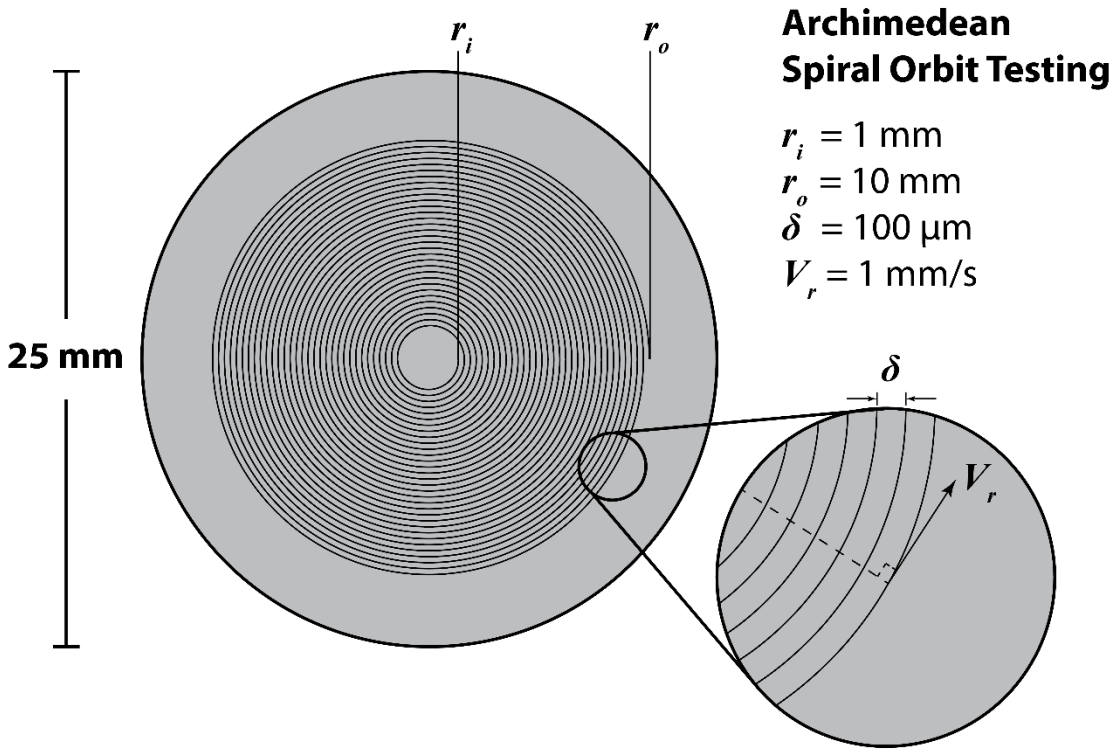

Fig. 7-3. Annotated schematic of an Archimedean spiral wear scar created during a spiral orbit test. Spacing between spirals (**δ**) was 100 µm with an initial radius of 1 mm and outer radius of 10 mm. Angular speed and retraction of the pin head were matched such that tangential velocity during sliding ($\mathbf{V_r}$) was 1 mm/s

In line with the study on load dependence, preliminary experiments were carried out on a spiral orbit tribometer at 100 mN and 1000 mN in dry nitrogen and humid nitrogen. The spiral orbit tribometer was used to allow for large, compact worn areas that could then provide a large enough surface area to study in the XRD to monitor any changes to the structure of the film such. Specifically, these tests were designed to observe whether or not

load influenced the formation of basal orientation during the first 10's of cycles when run-in occurred. This study was inspired by an experiment done by Fleischauer which showed a noticeable increase in the 2θ diffraction pattern peak at 14° indicating a growth of basal orientation during the first cycle of sliding for sputtered coatings prepared with various sputtering conditions [121]. The shape of the spiral was archimedean which restricts the radius to grow in equal spacing. Spacing used in our experiments was 100 μm from an inner radius of 1mm to 9mm outer radius. Experiments were run at a tangential velocity of 1 mm/s (Figure 7-3).

7.4 Results

7.4.1 Temperature Resolved Friction Tests

Temperature resolved friction data revealed a thermal dependence on the friction behavior of PVD sputtered MoS_2 films (Figure 7-4 A). During initial sliding, while ramping temperature down to -150°C, the coating exhibits friction coefficient behavior higher than that of the return to room temperature. Below 200K and for the remainder of the test, friction shows a gradual increase in friction at lower temperatures. These results are similar to those showed in a previous publication by Babuska et. al with similar activation energies (0.8 kJ/mol) using the same experimental setup and sputtered coatings [159]. We can then plot the room temperature normalized friction coefficient vs inverse normalized temperature to ascertain if friction is thermally driven and follows typical Arrhenius behavior (Figure 7-4 B). The return portion of the test appears to fit best to a modified exponential form instead of a purely Arrhenius behavior. This modified

exponential also interprets friction as having real bounds at T=0K instead of infinity as would be the case with a typical Arrhenius function.

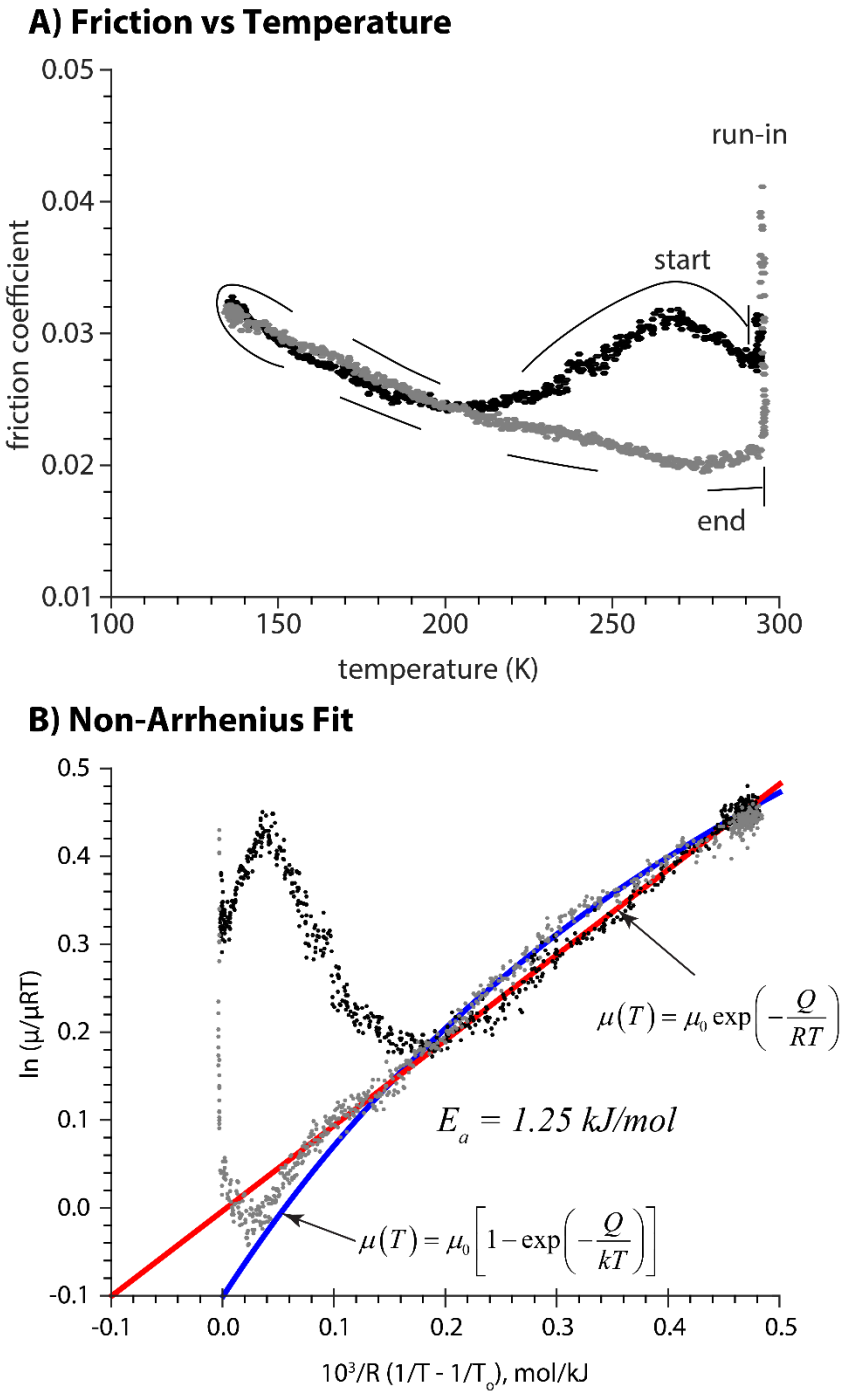

Fig. 7-4. (A) Friction results from temperature ramp done on cryogenic tribometer at 1N load, 1/8" countersurface at ~ 3 mm/s. As temperature was ramped from room temperature down to -150°C and back, an Arrhenius like trend was noticed and (B) shown to exhibit a non-Arrhenius exponential fit

7.4.2 Molecular Dynamics: Temperature & Commensurability

Molecular dynamics simulations carried out by collaborators at Sandia (described in methods) confirmed this temperature relationship. A series of simulations carried out at separate temperatures showed a similar trend in activation energy (1.37 kJ/mol) vs experiments (1.25 kJ/mol), yet were noticeably higher in friction coefficient (Figure 5 A). When normalized by the theoretical minimum friction coefficient at T=0K, however, these curves fall quite well on top of one another (Figure 7-5 A). Even at lower temperatures the simulations were able to similar behaviors with friction approaching a constant value at T=0K.

Nudged elastic band (NEB) simulations were also employed to understand how commensurability would affect the energy barrier to sliding. A unit cell of MoS_2 misoriented 30° relative to the MoS_2 basal plane below exhibited 3 times less peak energy barrier to sliding (0.065 J/atom) than a commensurate flake in sliding (0.195 J/atom) (Figure 7-6).

7.4.3 Temperature Dependent Friction Transients

Stop time experiments run at different dwell times at room temperature and -50°C showed interesting differences (Figure 7-7). At room temperature with dwell times below 10 minutes, no difference was noticed between the steady state friction during initial run-in and the initial friction for the test to follow on the same track. For the same range of dwell times (below 10 minutes) run at -50°C, no appreciable increase in friction transients were noticed, but the friction was on average higher than tests run at higher temperatures. After 10 minutes of dwell time friction transients became noticeable. For the room

temperature case, initial friction after dwell nearly doubled from μ = 0.04 to μ = 0.08. At -50°C, this relationship was not as pronounced, with $\Delta\mu \approx 0.01$.

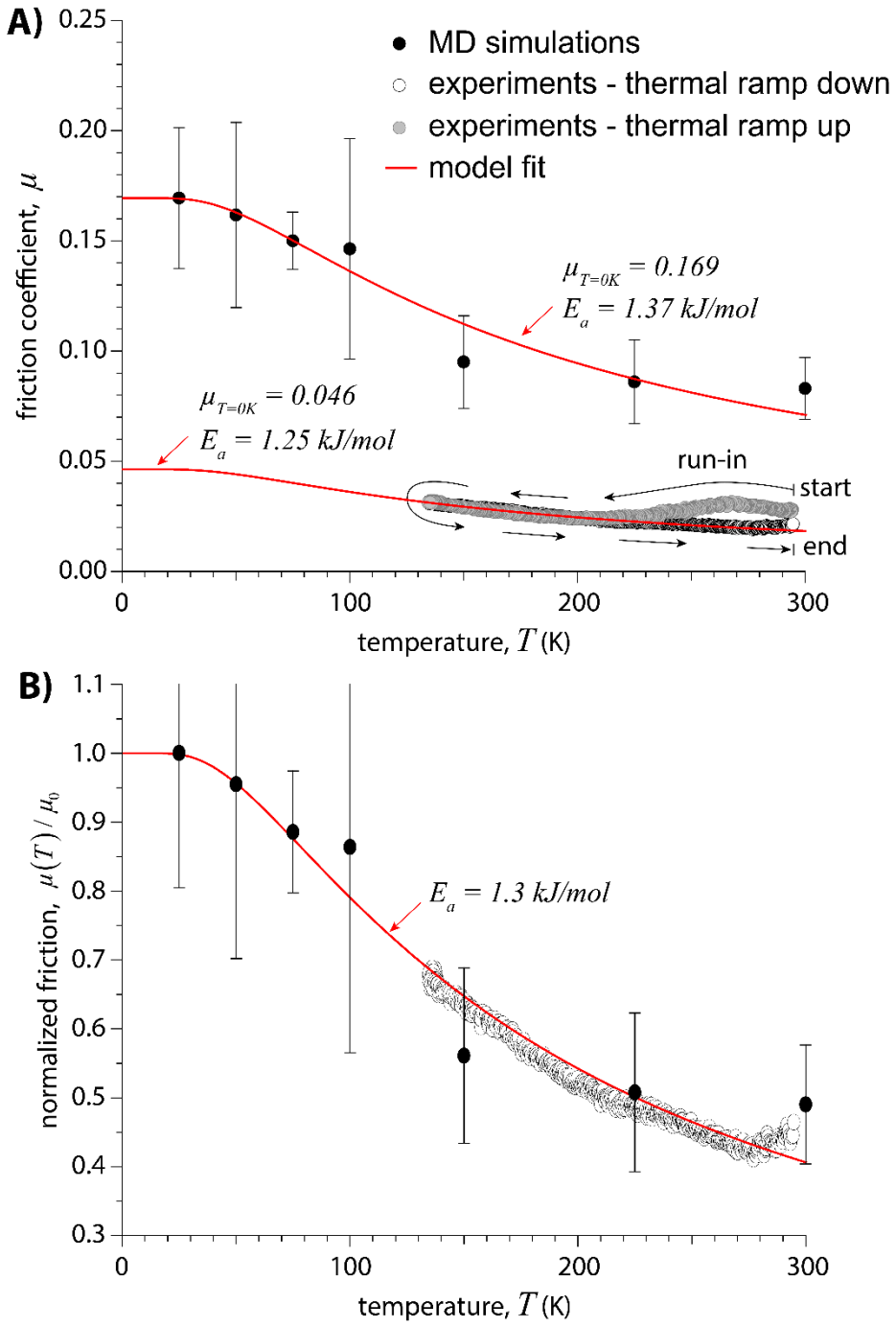

Fig. 7-5. (A) Friction from Figure 7-4 results and MD simulations showing activation energies of fits through data and (B) the friction data normalized by 0K initial friction estimates.

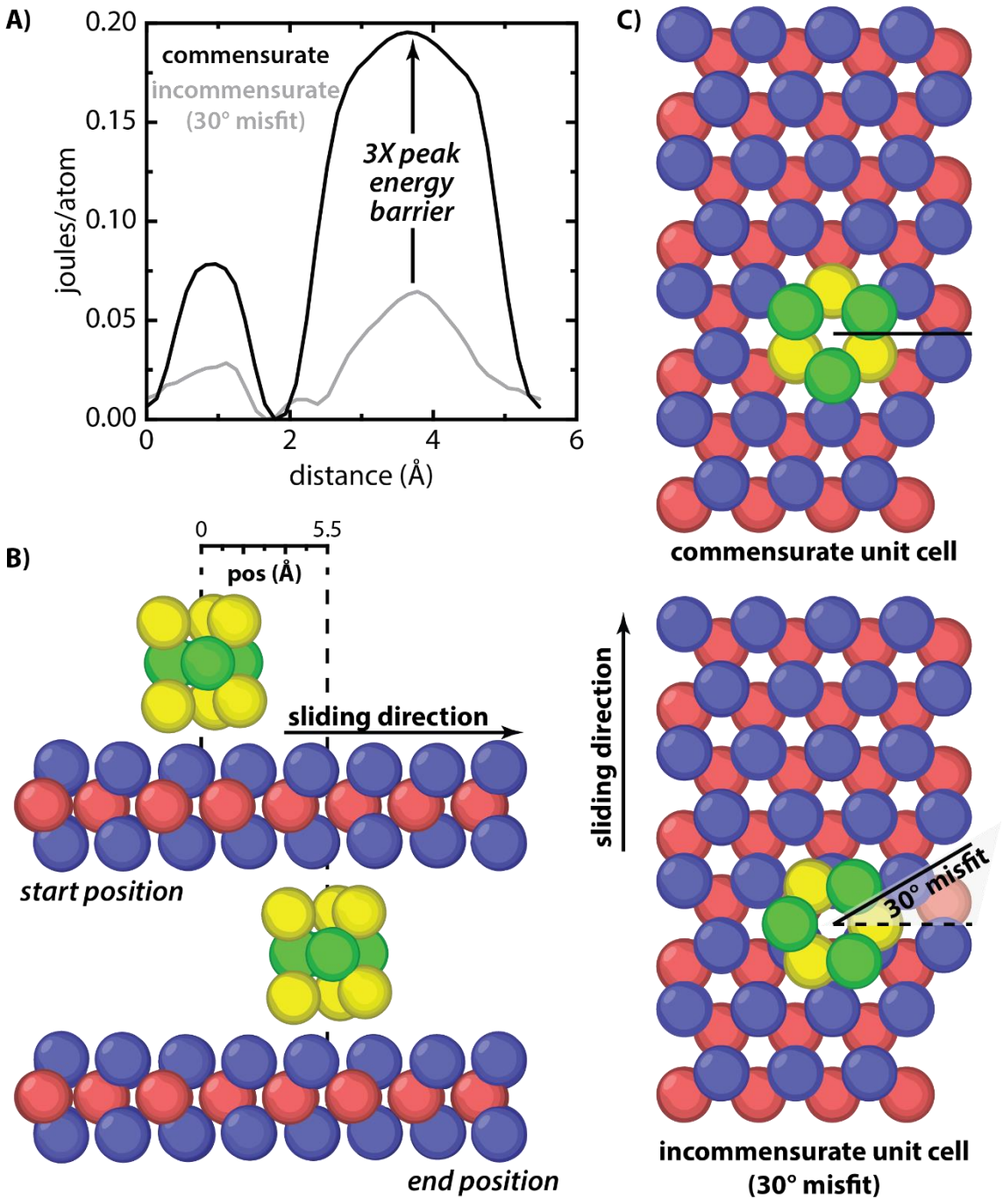

Fig. 7-6. (A) Results from NEB MD simulations showing the difference in energy barrier to sliding for commensurate and incommensurate unit cells of MoS_2 relative to substrate. (B) Side view of simulation showing sliding direction and distance slid and (C) top view

Additional friction transient studies were carried out with intermittent exposures to air.

It should be noted that these intermittent poisoning experiments were carried out on a

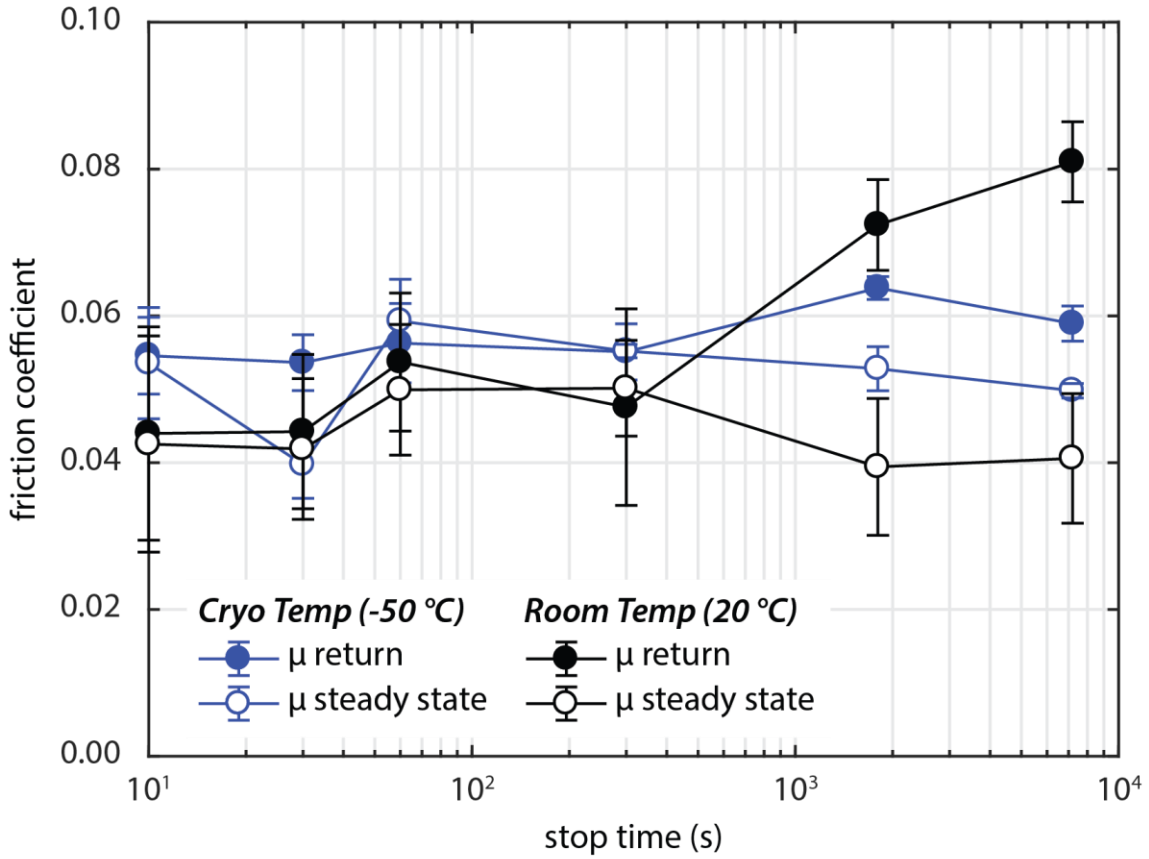

Fig. 7-7. Results from dwell time study. Steady state friction coefficients are determined from the last 50 sliding cycles and compared to initial friction upon resuming sliding after 10s, 30s, 1min, 5min, 30 min and 2 hr dwells. Error bars shown are deviation from sample set of 3 tests per dwell time. Test was conducted at 20°C and -50°C

separate tribometer than the one to do low temperature comparisons which resulted in friction coefficients in general lower by ~ 0.01. In general, dwell times that consisted of an intermittent poisoning of the environment did not appear to affect friction upon running in again as compared to dry dwell time studies at the same length (Figure 7-8 B). An example friction trace of a newly run-in coating and the following long and short dwell time experiment are shown in Figure 7-9. The shortest poisoned exposure time achievable was 5 minutes which showed similar re-run-in friction values to 10 minute exposures. Longer

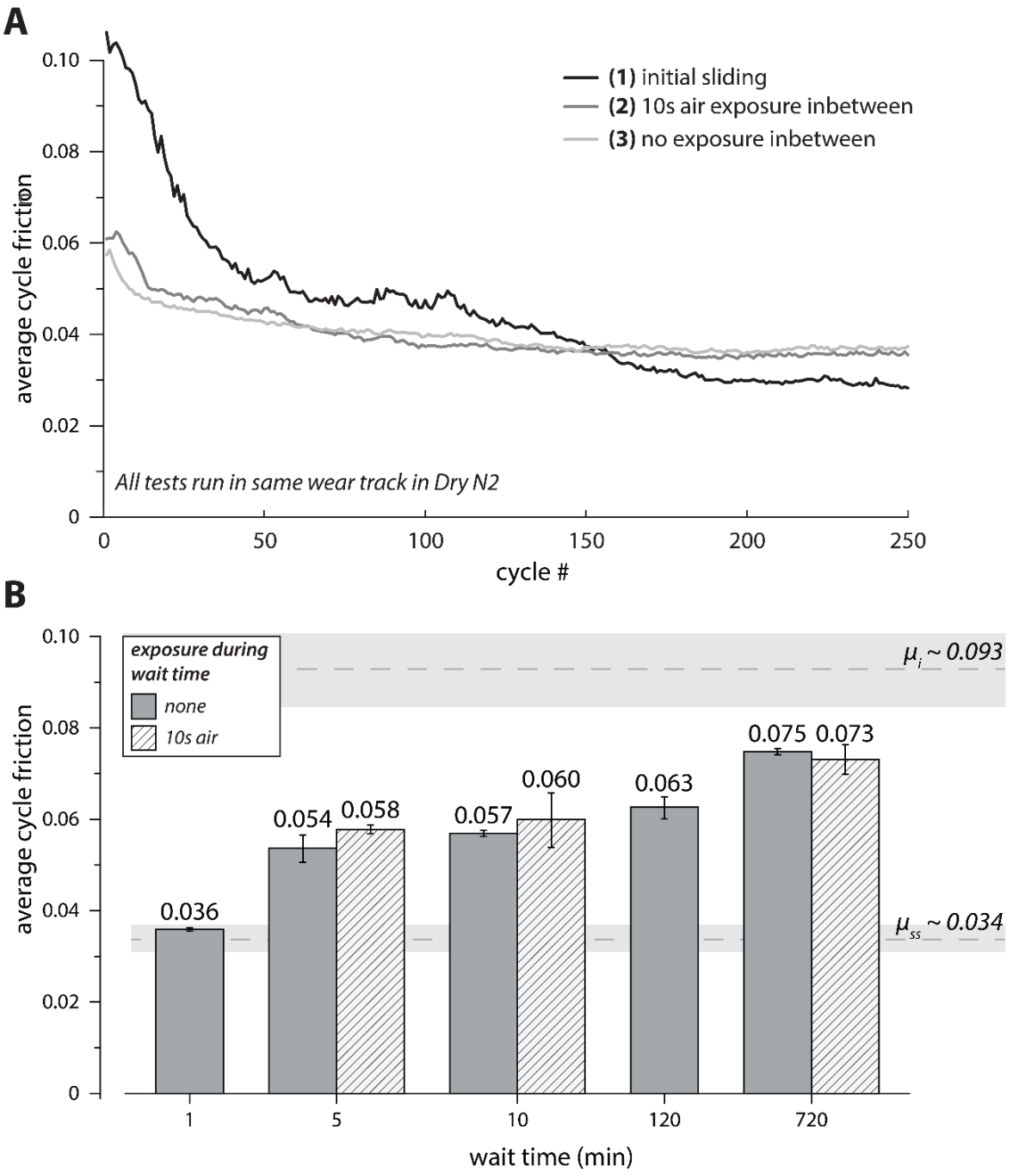

Fig. 7-8. (A) Representative friction traces for a complete cycle of initial run-in, run-in after poisoning and run-in after dry dwells for a given dwell time (B) Bar chart showing average initial friction for a given dwell time with error from 3 separate tests. Gray regions in the background show average initial friction on new tracks and average steady state friction with error across all tests.

dwell times of 12 hours in only dry nitrogen showed further increase in re-run-in friction than those of lower wait times but were fully exposed to ambient conditions for a brief amount of time.

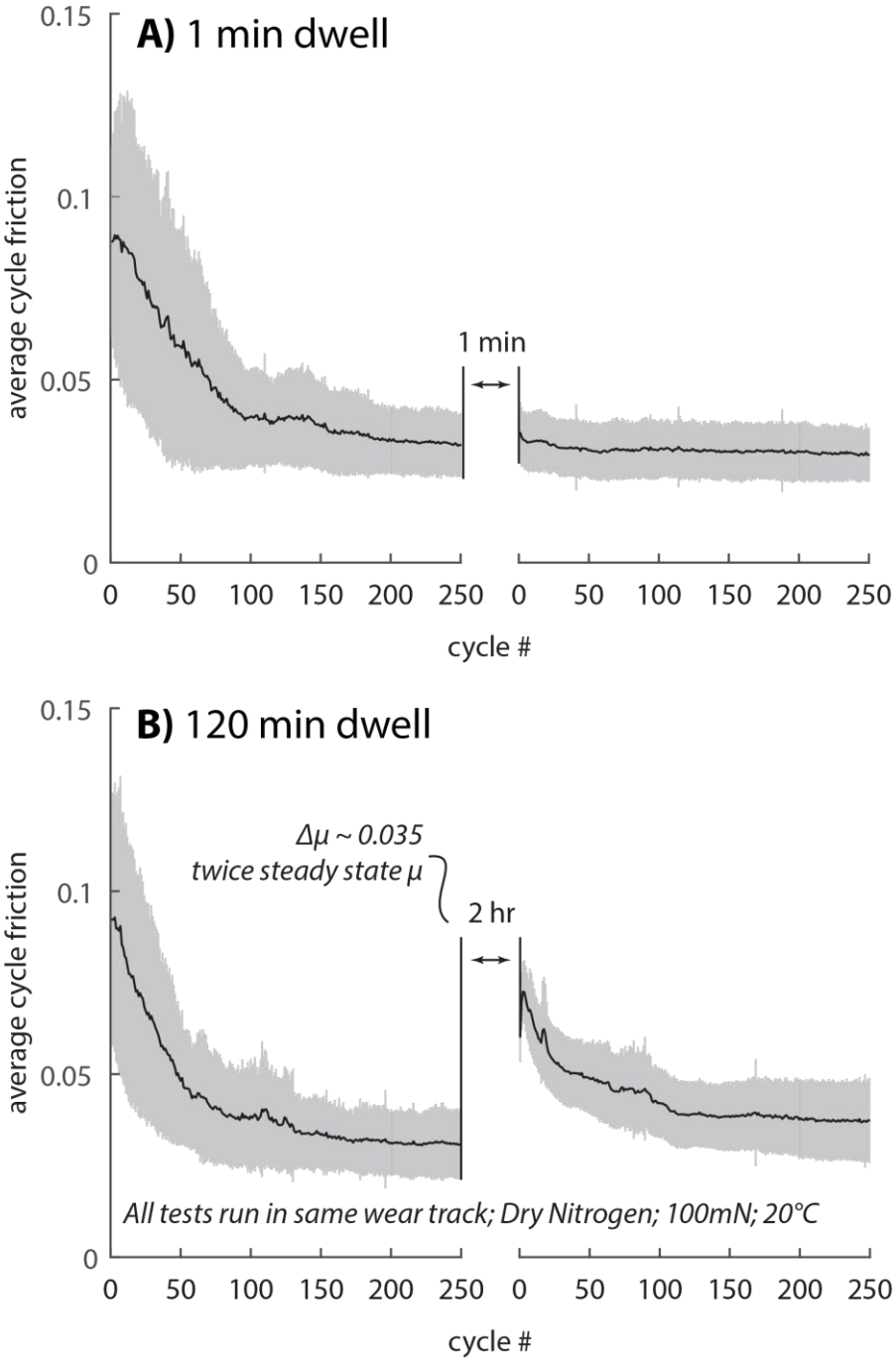

Fig. 7-9. Representative friction traces for stop time study experiments. In each case, the coating is first run in at an unworn location and let to sit for a period of time and then slid upon again in the same location.

7.4.4 Load & Substrate Dependence

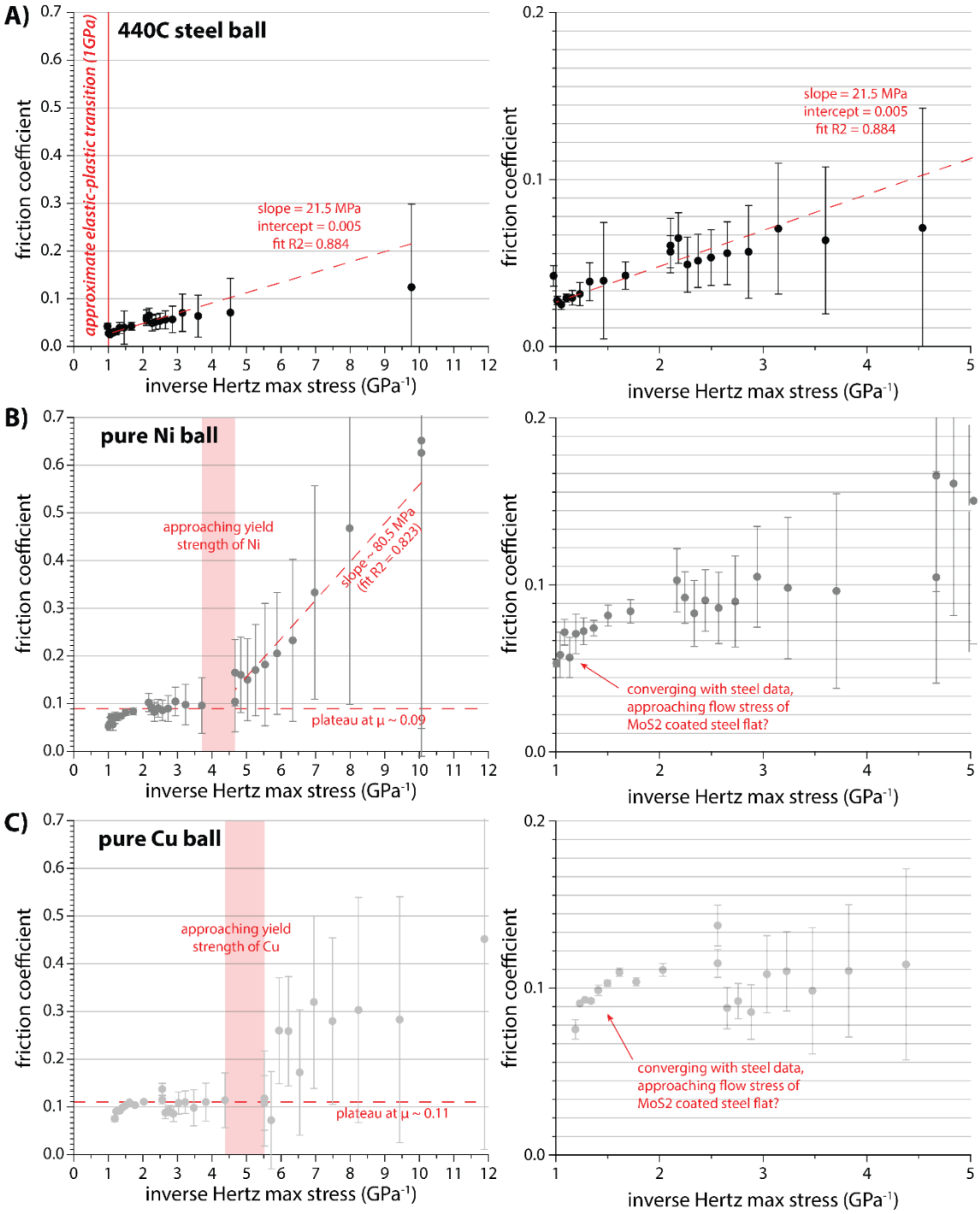

Fig. 7-10. Plots of friction coefficient vs. inverse Hertz max stress for 440C steel on MoS_2, pure Ni ball on MoS_2 and pure Cu ball on MoS_2 (B) The same plots as in (A) but focused on the high stress regions (< 5 GPa^{-1}) and low friction regimes (μ < 0.2)

A dependence of friction on load was noticed for the steel, copper and nickel pin materials (Figure 7-10). In each case tested, changes in friction behavior were noticed at stresses approaching the yield stresses of the materials tested. For the steel pin on steel coated MoS_2, a plateau in friction was approached at 1 GPa near the yield stress of either pin our counterface. A similar plateau can be seen for the nickel and copper specimens as well at higher contact pressures. For the nickel ball at pressures around the yield stress (~ 220 GPa) the precipitous drop in friction begins to slow with a similar behavior noticed for copper balls at ~ 200 GPa.

7.4.5 Spiral Orbit Run-In & XRD

Preliminary data for the spiral orbit XRD study is promising and reveals a relationship between applied load and basal orientation as well as insights into the role of transfer films. Friction data is presented for ordered coatings (Figure 7-11) while XRD results are shown for amorphous coatings (Figure 7-12 & Figure 7-13). Spiral orbit testing has proven to be a very useful method in creating large worn areas on a sample to enable XRD experiments that can monitor changes in crystallographic orientations. There are caveats, however, that should be noted and addressed when attempting to run spiral orbit experiments. The radius of sliding grows during testing and as this occurs, any tilt in the counterface sample will be amplified as you move further from the center, as such making servo-ing on load somewhat of an art more than a controlled aspect of the test. Unidirectional testing in general can also pose challenges in properly tearing the load at zero which is one reason why reciprocating experiments are so valuable.

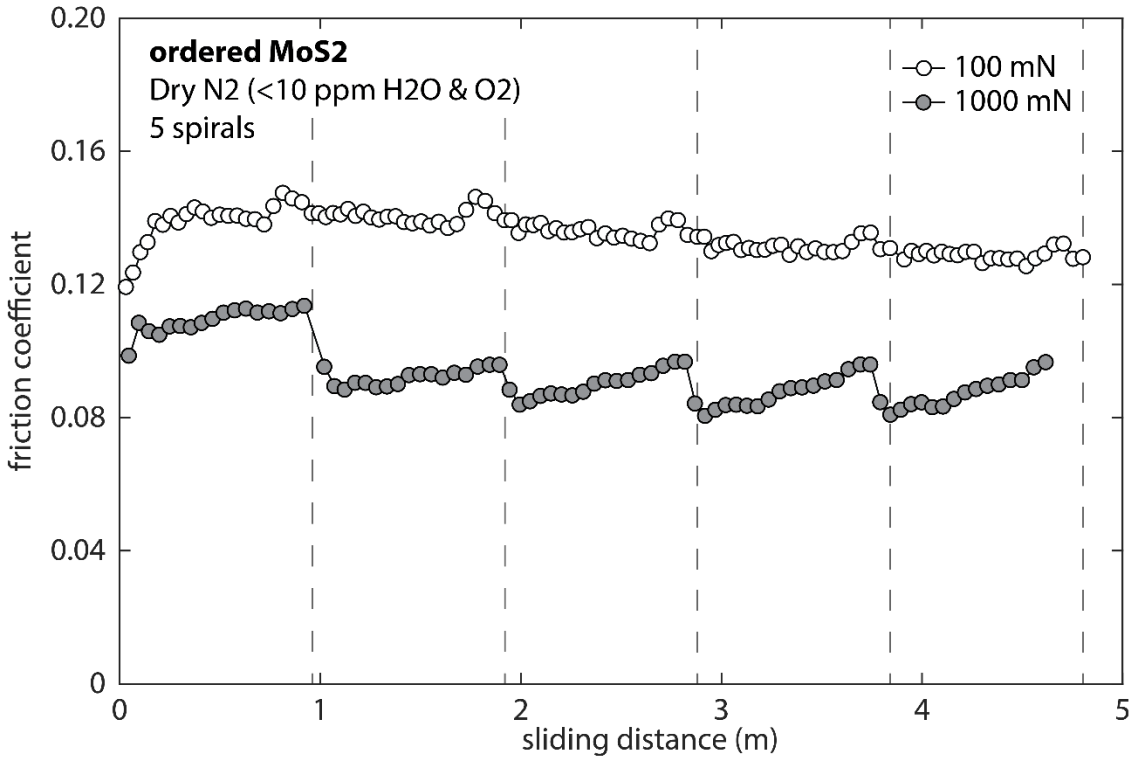

Fig. 7-11. Example of spiral orbit testing friction results for a sprayed *MoS_2* coating at 100mN and 1N applied load, 1mm/s tangential sliding speed. Dotted lines represent a complete spiral.

Friction results from spiral orbit testing on sputtered coupons in dry nitrogen revealed higher friction on average for 100 mN tests ($\mu \sim 0.13 – 0.14$) than 1000 mN ($\mu \sim 0.08 – 0.11$) tests (Figure 7-11) which agrees well with what we would expect from the inverse load relationship with friction (Figure 10) [117]. The values for friction coefficient, however are quite high for spray deposited MoS_2 coatings. These spiral orbit tests also show that in general friction does not increase upon continued sliding during a single spiral, with each complete spiral denoted by dashed lines (Figure 7-11). This suggests that prolonged sliding on unworn MoS_2, even with transfer to the ball, will not reduce friction coefficient. For comparison, typical 1000 cycle tests presented through this dissertation have total sliding distances of 1.6 m as compared to nearly 1 m for an individual spiral.

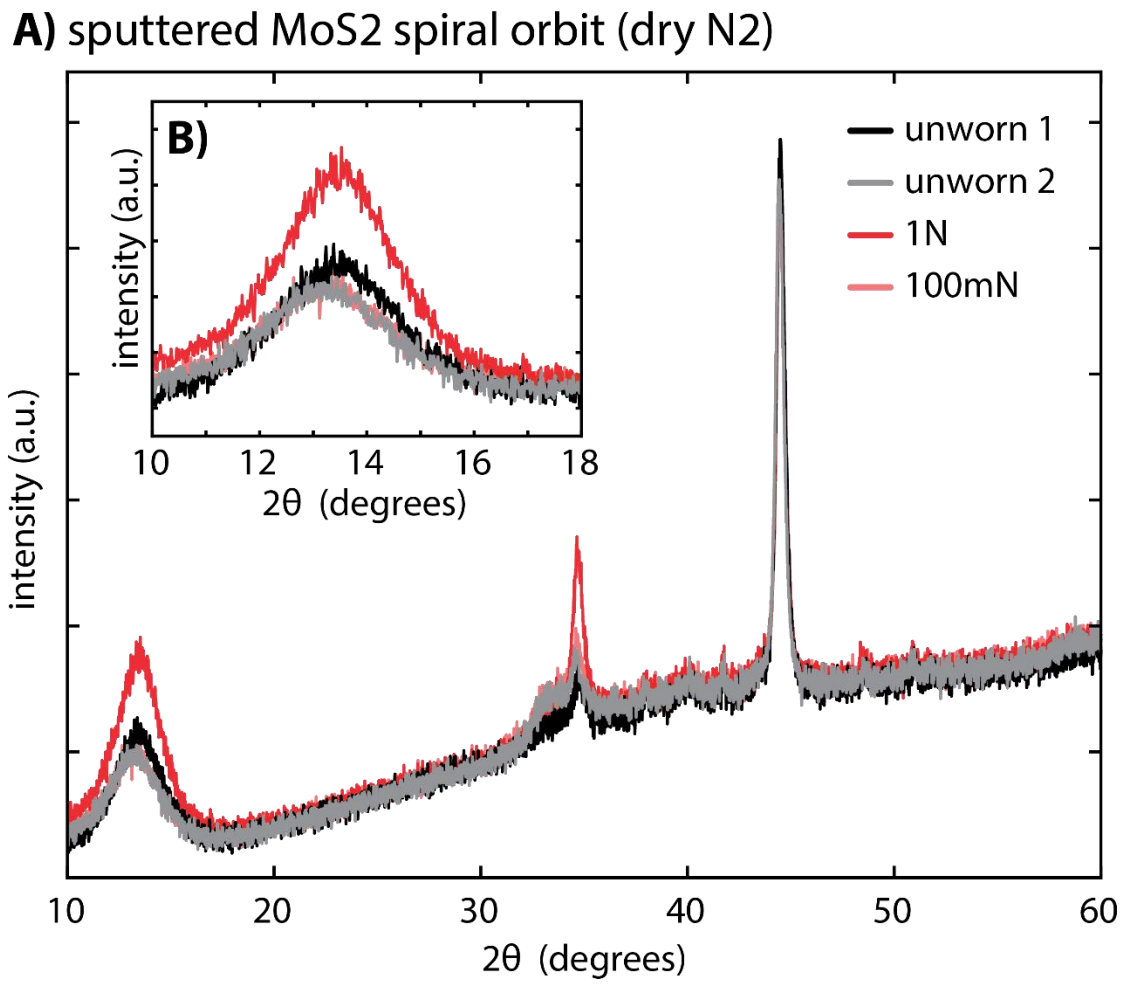

Fig. 7-12. (A) XRD diffraction pattern of two unworn sputtered *MoS_2* samples and samples run under 100 mN and 1 N load in dry nitrogen (B) Inset showing 14° peak intensity indicating differences in basal plane (100) representation.

Five separate coupons of sputter deposited MoS_2 were investigated via XRD after 10 spiral cycles in a nitrogen environment: two unworn sputtered samples, 1000mN in 20% RH N_2, 1000 mN in dry N_2 and 100 mN in dry N_2. These diffraction patterns were not scaled, but shifted slightly to match background intensity levels. Two unworn sputtered samples were compared to make sure that the batch of sputtered MoS_2 samples had comparable initial diffraction patterns to enable meaningful comparisons. There is a slight difference in diffraction patterns for these worn samples but not as significant as differences seen between different loads (Figure 7-12). From diffraction patterns for the

unworn sample and spirals run at different loads (Figure 7-12 A), it is evident that there is a higher intensity peak at $2\theta \approx 14°$ for coatings run-in at 1000 mN, denoting a stronger presence of surface parallel basally oriented MoS_2 in the film (Figure 7-12 B inset) as opposed to a lower load run-in at 100 mN. Also of interest is the development of a peak positioned at $2\theta \approx 34°$ for higher load experiments. This increase indicates development of additional basal orientation perpendicular to the substrate (100) suggesting that higher loads will in general form more crystalline orientations in MoS_2 [160]. When testing in a

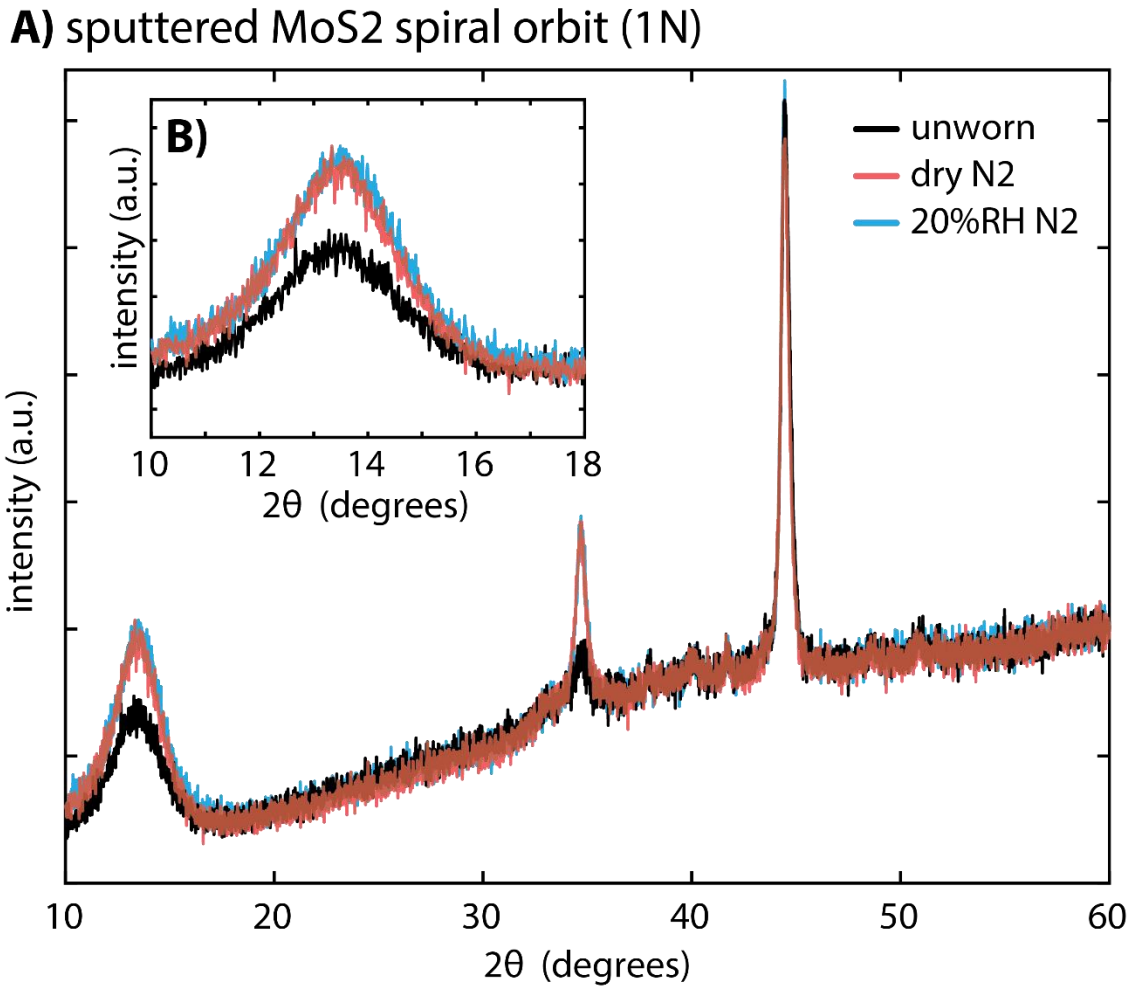

Fig. 7-13. (A) XRD diffraction pattern of unworn sputtered *MoS_2* and samples run under 1 N load in dry nitrogen and humid (20% RH) nitrogen (B) Inset showing 14° peak intensity indicating differences in basal plane (100) representation.

20% RH nitrogen environment at 1000 mN, the same results were seen as compared to testing in dry nitrogen (Figure 7-13).

7.5 Discussion

Temperature resolved friction testing and MD simulations showed a dependence of friction on temperature during sliding (Figure 7-5). By fitting a modified exponential form to the experimental data we were able to approximate an activation energy for sliding and bound the performance over a wide range of temperatures (0 – 300 K). Experimental results for the thermal dependence on friction differ somewhat from what is traditionally reported in literature for cryogenic temperatures [161], [162] that typically report a substantial increase in friction at temperatures below -20°C. Data shown here exhibits a smooth transition in gradually, yet minimally, increasing friction coefficient from ~ μ=0.02 – 0.05 from 300K to 0K respectively. The difference between our experiments and previous studies may be due to a variety of factors. Hamilton's study only tested composites MoS_2 samples or possibly affected by ice formation while Zhao's study used extreme contact pressures in an AFM to obtain their results. A more recent study by Dunckle took great care to test Ti-MoS_2 composite coatings in cryogenic vacuum conditions and obtained results very similar to those obtained by MD simulations (Figure 7-14) [163]. It is hard to compare the tests run by Dunckle to our own data due to the different contact geometries (multiple bearing gravity driven sled), coating type (Ti-MoS_2 composite) and applied loads (75 mN per bearing; 1/8" ⌀). A quick comparison can be made strictly on the differing loads applied given the same size in bearing (1/8" ⌀) by applying Hertz contact mechanics as shown by Singer [164]. With $\mu \approx L^{-1/3}$, friction would differ by 2 - 3 times, putting our

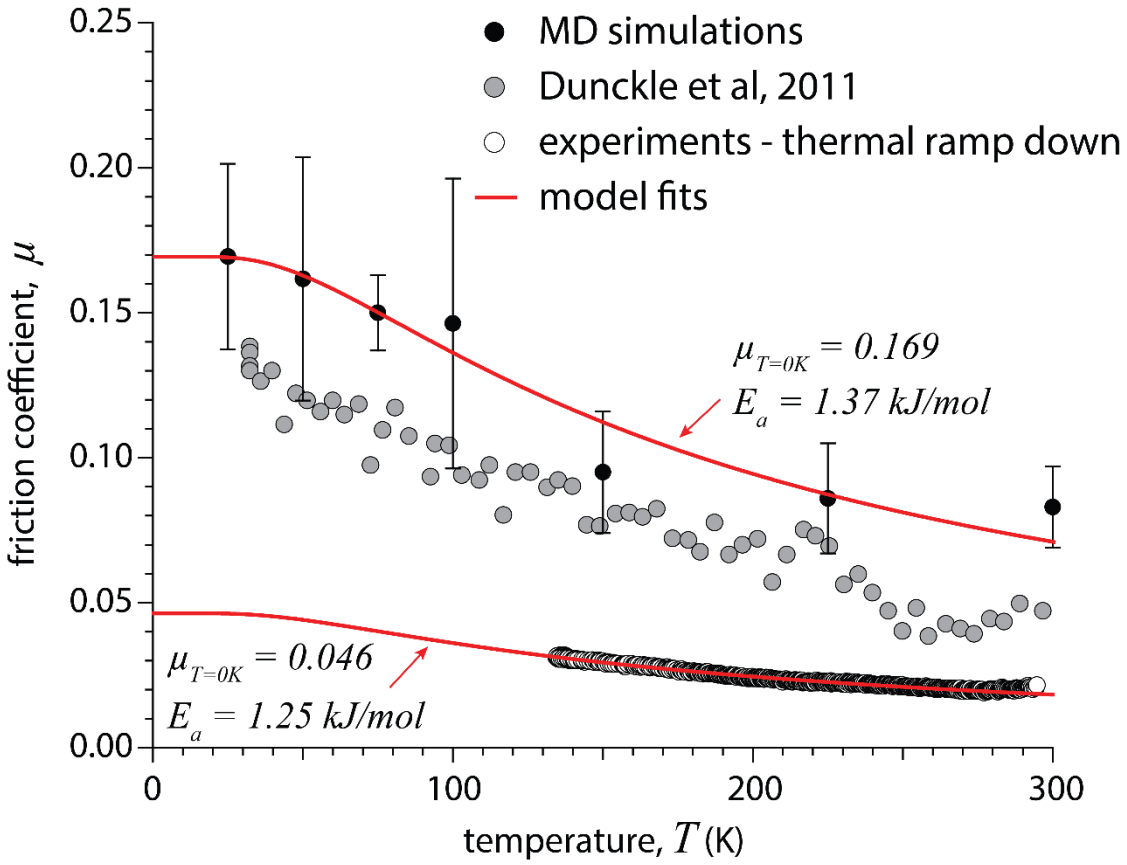

Fig. 7-14. Cycle averaged friction coefficients for temperature ramp experimental data, MD simulations (Figure 7-5) and data from Dunckle et al showing very similar trends in friction at cryogenic temperatures. [163]

own results directly in line with that of Dunckle's. This also agrees with the load dependence we've shown on various pin materials (Figure 7-10).

There still exists an appreciable difference between MD simulations and experiments (Figure 7-5). It is not expected that simulation and experiment perfectly overlap. Instead it is suggested that this difference is indicative of the state of structure of MoS_2. In the temperature resolved MD simulation (Figure 7-2), a highly defective, misoriented structure of nanocrystalline MoS_2 is simulated which is very different than that of an ordered film of MoS_2 formed during run-in. Orientation of MoS_2 flakes was hypothesized to be a contributor to this difference. NEB simulation results exploring the effect of

commensurability (Figure 7-6) also showed that mis-orientation between an MoS_2 unit cell and continuous sheet reduced the energy barrier to sliding by three-fold as compared to a unit cell sliding without a difference in commensurability or mis-orientation.

Stop time experiments were done in an attempt to observe possible flake rotation in the contact over time at different temperatures (Figure 7-7). Literature has shown that after a coating has been run-in to low steady state friction, the friction can rise again if left to sit without sliding for appreciable amounts of time. There are only a handful of publications directly studying these friction transients [27]–[30]. Haltner was the only one to study these transients extensively in multiple environments as well as in vacuum and still reported friction transients occurring in high vacuum (10^{-7} torr). His argument was that the return to high friction after dwell times was intimately tied to the free surface time, as in the time it took to accumulate a monolayer of water on the surface. This free surface time is directly related to the sticking coefficient (λ) for a giving molecule on a given surface. These calculations by Haltner assumed values of λ for water on MoS_2 in the range of 0.1 – 1. A separate study by Williams and McEvoy on properties of cleaved molybdenite reported far lower sticking coefficient values with $\lambda \sim 10^{-13}$ for a basal surface and $\lambda \sim 10^{-1}$ for edge sites [152]. Colbert had also shown that for 100nm thick sputter deposited pure MoS_2 coatings ~ 8 monolayers accumulate within 10 seconds in 25% RH, and over 24 hours only 1-2 monolayers were detected via adsorption measurements on a quartz crystal microbalance (QCM) to accumulate in a 4%RH environment. These values shown via QCM align well with Williams and McEvoy's estimates for sticking probabilities of water and make sense as most of the surface of the run-in coating should be basally oriented MoS_2. Colbert also showed extremely low diffusion coefficients of water into the MoS_2

surface in the range of $5x10^{-16}$ to $5x10^{-17}$. As such, it would seem that water in vacuum and inert environments does not appreciably accumulate on the run-in surfaces of MoS_2. It is suggested here that the return to increased friction over time is due to the settling of MoS_2 flakes into commensurate contact over time. When the temperature of the contact is reduced to -50°C, flake rotation is slowed and the time until re-run-in is reduced (Figure 7-7).

Environmental reversal testing served as an additional check on the role of water in experiments (Figure 7-8). Regardless of a test run after waiting undisturbed in a dry environment or after brief poisoning, transient increases in friction were the same for a given wait time and increased with time. These results suggest that the act of exposing the sample to air (minimum 40% RH during testing) has no effect on friction increase as compared to keeping the sample in an inert glove box (3 – 6 ppm H_2O). At room temperature, this would be equivalent to 10s in an environment with 1,500 – 3,000 times the amount of water in the atmosphere. There was also a concern that while rapidly pumping the antechamber down before re-entry, water may be desorbing and the transient increase would always be similar to those at 5 & 10 minutes ($\mu \approx 0.055–0.06$). To test this, 12 hour wait times were done with the 10s poisoning towards the end of the wait, with the thought if desorption of water was occurring, friction would remain at $\mu \approx 0.055–0.06$. This was not the case and the dry and poisoned 12 hr waits returned similar transient increases in friction.

If it is assumed that water is present on the surface earlier than stop times we can test and only serves to increase friction over time due to gradual adsorption of monolayers, it would be expected that a brief spike in water of the surrounding atmosphere would in some

way alter or increase friction. As this is not the case, it is thought that water adsorbed to the surface does not play a role in increasing friction as it primarily does not want to be present on the inert basal surface. It is more likely to adhere and possibly diffuse at edge sites. It may be that water can only diffuse and interact to an extent for ordered coatings, yielding a limit that is indicative of the maximum initial friction of $\mu \approx 0.10$. This would mean that sputtered coatings could exhibit far higher initial friction with much more diffused water. This also agrees well with our results showing the large difference in initial friction for sprayed vs sputtered coatings (Section 5). Yet, still, these ordered/sprayed coatings have proven to be extremely resilient in the face of aggressive oxidative environments, with oxidation limited to the first monolayer (Section 6). More work must be done to assess diffusion of water into ordered coatings, polycrystalline MoS_2 and a single crystal of MoS_2 to better understand the capability of water to diffuse in MoS_2.

It is hard to exactly determine if the transient increase in friction overtime would be due to a relaxation of sorts of the microstructure developed in the wear track, such as crystallite rotation, or diffusion of water through boundaries between cohesive crystallites in the wear track. A better understanding of the resulting structure during sliding in the wear track of MoS_2 (crystallite size, orientation, defect density) would be of great help and shed light into the notion that optimal crystallite sizes exist based upon sliding conditions [22], [121], [165], [166].

Preliminary results from XRD done on samples worn via spiral orbit experiments suggest that load may play a role in the recrystallization of MoS_2 with a more intense peak for basal orientation in the high load (1 N) case (Figure 7-12). No significant difference was noticed for tests run in humid nitrogen meaning that presence of water does not inhibit

sliding induced reorientation of basal planes (Figure 7-13). Along with an increase in the peak at 34° indicating growth of (100) orientation, this may mean that higher loads induce recrystallization regardless of orientation. No experimental evidence, however, was seen indicating applied load influenced the time until run-in or steady state friction was reached (Figure 7-15). This will be an interesting study moving forward to try and decouple the effects of load dependent recrystallization on run-in from the known load dependence on steady state friction behavior. Use of XRD to study the changing microstructure of MoS_2 films during run-in is a very promising technique but may benefit more from more powerful and focused X-Ray sources such as those found in synchrotron facilities.

7.6 Chapter Summary

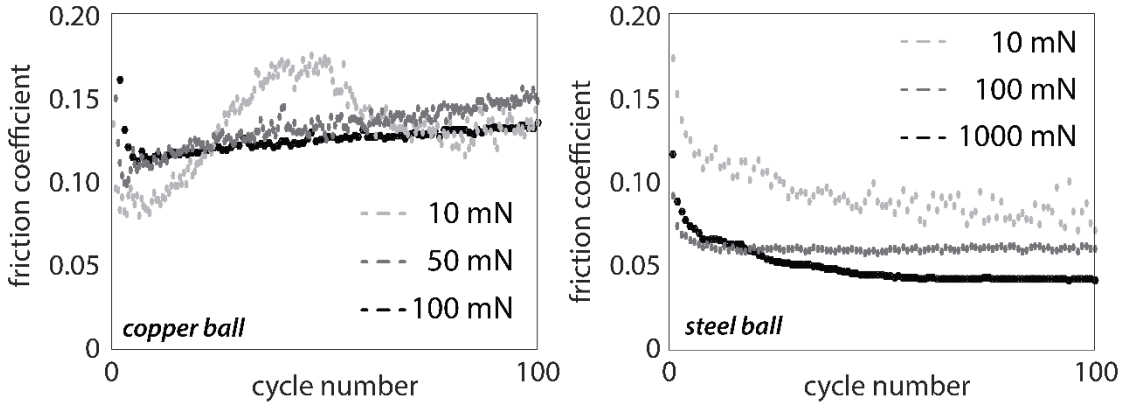

Fig. 7-15. Evolution of friction coefficient for copper and steel on pure *MoS_2* at different contact pressures.

Temperature resolved friction tests revealed a dependence of friction on temperature that could be fit to an Arrhenius like exponential and obtain an activation energy for sliding of 1.25 kJ/mol. MD simulations carried out by collaborators to mirror this study also gave a similar activation energy (1.37 kJ/mol), yet at higher friction coefficients. Cryogenic experiments done by Dunckle et al also agree very well with trends shown by our

experiments and MD simulations, with experimental data sets easily scalable between one another when accounting for differences in load. Structurally, the MD simulation and tribological test are very different with highly defective nanocrystalline MoS_2 sheets in simulation and a well run-in coating for experiments. A model is proposed that takes into account temperature and microstructural features such as flake orientation that can account for this gap. We experimentally demonstrated via dwell time studies that transient increases in friction after reaching steady state may be due to crystallite relaxation and reorientation over time. By dropping the temperature of the contact we were able to observe the return to high initial friction decrease with time suggesting a repression of flake rotation to high friction, low energy commensurate states. Environmental reversals between inert environments and laboratory air showed no difference as dwell time in between re-run-in was increased, suggesting adsorbed water was not playing a role in increased friction, but possibly diffusion of water into MoS_2 at edge sites. Ordered surfaces of MoS_2, however have proven to be very resistance to other environmental contaminants, with a demonstrated ability to limit oxidation to the initial surface.

Spiral orbit experiments enabled large worn areas of MoS_2 to be investigated with XRD. Results indicated that increased applied load was able to increase the degree of surface parallel basal crystallites, regardless of environment. Studies done to confirm the known load dependence in MoS_2 did not reveal any time dependent run-in behavior based on load.

8. Conclusions

Molybdenum Disulfide has been applied as a solid lubricant to surfaces for nearly a century now. In that time, much has been discovered about its lubrication properties in many different testing conditions across deposition techniques, motivated by many different applications. The purpose of this dissertation was to demonstrate that by tailoring and monitoring changes to the microstructure of MoS_2, much can be learned about its lubrication performance and resistance to environmental contaminants. This was accomplished by utilizing nitrogen spray deposited coating that exhibit a highly ordered surface parallel basal texture in the as deposited state (confirmed by XRD & TEM cross-sections) as a comparator to more amorphous PVD MoS_2 films.

Despite a somewhat patchy coverage as revealed by SEM/EDS, the sprayed coatings were able to provide low friction upon initial sliding, regardless of environment. The same cannot be said about amorphous PVD coatings which consistently exhibited higher initial friction as well as a dramatic increase in friction over sprayed coatings in humid air.

The reduction in initial friction for ordered films is attributed to the surface parallel basal orientation as deposited, reducing need for reorientation and recrystallization during run-in. The significantly higher friction for sputtered coatings in air is thought to be due to the inability of the crystallites to form a longer range order. XRD has shown that they may still basally orient in humid conditions, consistent with studies of films burnished in air, but are unable to recrystallize and stay in the wear track, leading to high friction and wear.

It was also shown via preliminary work with XRD enabled by large worn areas via spiral orbit experiments that load may play a role in the recrystallization process, with a slightly higher 2θ signal at 14.4° possibly indicating a more developed parallel basal

texture on the surface. No experimental evidence, however, was seen indicating applied load influenced the time until run-in or steady state friction was reached. This will be an interesting study moving forward to try and decouple the effects of load dependent recrystallization on run-in from the known load dependence on steady state friction behavior.

In addition to basal orientation, it was thought that in plane orientation may be a factor for the increased friction noticed in coatings already run-in. This transition from commensurate (low energy state, high energy barrier to sliding) to incommensurate (higher energy state, lower energy barrier to sliding) contact was demonstrated via MD simulations and further explored by monitoring the reduction in increased run-in over time at lower temperatures, possibly indicating a thermal dependence to crystallite relaxation. As such, the dependence of temperature on friction was assessed and found to fit an Arrhenius like exponential with an activation energy of 1.25 kJ/mol. MD simulations carried out by collaborators to mirror this study gave a similar activation energy (1.37 kJ/mol), yet at higher friction coefficients. Structurally, the MD simulation and tribological test are very different with highly defective nanocrystalline MoS_2 sheets in simulation and a well run-in coating for experiments. A model is proposed that takes into account temperature and microstructural features such as flake orientation that can account for this gap.

Environmental reversal testing between inert and laboratory air was used to confirm water was not effecting temperature resolved dwell studies. These dry and air poisoned dwell studies showed no appreciable differences, suggesting water adsorbed to the surface did not have an appreciable effect on run-in. The study, however, was not able to rule out diffusion of water into the MoS_2 coating, possibly at edge sites. Ordered surfaces of MoS_2,

however have proven to be very resistance to other environmental contaminants, with a demonstrated ability to limit oxidation to the initial surface.

HS-LEIS and XPS were used to provide new insights regarding the surface composition of thin MoS_2 films after exposure to oxygen at various temperatures. Highly ordered MoS_2 films with surface-parallel basal orientation are significantly more resistant to oxidation than amorphous (sputtered) MoS_2 films. Amorphous microstructures were very susceptible to oxidation throughout the depth of the film in either type of environment tested. In ordered microstructures, high temperature oxygen gas appeared to mostly physisorb to the surface of ordered coatings and likely interact with any available edge sites while atomic oxygen exposures were able to oxidize the entire surface of the ordered coating. As mentioned above, these sprayed/ordered coatings limited oxidation to the first atomic layer in either case (as revealed by HS-LEIS and XPS), which enables consistently lower friction on initial sliding and substantially shorter time until reaching steady state friction performance. This result can impact numerous applications for MoS_2 in oxidative environments, including lubrication for space machines and mechanisms. Figure 8-1 provides a visual aid of the hypothesized mechanisms outlined in this dissertation governing friction behavior in MoS_2 lubricated contacts.

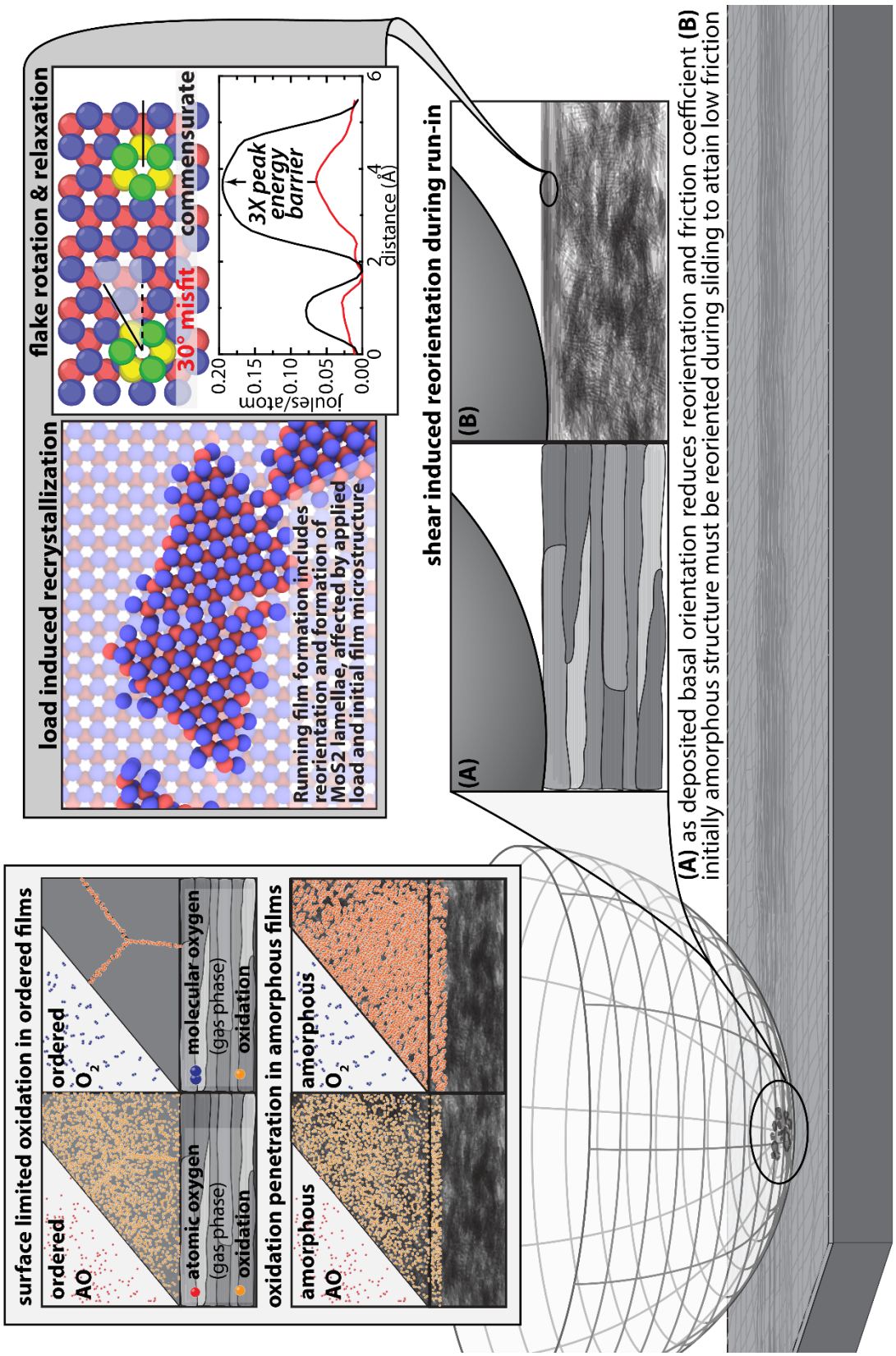

Fig. 8-1. Hypothesized mechanisms of MoS2 oxidation and kinetics of running film formation.

9. Proposed Studies & Future Directions of MoS2 Based Solid Lubricant Research

9.1 Motivation & Remaining Questions

There is an obvious need to better understand the crystallographic texture and morphology of a MoS_2 film in the wear track due to recrystallization during run-in and possible orientation dependent friction. This would also enable an idea of how the size and shape of an MoS_2 crystallite evolve under certain operating conditions. Throughout the literature, a better understanding of how crystallite size affects friction and wear performance have consistently been cited as a target for future studies, including this dissertation.

It can become especially confusing when you think of what the benefits and drawbacks of small/large crystallites may be to performance. For example, it is thought that large, ordered crystalline domains provide less edge sites for chemical reaction from environmental contaminants and provide a stable, surface parallel basal surface to reduce recrystallization and reorientation during run-in as we have shown. There is also the notion that smaller crystallites will help bond MoS_2 to the counterface for a more robust transfer film [22], [121], allow for more densely packed coatings that enable sliding interfaces to form more readily [166], and a factor in coating deposition [84].

So, a rift remains between what is thought to be good for run-in (environmental resistance, low initial friction) and ultimately establishing long-term, low steady-state friction and wear. Also, the role of water in lubrication of MoS_2 and how it interacts with the microstructure is still unknown. And as we get down to this level, trying to understand

crystallite interaction, one the most important questions, and hardest to answer, is where does slip occur? Is it constantly changing? How do we monitor this?

9.2 Continuation of Current Work – Supporting and Extending Findings & Results

9.2.1 Understanding Oxidation-based degradation of MoS_2

Oxidation studies carried out on the HS-LEIS and XPS were useful in establishing metrics and methods for assessing the fine gradient of oxide accumulation on the surface of MoS_2 films with respect to their microstructures. These studies showed how microstructure could limit oxidation but only at a single set of operating conditions. To be useful in materials design and engineering for suitable applications, a better understanding of the mechanism with which oxidation degrades these films across a range of different exposure lengths and temperatures is necessary. By varying the temperature and length of exposures, we can better assess in what way oxidation affects these films, such as a simple means of mass transport or reaction limited thermodynamics. The same methods of highly surface sensitive HS-LEIS depth profiling, XPS and tribological testing can be used in this new experimental matrix and help to expand our understanding of the oxidation-based degradation of MoS_2.

9.2.2 Dwell Time Studies & the Theory of Thermally Driven Crystallite Re-Orientation

Studies assessing differences in run-in behavior over time provided an interesting view of how the structure of MoS_2 films may be affecting friction behavior. Specifically, developed methods including dwell time experiments, molecular dynamics simulations and XRD characterization of large worn areas via spiral orbit testing outlined in section 7 assessed how MoS_2 crystallites in the wear track may be altering run-in behavior of MoS_2.

This concept of thermally driven crystallite re-orientation, however, is a difficult phenomenon to verify experimentally and the macroscale and as such would need additional testing to bolster our current findings. For instance, dwell time experiments carried out in different atmospheres, temperatures and a wider range of loading conditions would help to paint a better picture of the kinetics of running film formation and how it affects performance. With more data at different testing conditions, it may be possible to pull out different activation energies or time constants related to the run-in process via dwell time experiments. This is also true for XRD spiral orbit testing, where a range of loads, environments and temperatures can help to map out the change in basal orientation with respect to these different parameters in relation to friction behavior.

9.3 Future Work – Proposed Experiments to Move the State of Literature Forward

9.3.1 Monitoring Diffusion of Water in HS-LEIS

The role of water's presence in altering the lubrication of MoS_2 is still not fully understood. Many hypotheses have been proposed in the literature over decades yet none can conclusively answer this question. Our results indicate that either diffusion into the near surface or microstructural relaxation may cause increased initial friction after run-in. Even with QCM studies as done by Colbert, it is difficult to separate diffusion from adsorption. We believe our results (see Section 7) have ruled out adsorption as a cause to higher initial friction.

It is proposed that a study similar to our own LEIS study with oxidation be employed with isotopically tagged heavy water (H_2O^{18}). If done properly, this may be able to show if water is indeed able to diffuse into an ordered microstructure or limit itself to the surface as was seen for oxygen. This will help to narrow down possible sources of increased initial

friction in MoS_2. It is expected that, similar to oxygen, ordered films will excel at reducing the penetration of environmental species and also provide less surface area (as compared to amorphous films) for water to accumulate on the surface.

9.3.2 UHV Tribotesting

Further experiments in UHV conditions will also enable cleaner environments where coatings can be baked out and pumped down where water's presence is negligible. To enable these studies a custom built UHV tribometer was constructed at Sandia Nation Laboratories. The instrument is a linear reciprocating microtribometer experiments under ultra-high vacuum levels (as low as $1x10^{-10}$ torr) and a large range of temperatures (5K – 800K) (Figure 9-1). By testing in ultrahigh vacuum, we will be able to limit, if not prevent the accumulation of water on the surface and rule out water's affect on friction after sitting for periods of time. Cryogenic studies of MoS_2 in vacuum will have a similar benefit in knowing that ice is more than likely not present and will enable friction studies at far lower temperatures than currently capable. Lower temperature data will be useful in verifying MD simulations and help further develop the model of friction behavior and the effect of water on lubrication.

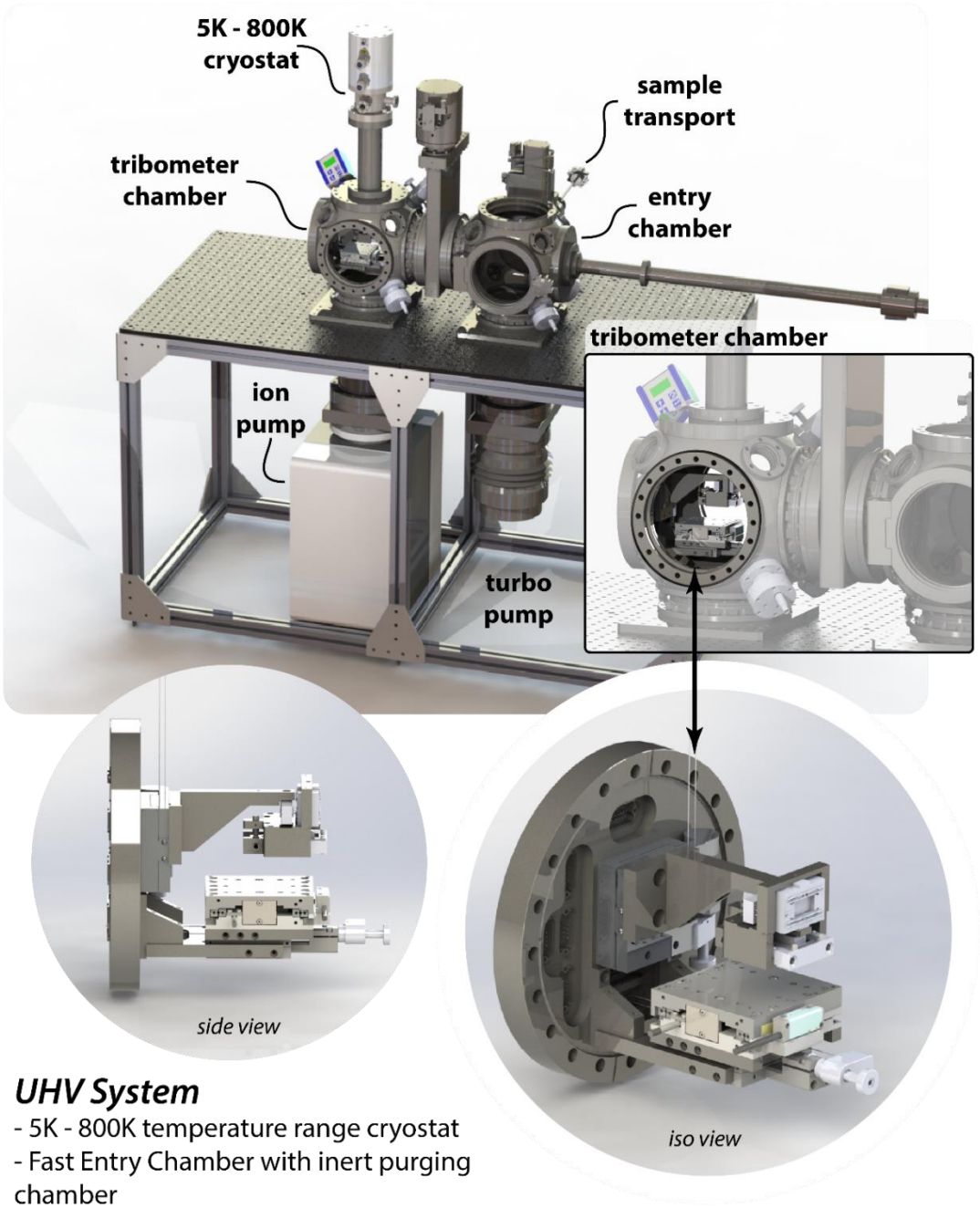

UHV System

- 5K - 800K temperature range cryostat
- Fast Entry Chamber with inert purging chamber
- Transportable sample rod to carry samples under vacuum for short periods of time
- UV Bakeout Lamps
- Modular design to allow for additional equipment in the future

UHV Rated Tribometer

- Cantilever flexure and capacitance probe based load metering
- Linear servo drive stage reciprocation & full XY sample positioning

Fig. 9-1: Annotated overview and schematic of UHV in-situ tribometer

9.3.3 Monitoring Microstructural Evolution during Run-in via Synchrotron X-Ray Microdiffraction

Previous experiments utilizing spiral orbit testing to view changes in the crystallographic structure provided information as to how load and environment affected the formation of basal planes. There are drawbacks, however, in using this method in that it takes upwards of 5-10 minutes to make an area large enough to scan, which as shown in Section 7, is enough time for friction to alter, possibly due to microstructural relaxation and crystallite rotation. The technique also does not allow for cycle resolved in-situ monitoring due to the amount of time it takes for the XRD to acquire a full diffraction pattern because of limitations in the amount and frequency of x-rays produced. To better monitor microstructural changes in smaller, controlled contacts, more powerful x-ray sources would be needed such as those found on a synchrotron. By using an in-situ tribometer on the beamline of a synchrotron, we should be able to sample far smaller areas such as in a typical linear wear scar and acquire diffraction patterns cycle by cycle. This information will be very useful in obtaining a better understanding of how crystallite orientation and possibly size can change during run-in across different loads and environments and not just snapshots before and after.

9.3.4 In-situ TEM Study of MoS_2 Crystallite Rotation, Recrystallization & Interactions

Visualizing a sliding interface or even individual crystallite interactions pose an extreme challenge for MoS_2 tribology, yet would enable much validation of current and proposed theories. Specifically, for flake interactions, in-situ TEM experiments would allow for a direct view of how crystallites orient themselves on larger monolayers. Section

7 attempts to understand flake re-orientation in the context of increased run-in over time and directly affected by temperature. With in-situ TEM experiments (even environmental-TEM), single crystallites of MoS_2 on larger monolayers of MoS_2 can be monitored at a range of temperatures, environments and initial energy states (commensurate or incommensurate). Apart from confirmation of our thermal dependent flake re-orientation theory (see Section 7), various information about the thermodynamics of the system can also be ascertained such as activation energies which may also be able to explain and help explore some of the kinetics of sliding.

10. References

[1] E. Rabinowicz, *Friction and Wear of Materials (2nd Edition)*. 1995.

[2] G. Amontons, “De la resistance causée dans les machines,” *Mem. Acad. R.*, vol. A, pp. 275–282, 1699.

[3] T. Mang, K. Bobzin, and T. Bartels, *Industrial tribology: Tribosystems, friction, wear and surface engineering, lubrication*. 2011.

[4] N. D. Spencer and W. T. Tysoe, “The Cutting Edge of Tribology: A Decade of Progress in Friction, Lubrication and Wear,” no. 1986, pp. 239–269, 2015.

[5] B. Bhushan, *Modern Tribology Handbook*. 2001.

[6] R. W. Carpick *et al.*, “The tribology opportunities study: Can tribology save a quad?” *Tribol. Lubr. Technol.*, vol. 72, no. 5, 2016.

[7] P. H. Jost, “Lubrication (tribology): education and research: a report on the present position and industry’s needs,” p. 79, 1966.

[8] H. P. Jost, “Tribology - Origin and future,” *Wear*, vol. 136, no. 1, pp. 1–17, 1990.

[9] H. P. Jost, “Tribology micro & macro economics: A road to economic savings,” *Tribol. Lubr. Technol.*, vol. 61, no. 10, pp. 18–22, 2005.

[10] P. Fleischauer and M. Hilton, “Assessment of the Tribiological Requirements of Advanced Spacecraft Mechanisms,” p. 30, 1991.

[11] P. D. Fleischauer and M. R. Hilton, “Applications of space tribology in the USA,” *Tribol. Int.*, vol. 23, no. 2, pp. 135–139, 1990.

[12] T. Mang and W. Dresel, *Lubricants and Lubrication*. 2007.

[13] F. P. Bowden and D. Tabor, “The Friction and Lubrication of Solids,” *Am. J. Phys.*, vol. 19, p. 428, 1951.

[14] I. L. Singer, S. D. Dvorak, K. J. Wahl, and T. W. Scharf, “Role of third bodies in friction and wear of protective coatings,” *J. Vac. Sci. Technol. A Vacuum, Surfaces, Film.*, vol. 21, no. 5, p. S232, 2003.

[15] I. L. Singer, “How third-body processes affect friction and wear,” *MRS Bull.*, vol. 23, no. 6, pp. 37–40, 1998.

[16] K. J. Wahl and W. Gregory Sawyer, “Observing Interfacial Sliding Processes in Solid-Solid Contacts,” *MRS Bull.*, vol. 33, no. 12, pp. 1159–1167, Dec. 2008.

[17] T. W. Scharf and S. V Prasad, “Solid lubricants: A review,” *J. Mater. Sci.*, vol. 48, no. 2, pp. 511–531, 2013.

[18] J. Moser and F. Levy, “Crystal Reorientation and Wear Mechanisms in Mos2 Lubricating Thin-Films Investigated By Tem,” *J. Mater. Res.*, vol. 8, no. 1, pp. 206–213, 1993.

[19] J. J. Hu, R. Wheeler, J. S. Zabinski, P. A. Shade, A. Shiveley, and A. A. Voevodin, “Transmission Electron Microscopy Analysis of Mo–W–S–Se Film Sliding Contact Obtained by Using Focused Ion Beam Microscope and In-Situ Microtribometer,” *Tribol. Lett.*, vol. 32, no. 1, 2008.

[20] T. W. Scharf, R. S. Goeke, P. G. Kotula, and S. V. Prasad, “Synthesis of Au-MoS2 nanocomposites: Thermal and friction-induced changes to the structure,” *ACS Appl. Mater. Interfaces*, vol. 5, no. 22, pp. 11762–11767, 2013.

[21] J. K. Lancaster, “Anisotropy in the mechanical properties of lamellar solids and its effect on wear and transfer,” *Wear*, vol. 9, no. 3, pp. 169–188, 1966.

[22] P. D. Fleischauer and R. Bauer, “The Influence of Surface Chemistry on MoS2 Transfer Film Formation,” *A S L E Trans.*, vol. 30, no. 2, pp. 160–166, 1987.

[23] T. W. Scharf and I. L. Singer, “Monitoring Transfer Films and Friction Instabilities with In Situ Raman Tribometry,” *Tribol. Lett.*, vol. 14, no. 1, pp. 3–8, 2003.

[24] P. D. Fleischauer, “Effects of Crystallite Orientation on Environmental Stability and Lubrication Properties of Sputtered MoS2 Thin Films,” *A S L E Trans.*, vol. 27, no. 1, pp. 82–88, 1984.

[25] T. W. Scharf, P. G. Kotula, and S. V. Prasad, “Friction and wear mechanisms in MoS2/Sb2O3/Au nanocomposite coatings,” *Acta Mater.*, vol. 58, no. 12, pp. 4100–4109, 2010.

[26] J. J. Hu, R. Wheeler, J. S. Zabinski, P. A. Shade, A. Shiveley, and A. A. Voevodin, “Transmission electron microscopy analysis of Mo-W-S-Se film sliding contact obtained by using focused ion beam microscope and in situ microtribometer,” *Tribol. Lett.*, vol. 32, no. 1, pp. 49–57, 2008.

[27] V. R. Johnson and G. W. Vaughn, “Investigation of the mechanism of MoS2 lubrication in vacuum,” *J. Appl. Phys.*, vol. 27, no. 10, pp. 1173–1179, 1956.

[28] A. J. Haltner, “An evaluation of the role of vapor lubrication mechanisms in MoS 2,” *Wear*, vol. 7, no. 1, pp. 102–117, 1964.

[29] M. T. Lavik, T. B. Daniel, and A. N. Abbott, “Friction of Molybdenum Diselenide,” *J. Appl. Phys.*, vol. 32, no. 9, p. 1795, Sep. 1961.

[30] M. Matsunaga and K. Hoshimoto, “Frictional behaviour of molybdenum disulphide in high vacuum - Part II,” *Wear*, vol. 38, no. 2, pp. 371–384, 1976.

[31] M. Tagawa *et al.*, “Space environmental effects on MoS2 and diamond-like carbon lubricating films: Atomic oxygen-induced erosion and its effect on tribological properties,” *Surf. Coatings Technol.*, vol. 202, no. 4–7, pp. 1003–1010, 2007.

[32] M. Tagawa *et al.*, “Hyperthermal atomic oxygen interaction with MoS2 lubricants and relevance to space environmental effects in low earth orbit - Effects on friction coefficient and wear-life,” *Tribol. Lett.*, vol. 18, no. 4, pp. 437–443, 2005.

[33] M. Tagawa *et al.*, “Wear-life of the molybdenum disulfide sputtered film under hyperthermal atomic oxygen bombardment: In-situ wear-life evaluations,” *Eur. Sp. Agency, Special Publ. ESA SP*, no. 524, pp. 311–314, 2003.

[34] M. Tagawa, K. Yokota, N. Ohmae, K. Matsumoto, and M. Suzuki, “Hyperthermal atomic oxygen interaction with MoS2 lubricants relevance to space environmental effects in low earth orbit - Atomic oxygen-induced oxidation,” *Tribol. Lett.*, vol. 17, no. 4, pp. 859–865, 2004.

[35] J. A. Martin, J. B. Cross, and L. E. Pope, “MoS2 interaction with 1.5 eV atomic oxygen,” *Mat. Res. Soc. Symp. Proc*, vol. 140, pp. 271–276, 1989.

[36] J. B. Cross, J. A. Martin, L. E. Pope, and S. L. Koontz, “Atomic Oxygen MoS2 Chemical Interactions,” *Surf. Coat. Technol.*, vol. 42, no. 1, pp. 41–48, 1990.

[37] R. L. Fusaro, “Lubrication and failure mechanisms of molybdenum disulfide films. 1: Effect of atmosphere,” ntrs.nasa.gov, 1978.

[38] D. A. W. J. Gee, G. Salomon, and J. H. Zaat, “On the Mechanisms of MoS2-Film Failure in Sliding Friction,” *A S L E Trans.*, vol. 8, no. 2, pp. 156–163, 1965.

[39] G. Salomon, A. W. J. De Gee, and J. H. Zaat, “Mechano-chemical factors in MoS2-film lubrication,” *Wear*, vol. 7, no. 1, pp. 87–101, 1964.

[40] R. P. Pardee, “The Effect of Humidity on Low-Load Frictional Properties of a Bonded Solid Film Lubricant,” *A S L E Trans.*, vol. 15, no. 2, pp. 130–142, 1972.

[41] C. Pritchard and J. W. Midgley, “The effect of humidity on the friction and life of

unbonded molybdenum disulphide films," *Wear*, vol. 13, no. 1, pp. 39–50, 1969.

[42] A. J. Haltner and C. S. Oliver, "Effect of Water Vapor on Friction of Molybdenum Disulfide," *Ind. Eng. Chem. Fundam.*, vol. 5, no. 3, pp. 348–355, 1966.

[43] S. Ross and A. Sussman, "Surface Oxidation of Molybdenum Disulfide," *J. Phys. Chem.*, vol. 59, no. 9, pp. 889–892, 1955.

[44] D. D. Make, C. Gao, L. Bredell, and D. Kuhhnann-wilsdorf, "Micromechanics of MoS2 lubrication," vol. 164, pp. 480–491, 1993.

[45] M. Uemura, K. Saito, and K. Nakao, "A Mechanism of Vapor Effect on Friction Coefficient of Molybdenum Disulfide," *Tribol. Trans.*, vol. 33, no. 4, pp. 551–556, 1990.

[46] R. Holinski and J. Gänsheimer, "A study of the lubricating mechanism of molybdenum disulfide," *Wear*, vol. 19, no. 3, pp. 329–342, 1972.

[47] R. M. Johnston and a J. W. Moore, "Water Adsorption on Molybdenum Disulfide Containing Surface Contaminants," *J. Phys. Chem.*, vol. 68, no. 11, pp. 3399–3406, 1964.

[48] J. K. G. Panitz, "The tribological properties of MoS2 coatings in vacuum, low relative humidity, and high relative humidity environments," *J. Vac. Sci. Technol. A Vacuum, Surfaces, Film.*, vol. 6, no. 3, p. 1166, 1988.

[49] H. S. Khare and D. L. Burris, "Surface and subsurface contributions of oxidation and moisture to room temperature friction of molybdenum disulfide," *Tribol. Lett.*, vol. 53, no. 1, pp. 329–336, 2014.

[50] H. S. Khare and D. L. Burris, "The effects of environmental water and oxygen on the temperature-dependent friction of sputtered molybdenum disulfide," *Tribol.*

Lett., vol. 52, no. 3, pp. 485–493, 2013.

[51] T. Kubart, T. Polcar, L. Kopeck, R. Novak, and D. Novakova, "Temperature dependence of tribological properties of MoS2 and MoSe2 coatings," *Surf. Coat. Technol.*, vol. 193, no. 1, pp. 230–233, 2005.

[52] J. Gänsheimer, "Influence of Certain Vapors and Liquids on the Frictional Properties of Molybdenum Disulfide," *A S L E Trans.*, vol. 10, no. 4, pp. 390–399, 1967.

[53] B. C. Windom, W. G. Sawyer, and D. W. Hahn, "A raman spectroscopic study of MoS2 and MoO3: Applications to tribological systems," *Tribol. Lett.*, vol. 42, no. 3, pp. 301–310, 2011.

[54] X. Zhao and S. S. Perry, "The role of water in modifying friction within MoS2 sliding interfaces," *ACS Appl. Mater. Interfaces*, vol. 2, no. 5, pp. 1444–1448, 2010.

[55] M. N. Gardos, "The Synergistic Effects of Graphite of the Friction and Wear of MoS2 Films in Air," *Tribol. Trans.*, vol. 31, no. 2, pp. 214–227, 1988.

[56] T. B. Stewart and P. D. Fleischauer, "Chemistry of sputtered molybdenum disulfide films," *Inorg. Chem.*, vol. 21, no. 6, pp. 2426–2431, 1982.

[57] M. R. Hilton and P. D. Fleischauer, "Structural Studies of Sputter-Deposited MoS2 Solid Lubricant Films," *MRS Proc.*, vol. 140, pp. 227–238, 1988.

[58] P. D. Fleischauer, "Fundamental aspects of the electronic structure, materials properties and lubrication performance of sputtered MoS2 films," *Thin Solid Films*, vol. 154, no. 1–2, 1987.

[59] J. R. Lince and P. D. Fleischauer, "Crystallinity of rf-sputtered MoS2 films," *J. Mater. Res.*, vol. 2, no. 6, pp. 827–838, 1987.

[60] P. Niederhauser, H. E. Hintermann, and M. Maillat, "Moisture-resistant MoS2-

based composite lubricant films," *Thin Solid Films*, vol. 108, no. 2, pp. 209–218, 1983.

[61] M. R. Hilton, R. Bauer, S. V. Didziulis, M. T. Dugger, J. M. Keem, and J. Scholhamer, "Structural and tribological studies of MoS2 solid lubricant films having tailored metal-multilayer nanostructures," *Surf. Coatings Technol.*, vol. 53, no. 1, pp. 13–23, 1992.

[62] T. W. Scharf, D. R. Diercks, B. P. Gorman, S. V Prasad, and M. T. Dugger, "Atomic Layer Deposition of Tungsten Disulphide Solid Lubricant Nanocomposite Coatings on Rolling Element Bearings," *Tribol. Trans.*, vol. 52, no. 3, pp. 284–292, 2009.

[63] P. Stoyanov, R. R. Chromik, D. Goldbaum, J. R. Lince, and X. Zhang, "Microtribological Performance of Au–MoS2 and Ti–MoS2 Coatings with Varying Contact Pressure," *Tribol. Lett.*, vol. 40, no. 1, pp. 199–211, 2010.

[64] I. L. Singer, S. D. Dvorak, K. J. Wahl, and T. W. Scharf, "Role of third bodies in friction and wear of protective coatings," *J. Vac. Sci. Technol. A*, vol. 21, no. 5, pp. S232–S240, 2003.

[65] G. J. Dudder, X. Zhao, B. Krick, W. G. Sawyer, and S. S. Perry, "Environmental effects on the tribology and microstructure of MoS 2-Sb 2O 3-C Films," *Tribol. Lett.*, vol. 42, no. 2, pp. 203–213, 2011.

[66] J. J. Hu, J. E. Bultman, and J. S. Zabinski, "Microstructure and lubrication mechanism of multilayered MoS2/Sb2O3 thin films," *Tribol. Lett.*, vol. 21, no. 2, 2006.

[67] J. S. Zabinski, J. E. Bultman, J. H. Sanders, and J. J. Hu, "Multi-environmental lubrication performance and lubrication mechanism of MoS2/Sb2O3/C composite

films," *Tribol. Lett.*, vol. 23, no. 2, pp. 155–163, 2006.

[68] C. Muratore and A. A. Voevodin, "Chameleon Coatings: Adaptive Surfaces to Reduce Friction and Wear in Extreme Environments," *Annu. Rev. Mater. Res.*, vol. 39, no. 1, pp. 297–324, 2009.

[69] C. C. Baker, R. R. Chromik, K. J. Wahl, J. J. Hu, and A. A. Voevodin, "Preparation of chameleon coatings for space and ambient environments," *Thin Solid Films*, vol. 515, no. 17, pp. 6737–6743, 2007.

[70] A. A. Voevodin and J. S. Zabinski, "Nanocomposite and nanostructured tribological materials for space applications," *Compos. Sci. Technol.*, vol. 65, no. 5, pp. 741–748, 2005.

[71] R. R. Chromik, C. C. Baker, A. A. Voevodin, and K. J. Wahl, "In situ tribometry of solid lubricant nanocomposite coatings," *Wear*, vol. 262, no. 9--10, pp. 1239–1252, 2007.

[72] L. Rapoport *et al.*, "Friction and wear of MoS2 films on laser textured steel surfaces," *Surf. Coatings Technol.*, vol. 202, no. 14, pp. 3332–3340, 2008.

[73] W. O. Winer, "Molybdenum disulfide as a lubricant: A review of the fundamental knowledge," *Wear*, vol. 10, pp. 422–452, 1967.

[74] R. R. M. Johnston and A. J. W. Moore, "The burnishing of molybdenum disulphide on to metal surfaces," *Wear*, vol. 7, no. 6, pp. 498–512, Nov. 1964.

[75] B. Vierneusel, T. Schneider, S. Tremmel, S. Wartzack, and T. Gradt, "Humidity resistant MoS2 coatings deposited by unbalanced magnetron sputtering," *Surf. Coat. Technol.*, vol. 235, pp. 97–107, 2013.

[76] C. Muratore and A. A. Voevodin, "Control of molybdenum disulfide basal plane

orientation during coating growth in pulsed magnetron sputtering discharges," *Thin Solid Films*, vol. 517, no. 19, pp. 5605–5610, 2009.

[77] P. A. Bertrand, "Orientation of rf-sputter-deposited MoS2 films," *J. Mater. Res.*, vol. 4, no. 1, pp. 180–184, 1989.

[78] J. K. G. Panitz, L. E. Pope, C. R. Hills, J. E. Lyons, and D. J. Staley, "A statistical study of the combined effects of substrate temperature, bias, annealing and a Cr3Si2 undercoating on the tribological properties of r.f. sputtered MoS2 coatings," *Thin Solid Films*, vol. 154, no. 1–2. pp. 323–332, 1987.

[79] T. Spalvins, "Structure of Sputtered Molybdenum Disulfide Films at Various Substrate Temperatures," *A S L E Trans.*, vol. 17, no. 1, pp. 1–7, 1974.

[80] J. Moser, H. Liao, and F. Levy, "Texture characterisation of sputtered MoS2 thin films by cross-sectional TEM analysis," *J. Phys. D Appl. Phys.*, vol. 23, no. 5, pp. 624–626, 1990.

[81] J. Moser and F. Levy, "Growth mechanisms and near-interface structure in relation to orientation of M0S2 sputtered thin films," *J. Mater. Res.*, vol. 7, no. October 1991, p. 734, 1992.

[82] T. Spalvins, "Morphological and Frictional Behavior of Sputtered MoS2 Films," *Thin Solid Films*, vol. 96, no. 1, pp. 17–24, 1982.

[83] T. Spalvins and A. S. Engineering, "Lubrication With Sputtered MoS2 Films: Principles, Operation, Limitations," 1991.

[84] N. J. Mikkelsen and G. Sørensen, "Solid lubricating films produced by ion bombardment of sputter deposited MoSx films," *Surf. Coatings Technol.*, vol. 51, no. 1–3, pp. 118–123, 1992.

[85] I. L. Wahl, K J; Seitzman, L E; Bolster, R N; Singer, “Low Friction, High Endurance Ion-Beam Deposited Pb-Mo-S Coatings,” *Surf. Coatings Technol.*, vol. 73, no. 3, pp. 152–159, 1995.

[86] L. E. Seitzman *et al.*, “Relationship of Endurance to Microstructure of IBAD MoS2 Coatings,” *Tribol. Trans.*, vol. 38, no. 2, pp. 445–451, 1995.

[87] L. E. Seitzman, R. N. Bolster, and I. L. Singer, “Effects of temperature and ion-to-atom ratio on the orientation of IBAD MoS2 coatings,” *Thin Solid Films*, vol. 260, no. 2, pp. 143–147, 1995.

[88] D. N. Dunn, L. E. Seitzman, and I. L. Singer, “MoS2 deposited by ion beam assisted deposition: 2H or random layer structure?,” *J. Mater. Res.*, vol. 13, no. 10, pp. 3001–3007, 1998.

[89] K. J. Wahl, D. N. Dunn, and I. L. Singer, “Effects of ion implantation on microstructure, endurance and wear behavior of IBAD MoS2,” *Wear*, vol. 237, no. 1, pp. 1–11, 2000.

[90] J. F. Curry *et al.*, “Highly Oriented MoS2 Coatings: Tribology and Environmental Stability,” *Tribol. Lett.*, vol. 64, no. 1, p. 11, 2016.

[91] M. Hirano, K. Shinjo, R. Kaneko, and Y. Murata, “Observation of Superlubricity by Scanning Tunneling Microscopy,” *Phys. Rev. Lett.*, vol. 78, no. 8, pp. 1448–1451, 1997.

[92] M. Dienwiebel, G. S. Verhoeven, N. Pradeep, J. W. M. Frenken, J. A. Heimberg, and H. W. Zandbergen, “Superlubricity of graphite,” *Phys. Rev. Lett.*, vol. 92, no. 12, p. 126101, 2004.

[93] D. L. Burris and W. G. Sawyer, “Addressing Practical Challenges of Low Friction

Coefficient Measurements," *Tribol. Lett.*, vol. 35, no. 1, pp. 17–23, Apr. 2009.

[94] B. a. Krick, J. R. Vail, B. N. J. Persson, and W. G. Sawyer, "Optical In Situ Micro Tribometer for Analysis of Real Contact Area for Contact Mechanics, Adhesion, and Sliding Experiments," *Tribol. Lett.*, vol. 45, no. 1, pp. 185–194, Oct. 2011.

[95] M. Varenberg, A. Peressadko, S. Gorb, E. Arzt, and S. Mrotzek, "Advanced testing of adhesion and friction with a microtribometer," *Rev. Sci. Instrum.*, vol. 77, no. 6, 2006.

[96] D. L. Burris, W. G. Sawyer, and D. L. B. Æ. W. G. Sawyer, "Addressing Practical Challenges of Low Friction Coefficient Measurements," *Tribol. Lett.*, vol. 35, no. 1, pp. 17–23, 2009.

[97] I.-T. GmbH, "Surface Lab." 2013.

[98] H. H. Brongersma, "Low-Energy Ion Scattering," in *Characterization of Materials*, E. N. Kaufman, Ed. Wiley, 2012, pp. 2024–2044.

[99] E. N. Kaufmann, *Characterization of materials*. Wiley-Interscience, 2003.

[100] B. Schönfeld, J. J. Huang, and S. C. Moss, "Anisotropic mean-square displacements (MSD) in single-crystals of 2H-and 3R-MoS2," *Acta Crystallogr. Sect. B Struct. Sci.*, vol. 39, no. 4, pp. 404–407, 1983.

[101] D. L. Smith, *Thin - film deposition : principles and practice*. 1995.

[102] I. L. Singer and D. C. Washington, "Solid Lubricating Films for Extreme Environments," *MRS Proc.*, vol. 140, pp. 215–226, 1988.

[103] W. O. Winer, "Molybdenum disulfide as a lubricant: A review of the fundamental knowledge," *Wear*, vol. 10, pp. 422–452, 1967.

[104] M. R. Hilton, R. Bauer, and P. D. Fleischauer, "Tribological performance and

deformation of sputter-deposited MoS2 solid lubricant films during sliding wear and indentation contact," *Thin Solid Films*, vol. 188, no. 2, pp. 219–236, 1990.

[105] J. S. Zabinski, M. S. Donley, S. D. Walck, T. R. Schneider, and N. T. Mcdevitt, "The Effects of Dopants on the Chemistry and Tribology of Sputter-Deposited MoS $_2$ Films," *Tribol. Trans.*, vol. 38, no. 4, pp. 894–904, 1995.

[106] J. M. Martin, C. Donnet, T. Le Mogne, and T. Epicier, "Superlubricity of molybdenum disulphide," *Phys. Rev. B Condens. Matter*, vol. 48, no. 14, pp. 10583–10586, 1993.

[107] H. S. Khare and D. L. Burris, "The effects of environmental water and oxygen on the temperature-dependent friction of sputtered molybdenum disulfide," *Tribol. Lett.*, vol. 52, no. 3, pp. 485–493, 2013.

[108] H. S. Khare and D. L. Burris, "Surface and subsurface contributions of oxidation and moisture to room temperature friction of molybdenum disulfide," *Tribol. Lett.*, vol. 53, no. 1, pp. 329–336, 2014.

[109] C. Pritchard and J. W. Midgley, "The effect of humidity on the friction and life of unbonded molybdenum disulphide films," *Wear*, vol. 13, no. 1. pp. 39–50, 1969.

[110] M. Uemura, K. Saito, and K. Nakao, "A Mechanism of Vapor Effect on Friction Coefficient of Molybdenum Disulfide," *Tribol. Trans.*, vol. 33, no. 4, pp. 551–556, 1990.

[111] S. M. Aouadi *et al.*, "Adaptive Mo2N/MoS2/Ag Tribological Nanocomposite Coatings for Aerospace Applications," *Tribol. Lett.*, vol. 29, no. 2, pp. 95–103, 2008.

[112] A. a. Voevodin and J. S. Zabinski, "Nanocomposite and nanostructured tribological materials for space applications," *Compos. Sci. Technol.*, vol. 65, no. 5 SPEC. ISS.,

pp. 741–748, 2005.

[113] S. V Prasad, N. T. McDevitt, and J. S. Zabinski, “Tribology of tungsten disulfide–nanocrystalline zinc oxide adaptive lubricant films from ambient to 500°C,” *Wear*, vol. 237, no. 2, pp. 186–196, 2000.

[114] L. E. Seitzman, I. L. Singer, R. N. Bolster, and C. R. Gossett, “Effect of a titanium nitride interlayer on the endurance and composition of a molybdenum disulfide coating prepared by ion-beam-assisted deposition,” *Surf. Coatings Technol.*, vol. 51, no. 1–3, 1992.

[115] R. S. Colbert, B. A. Krick, A. C. Dunn, J. R. Vail, N. Argibay, and W. G. Sawyer, “Uncertainty in pin-on-disk wear volume measurements using surface scanning techniques,” *Tribol. Lett.*, vol. 42, no. 1, pp. 129–131, 2011.

[116] T. L. Schmitz, J. E. Action, D. L. Burris, J. C. Ziegert, and W. G. Sawyer, “Wear-Rate Uncertainty Analysis,” *J. Tribol.*, vol. 126, no. 4, p. 802, 2004.

[117] I. L. Singer, R. N. Bolster, J. Wegand, S. Fayeulle, and B. C. Stupp, “Hertzian stress contribution to low friction behavior of thin MoS 2 coatings,” *Appl. Phys. Lett.*, vol. 57, no. 10, pp. 995–997, 1990.

[118] T. W. Scharf and S. V. Prasad, “Solid lubricants: A review,” *J. Mater. Sci.*, vol. 48, no. 2, pp. 511–531, 2013.

[119] J. F. Archard and W. Hirst, “The Wear of Metals under Unlubricated Conditions,” *Proc. R. Soc. London A Math. Phys. Eng. Sci.*, vol. 236, no. 1206, pp. 397–410, 1956.

[120] M. R. Ripoll, R. Simic, J. Brenner, and B. Podgornik, “Friction and lifetime of laser surface-textured and MoS2-Coated Ti 6Al4V under Dry reciprocating sliding,”

Tribol. Lett., vol. 51, no. 2, pp. 261–271, 2013.

[121] P. D. Fleischauer and R. Bauer, “Chemical and Structural Effects on the Lubrication Properties of Sputtered MoS2 Films,” *Tribol. Trans.*, vol. 31, no. 2, pp. 239–250, 1988.

[122] E. W. Roberts and W. B. Price, “In-Vacuo, Tribological Properties of "High-Rate" Sputtered MoS2 Applied to Metal and Ceramic Substrates,” in *{MRS} Proceedings*, 1988, vol. 140, p. 251.

[123] C. Müller, C. Menoud, M. Maillat, and H. E. Hintermann, “Thick compact MoS2 coatings,” *Surf. Coat. Technol.*, vol. 36, no. 1, pp. 351–359, 1988.

[124] M. Suzuki, “Comparison of tribological characteristics of sputtered MoS2 films coated with different apparatus,” *Wear*, vol. 218, no. 1, pp. 110–118, 1998.

[125] M. Mosleh, S. J. P. Laube, and N. P. Suh, “Friction of Undulated Surfaces Coated with MoS2 by Pulsed Laser Deposition,” *Tribol. Trans.*, vol. 42, no. 3, pp. 495–502, 1999.

[126] J. Kibsgaard, Z. Chen, B. N. Reinecke, and T. F. Jaramillo, “Engineering the surface structure of MoS2 to preferentially expose active edge sites for electrocatalysis,” *Nat. Mater.*, vol. 11, no. 11, pp. 963–969, 2012.

[127] RadisavljevicB *et al.*, “Single-layer MoS2 transistors,” *Nat Nano*, vol. 6, no. 3, pp. 147–150, 2011.

[128] H. Wang *et al.*, “Integrated Circuits Based on Bilayer MoS2 Transistors.,” *Nano Lett.*, vol. 12, no. 9, pp. 4674–80, 2012.

[129] C. P. Lu, G. Li, J. Mao, L. M. Wang, and E. Y. Andrei, “Bandgap, mid-gap states, and gating effects in MoS2,” *Nano Lett.*, vol. 14, no. 8, pp. 4628–4633, 2014.

[130] O. Lopez-Sanchez, D. Lembke, M. Kayci, A. Radenovic, and A. Kis, “Ultrasensitive photodetectors based on monolayer MoS2,” *Nat. Nanotechnol.*, vol. 8, no. 7, pp. 497–501, 2013.

[131] R. S. Sundaram *et al.*, “Electroluminescence in single layer MoS2,” *Nano Lett.*, vol. 13, no. 4, pp. 1416–1421, 2013.

[132] V. Buck, “Preparation and properties of different types of sputtered MoS2 films,” *Wear*, vol. 114, no. 3, pp. 263–274, 1987.

[133] P. D. Fleischauer and J. R. Lince, “A comparison of oxidation and oxygen substitution in MoS2 solid film lubricants,” *Tribol. Int.*, vol. 32, no. 11, pp. 627–636, Nov. 1999.

[134] D. J. Late, B. Liu, H. S. S. R. Matte, V. P. Dravid, and C. N. R. Rao, “Hysteresis in single-layer MoS2 field effect transistors,” *ACS Nano*, vol. 6, no. 6, pp. 5635–5641, 2012.

[135] G.-H. Lee *et al.*, “Highly Stable, Dual-Gated MoS2 Transistors Encapsulated by Hexagonal Boron Nitride with Gate-Controllable Contact, Resistance, and Threshold Voltage,” *ACS Nano*, vol. 9, no. 7, pp. 7019–7026, 2015.

[136] C. Muratore, J. E. Bultman, S. M. Aouadi, and A. A. Voevodin, “In situ Raman spectroscopy for examination of high temperature tribological processes,” *Wear*, vol. 270, no. 3--4, pp. 140–145, 2011.

[137] T. Liang, W. G. Sawyer, S. S. Perry, S. B. Sinnott, and S. R. Phillpot, “Energetics of Oxidation in MoS2 Nanoparticles by Density Functional Theory,” *J. Phys. Chem. C*, vol. 115, no. 21, pp. 10606–10616, 2011.

[138] T. Liang, W. G. Sawyer, S. S. Perry, S. B. Sinnott, and S. R. Phillpot, “First-

principles determination of static potential energy surfaces for atomic friction in MoS2 and MoO3," *Phys. Rev. B Condens. Matter Mater. Phys.*, 2008.

[139] B. A. Krick, J. R. Vail, B. N. J. Persson, and W. G. Sawyer, "Optical In Situ Micro Tribometer for Analysis of Real Contact Area for Contact Mechanics, Adhesion, and Sliding Experiments," *Tribol. Lett.*, vol. 45, no. 1, pp. 185–194, 2012.

[140] S. Průša *et al.*, "Highly Sensitive Detection of Surface and Intercalated Impurities in Graphene by LEIS," *Langmuir*, vol. 31, no. 35, pp. 9628–9635, 2015.

[141] H. R. J. ter Veen, T. Kim, I. E. Wachs, and H. H. Brongersma, "Applications of High Sensitivity-Low Energy Ion Scattering (HS-LEIS) in heterogeneous catalysis," *Catal. Today*, vol. 140, no. 3–4, pp. 197–201, 2009.

[142] A. Kauling *et al.*, "Surface composition/organization of ionic liquids with Au nanoparticles revealed by high-sensitivity low-energy ion scattering.," *Langmuir*, vol. 29, no. 46, pp. 14301–6, 2013.

[143] J. A. Kilner, S. J. Skinner, and H. H. Brongersma, "The isotope exchange depth profiling (IEDP) technique using SIMS and LEIS," *J. Solid State Electrochem.*, vol. 15, no. 5, pp. 861–876, 2011.

[144] National Institute of Standards and Technology, "NIST X-ray Photoelectron Spectroscopy Database," *June 06, 2000*. .

[145] J. Baltrusaitis *et al.*, "Generalized molybdenum oxide surface chemical state XPS determination via informed amorphous sample model," *Appl. Surf. Sci.*, vol. 326, pp. 151–161, 2015.

[146] R. G. Dickinson and L. Pauling, "The Crystal Structure of Molybdenite," *J. Am. Chem. Soc.*, vol. 45, no. 6, pp. 1466–1471, 1923.

[147] T. Spalvins, “Deposition of MoS2 Films by Physical Sputtering and Their Lubrication Properties in Vacuum,” *A S L E Trans.*, vol. 12, no. 1, pp. 36–43, 1969.

[148] G. Colas, A. Saulot, E. Regis, and Y. Berthier, “Investigation of crystalline and amorphous MoS2 based coatings: Towards developing new coatings for space applications,” *Wear*, vol. 330--331, pp. 448–460, 2015.

[149] P. D. Fleischauer and M. R. Hilton, “International applications of space tribology,” pp. 135–139, 1990.

[150] J. J. Hu, R. Wheeler, J. S. Zabinski, P. A. Shade, A. Shiveley, and A. A. Voevodin, “Transmission Electron Microscopy Analysis of {Mo--W--S--Se} Film Sliding Contact Obtained by Using Focused Ion Beam Microscope and In~Situ Microtribometer,” *Tribol. Lett.*, vol. 32, no. 1, 2008.

[151] R. L. Fusaro, “Preventing Spacecraft Failures Due to Tribological Problems,” no. April, 2001.

[152] R. H. Williams and a J. McEvoy, “Some properties of molybdenite cleavage surfaces,” *J. Phys. D. Appl. Phys.*, vol. 4, no. 3, p. 316, 1971.

[153] J. M. Martin, H. Pascal, C. Donnet, T. Le Mogne, J. L. Loubet, and T. Epicier, “Superlubricity of MoS2: crystal orientation mechanisms,” *Surf. Coat. Technol.*, vol. 68, pp. 427–432, 1994.

[154] T. Onodera *et al.*, “A Computational Chemistry Study on Friction of h-MoS2. Part I. Mechanism of Single Sheet Lubrication,” *J. Phys. Chem. B*, vol. 113, no. 52, pp. 16526–16536, 2009.

[155] T. Onodera *et al.*, “A Computational Chemistry Study on Friction of h-MoS2. Part {II}. Friction Anisotropy,” *J. Phys. Chem. B*, vol. 114, no. 48, pp. 15832–15838,

2010.

[156] O. Hod, “Superlubricity - a new perspective on an established paradigm,” 2012.

[157] M. Dienwiebel, N. Pradeep, G. S. Verhoeven, H. W. Zandbergen, and J. W. M. Frenken, “Model experiments of superlubricity of graphite,” *Surf. Sci.*, vol. 576, no. 1--3, pp. 197–211, 2005.

[158] M. M. van Wijk, M. Dienwiebel, J. W. M. Frenken, and A. Fasolino, “Superlubric to stick-slip sliding of incommensurate graphene flakes on graphite,” *Phys. Rev. B Condens. Matter*, vol. 88, no. 23, p. 235423, 2013.

[159] T. F. Babuska, A. A. Pitenis, M. R. Jones, B. L. Nation, W. G. Sawyer, and N. Argibay, “Temperature-Dependent Friction and Wear Behavior of PTFE and MoS2,” *Tribol. Lett.*, vol. 63, no. 2, p. 15, 2016.

[160] J. R. Lince and P. D. Fleischauer, “Crystallinity of rf-sputtered MoS2 films,” *J. Mater. Res.*, vol. 2, no. 6, pp. 827–838, 1987.

[161] X. Zhao, S. R. Phillpot, W. G. Sawyer, S. B. Sinnott, and S. S. Perry, “Transition from thermal to athermal friction under cryogenic conditions,” *Phys. Rev. Lett.*, vol. 102, no. 18, p. 186102, 2009.

[162] M. a. Hamilton *et al.*, “A possible link between macroscopic wear and temperature dependent friction behaviors of MoS 2 coatings,” *Tribol. Lett.*, vol. 32, no. 2, pp. 91–98, 2008.

[163] C. G. Dunckle, M. Aggleton, J. Glassman, and P. Taborek, “Friction of molybdenum disulfidetitanium films under cryogenic vacuum conditions,” *Tribol. Int.*, vol. 44, no. 12, pp. 1819–1826, 2011.

[164] I. L. Singer, R. N. Bolster, J. Wegand, S. Fayeulle, and B. C. Stupp, “Hertzian stress

contribution to low friction behavior of thin MoS2 coatings," *Appl. Phys. Lett.*, vol. 57, no. 10, pp. 995–997, 1990.

[165] N. J. N. Mikkelsen, G. Sorensen, and G. Sørensen, "Solid lubricating films produced by ion bombardment of sputter deposited MoSx films," *Surf. Coatings Technol.*, vol. 51, no. 1–3, pp. 118–123, 1992.

[166] E. E. Hoffman and L. D. Marks, "Soft Interface Fracture Transfer in Nanoscale MoS2," *Tribol. Lett.*, vol. 64, no. 1, 2016.

[167] B. a. Krick and W. G. Sawyer, "Space Tribometers: Design for Exposed Experiments on Orbit," *Tribol. Lett.*, vol. 41, no. 1, pp. 303–311, Sep. 2010.

[168] A. A. Voevodin, T. A. Fitz, J. J. Hu, and J. S. Zabinski, "Nanocomposite tribological coatings with 'chameleon' surface adaptation," *J. Vac. Sci. Technol. A Vacuum, Surfaces, Film.*, vol. 20, no. 4, pp. 1434–1444, 2002.

11. Vita

John Curry was born and raised in Whitehouse St, NJ on September 8, 1989 under loving parents James and Claire Curry. After graduating from Hunterdon Central Regional High School in 2008, he attended Lehigh University where he received his BS in 2012, ME in 2014 and Ph.D. in 2017 all in Mechanical Engineering. During John's graduate studies, he served as a teaching assistant in Graphics for Engineering Design for four semesters, teaching students the principles of engineering design, CAD design, drawing and geometric tolerancing. During his graduate work in tribology, John earned the Society of Tribologists & Lubrication Engineers (STLE) Philadelphia Section 2015 Scholarship Award and STLE 2016 E. Elmer Klaus Fellowship Presidential Award. John has published four peer reviewed journal articles, two as first author with three out for review and presented at three separate conferences, attending 7 total during his graduate studies (shown below).

11.1 Journal Papers (Published, reverse chronological order)

1) **Curry, J.F.**, Argibay, N., Babuska, T.F., Nation, B., Martini, A., Strandwitz, N.C., Dugger, M.T., and Krick, B.A., "Highly Oriented MoS_2 Coatings: Tribology and Environmental Stability" Tribology Letters. 2016.
2) **Curry, J.F.**, Babuska, T.F., Brumbach, M.T., and Argibay, N., "Temperature-Dependent Friction and Wear of MoS_2/Sb_2O_3/Au Nanocomposites" Tribology Letters. 2016.
3) Erickson, G.M., Sidebottom, M.A., **Curry, J.F.**, Kay, D.I., Kuhn-Hendricks, S., Norell, M.A., Sawyer, W.G., and Krick, B.A., "Paleo-tribology: Development of wear measurement techniques and a three-dimensional model revealing how grinding dentitions self-wear to enable functionality" Surface Metrology. 2015.
4) Harris, K.L., **Curry, J.F.**, Pitenis, A.A., Rowe, K.G., Sidebottom, M.A., Sawyer, W.G., and Krick, B.A., "Wear debris mobility, aligned surface roughness and the low wear behavior of filled polytetrafluoroethylene" Tribology Letters. 2015.

11.2 Journal Papers (Submitted)

5) **Curry, J.F.**, Luftman, H.S., Sidebottom, M.A., Strandwitz, N.C., Argibay, N., and Krick, B.A., "Probing the First Few Layers of MoS_2 with HS-LEIS: Effect of Microstructure on Oxidation" ACS Applied Materials & Interfaces. 2017
6) Chandross, M., **Curry, J.F.**, Babuska, T.F., Lu, P., Chandross, M., Furnish, T.A., Kustas, A.B., and Argibay, N., "Low Friction of Pure Metals in the Inverse Hall-Petch Regime" PNAS. 2017.
7) Argibay, N., Lu, P., O'Brien, C.J., Adams, D.P., Abdeljawad, F., Chandross, M., Clark, B.G., Boyce, B.L., Furnish, T.A., **Curry, J.F.**, Dugger, M.T., Rodriguez, M.A., Schuh, C.A., and Foiles, S.M., "Achieving Ultralow Wear with Nanocrystalline Metals" Science. 2017.

11.3 Journal Papers (In Preparation)

8) **Curry, J.F.**, Chandross, M., Babuska, T.F., Krick, B.A., and Argibay, N., "Energetics of MoS_2 Running Film Formation: Developing a Mechanistic Framework" Physical Review Letters. 2017.
9) **Curry, J.F.**, Goldstein, M., Counts, M., and Krick, B.A., "Design & Development of Multifunctional Tribometer to Asses Penetration of Multi-Purpose Lubricants" Tribology Transactions. 2017.

11.4 Conference Presentations

1) **Curry, J.F.**, Sidebottom, M.A., Counts, M., and Krick, B.A., "Uncertainties in Tribometry: A Multi-Functional Thrustwasher, Block-On-Ring, Rotary Pin-On-Disk and Reciprocating Tribometer" Society of Tribologists and Lubrication Engineers. STLE Annual Meeting, May 17-21, 2015. Dallas, TX.
2) Zeng, G., Tansu, N., **Curry, J.F.**, Sidebottom, M.A., and Krick, B.A., "Nanoscale Mechanisms in Ductile Wear of Brittle Material". Society of Tribologists and Lubrication Engineers. STLE Annual Meeting, May 17-21, 2015. Dallas, TX.
3) Krick, B.A., Sidebottom, M.A., **Curry, J.F.**, Pitenis, A.A, Harris, K.L., and Sawyer, W.G., "Ultralow Wear PTFE and Alumina Composites: The Role of Tribochemistry and Nanomechanics". Society of Tribologists and Lubrication Engineers. STLE Annual Meeting. May 17 – 21, 2015, Dallas, TX.
4) **Curry, J.F.**, Ju, L., Luftman, H.S., Strandwitz, N.C., Sidebottom, M.A., Argibay, N., and Krick, B.A., "Environmental Sensitivity of MoS_2 Coatings: Influence on the First Few Layers" Materials Research Society. 2016 MRS Spring Meeting & Exhibit, March 28 – April 1, 2016. Phoenix, AZ.
5) Babuska, T.F., Nation, B., Chandross, M., Argibay, N., **Curry, J.F.**, and Krick, B.A., "Temperature Dependent Wear and Friction of MoS_2 at the Extremes" Society of Tribologists and Lubrication Engineers. STLE Annual Meeting, May 15 – 19, 2016. Las Vegas, NV.

6) **Curry, J.F.**, Ju, L., Luftman, H.S., Strandwitz, N.C., Sidebottom, M.A., Argibay, N., and Krick, B.A., "Environmental Sensitivity of MoS_2 Coatings: Probing the First Few Layers" Society of Tribologists and Lubrication Engineers. STLE Annual Meeting, May 15 – 19, 2016. Las Vegas, NV.
7) Schulze, K., Uruena, J., Pitenis, A., **Curry, J.F.**, Sidebottom, M.A., Krick, B.A., Angelini, T., and Sawyer, W.G., "Slow Rise, Take it Easy: Local Mesh Size Control of Thermal Fluctuation Lubrication" Society of Tribologists and Lubrication Engineers. STLE Annual Meeting, May 15 – 19, 2016. Las Vegas, NV.
8) Erickson, G.M., Kuhn-Hendricks, S.M., Sidebottom, M.A., **Curry, J.F.**, Zeng, G., Norell, M.A. and Krick, B.A., "Wavy Enamel in Hadrosaurid Dinosaurs with Grinding Dentitions Functioned to Limit Fracture Damage Through Energy-robbing Crack Deflection and Channeling" Society of Vertebrate Paleontology 76th Annual Meeting, October 2016. Salt Lake City, UT.
9) Babuska, T.F., **Curry, J.F.**, Chandross, M., Dugger, M.T., Krick, B.A., and Argibay, N., "Understanding Friction in MoS_2, Part 1: Stress, Time and Temperature" American Vacuum Society. AVS 63rd International Symposium & Exhibition. November 6 – 11, 2016. Nashville, TN.
10) **Curry, J.F.**, Chandross, M., Babuska, T.F., Strandwitz, N.C., Luftman, H.S., Dugger, M.T., Argibay, N., and Krick, B.A., "Understanding Friction in MoS_2, Part 2: Water, Oxidation and Run-In" American Vacuum Society. AVS 63rd International Symposium & Exhibition. November 6 – 11, 2016. Nashville, TN.
11) Kustas, A.B., **Curry, J.F.**, Babuska, T.F., Chandross, M., Lu, P., Furnish, T.A., and Argibay, N., "The Remarkable Friction Behavior of Copper at Cryogenic Temperatures" American Vacuum Society. AVS 63rd International Symposium & Exhibition. November 6 – 11, 2016. Nashville, TN.
12) **Curry, J.F.**, Wilson, M., Babuska, T.F., Luftman, H.S., Strandwitz, N.C., Sidebottom, M.A., Chandross, M., Dugger, M.T., Argibay, N., and Krick, B.A., "Effects of Microstructure and Environment on the Run-In of MoS2" American Chemical Society. 253rd American Chemical Society National Meeting & Exposition, April 2 – 6, 2017. San Francisco, CA.
13) **Curry, J.F.**, Wilson, M., Babuska, T.F., Luftman, H.S., Strandwitz, N.C., Sidebottom, M.A., Chandross, M., Dugger, M.T., Argibay, N., and Krick, B.A., "Understanding friction in MoS2: Structure, oxidation and run-in" Society of Tribologists and Lubrication Engineers. STLE Annual Meeting, May 21 – 25. Atlanta, GA.
14) Babuska, T.F., **Curry, J.F.**, Nation, B., Chandross, M., Lu, P., and Argibay, N., "Low Friction in Metal contacts: Linking microstructural evolution and tribology." Society of Tribologists and Lubrication Engineers. STLE Annual Meeting, May 21 – 25. Atlanta, GA.

11.5 Invited Presentations

1) **Curry, J.F.**, Sidebottom, M.A., Krick, B.A. "Tribological Performance & LEIS Characterization of MoS_2 Coatings in dry and aerobic environments" Society of Tribologists and Lubrication Engineers. STLE Philadelphia Section Meeting. September 17, 2015. Oreland, PA.
2) Chandross, M., Babuska, T.F., **Curry, J.F.**, Dugger, M.T., Krick, B.A., and Argibay, N., "Understanding Friction in MoS2" The American Ceramic Society, 12th Pacific Rim Conference on Ceramic and Glass Technology (PACRIM 12). May 21 – 26, 2017. Waikoloa, Hawaii.

11.6 Poster Presentations

1) **Curry, J.F.**, Sidebottom, M.A., and Krick, B.A. "Tribological Properties of 3D Printed ABS: An Exploratory Study" Poster Presentation. Society of Tribologists and Lubrication Engineers. May 2014. Orlando, FL.
2) Smith, J.C., **Curry, J.F.**, Sidebottom, M.A., and Krick, B.A., "Effects of Relative Motion on Friction and Wear: Unidirectional vs Reciprocating Rotary Contacts" Poster Presentation. Society of Tribologists and Lubrication Engineers. May 2016. Las Vegas, NV.
3) Markham, J., **Curry, J.F.**, Gallant, E., Goldstein, M., Counts, M., and Krick, B.A., "Penetration & Characterization of Multi-Purpose Lubricants" Poster Presentation. Society of Tribologists and Lubrication Engineers. May 2016. Las Vegas, NV.
4) **Curry, J.F.**, Zeng, G., Toro, A., Sidebottom, M.A., and Krick, B.A., "Tribooxidational Effects on Wear of Ruby and Steel Alloys" Poster Presentation. Society of Tribologists and Lubrication Engineers. May 2016. Las Vegas, NV.
5) **Curry, J.F.**, Sidebottom, M.A., Luftman, H.S., Strandwitz, N.C., Babuska, T.F., Argibay, N., and Krick, B.A., "The Full MoS_2 Monty… Environment!" Poster Presentation. Gordon Research Conference. June 2016. Lewiston, ME.
6) Babuska, T.F., **Curry, J.F.**, Nation, B., Krick, B.A., Chandross, M., and Argibay, N., "The Full MoS_2 Monty… Temperature!" Poster Presentation. Gordon Research Conference. June 2016. Lewiston, ME.
7) Nation, B., Babuska, T.F., **Curry, J.F.**, Krick, B.A., Chandross, M., and Argibay, N., "The Full MoS_2 Monty… Stress!" Poster Presentation. Gordon Research Conference. June 2016. Lewiston, ME.
8) Grejtak, T., Sedaille, M., Curry, J.F., and Krick, B.A., "Optical In Situ Micro Tribometer for Analysis of Real Contact Area for Adhesive Contact Mechanics" Poster Presentation. Society of Tribologists and Lubrication Engineers May 21 – 25, 2017. Atlanta, GA.